ABSTRACT

Title of Dissertation: PLASTIC BALL GRID ARRAY SOLDER JOINT RELIABILITY ASSESSMENT UNDER COMBINED THERMAL CYCLING AND VIBRATION LOADING CONDITIONS

Haiyu Qi, Ph.D., 2006

Dissertation Directed By: **Chair Professor, Michael Pecht, Department of Mechanical Engineering**

Concurrent vibration and thermal environment is commonly encountered in the service life of electronic equipment, including those used in automotive, avionic, and military products. Though extensive research exists in literature for solder joint failures due to thermal cycling, limited research has been conducted on investigating solder joint failures due to a combination of vibration and thermal cycling.

In this study, experiments were conducted on PBGA assemblies under thermal cycling, vibration loading, and combined thermal cycling and vibration loading conditions. The results showed much earlier PBGA solder joint failure under combined loading compared with either thermal cycling or vibration loading alone. It was found that traditional linear superposition can overpredict the solder joint fatigue life since it neglects the interaction of the vibration and thermal cyclic loadings.

An incremental damage superposition approach using finite element analysis was applied to PBGA solder joint reliability assessment. This approach can model the nonlinear interactions between vibration loading and thermal cycling. It considers the

temperature effect on vibration response and the effect caused by thermomechanical mean stress affects. This approach was validated through experiments and reflects the actual damage trends.

Based on the incremental damage superposition approach, a rapid solder joint fatigue life prediction simulation approach for PBGA was also developed for combined temperature cycling and vibration loading conditions. This approach included a thermomechanical stress model and a vibration stress model to analyze the interconnect stress under thermal cycling and vibration loading conditions. The mean stress during thermal cycling was obtained from the response curve. The damage due to two different loadings was then calculated using the generalized strain approach and superposed. This approach was also validated using experimental data.

This work has also resulted in a rapid virtual qualification algorithm to predict solder joint reliability under combined temperature and vibration loading conditions. The importance of physics of failure principles in modeling and designing experiments were also explored and addressed. Industry should benefit from this study on reliability prediction, qualification, and accelerated testing design.

PLASTIC BALL GRID ARRAY (PBGA) SOLDER JOINT RELIABILITY ASSESSMENT UNDER COMBINED THERMAL CYCLING AND VIBRATION LOADING CONDITIONS

By

Haiyu Qi

Dissertation submitted to the Faculty of the Graduate School of the
University of Maryland, College Park, in partial fulfillment
of the requirements for the degree of
Doctor of Philosophy
2006

Advisory Committee:
Professor Michael Pecht, Chair
Professor Abhijit Dasgupta
Professor Bongtae Han
Associate Professor Patrick McCluskey
Associate Professor Charles Schwartz

© Copyright by
Haiyu Qi
2006

Dedication

To my parents, Jiayu Zhang and Jinghai Qi

To my wife, Ping Liu

To my son, Alexander Sijie Qi

To all love me and support me

Acknowledgements

I express my deep gratitude to Professor Michael Pecht, my dissertation advisor, for his perpetual support, encouragement and valuable guidance. His openness to discussions, patience, and constructive criticism made working on this dissertation satisfying. Working with him has indeed been an enriching experience for me.

I would also like to thank Prof. Dasgupta, Prof. Han, Prof. McCluskey, Prof. Schwartz for serving on my dissertation committee and providing valuable suggestions from time to time. I also appreciate Prof. Barker and Dr. Osterman's guidance on my dissertation work from time to time.

I gratefully acknowledge the CALCE consortium members to provide the financial and technical support on this work. I also express my thanks to the students, staff and faculty at CALCE, who have been supportive throughout.

Last but not the least, my parents and my family deserve my deepest appreciation for their love and support.

Table of Contents

Dedication ... ii

Acknowledgements ... iii

Table of Contents ... iv

Chapter 1: Introduction ... 1

1.1 Problem Statement and Objectives ... 1
1.2 Background and Literature Review ... 2
1.2.1 Life Prediction Approaches for Solder ... 2
1.2.2 Review of Cumulative Damage Approaches ... 8
1.3 Overview of the Dissertation ... 11

Chapter 2: Accelerated Testing ... 12

2.1 Design of Accelerated Stress Test ... 12
2.1.1 Test Loads and Test Matrix ... 12
2.1.2 Test Vehicle ... 13
2.1.3 Test Setup ... 14
2.1.4 Failure Monitoring and Detection ... 15
2.2 Vibration Response Characterization ... 16
2. 3 Accelerated Life Test Results ... 20
2.3.1 Temperature Cycling Test Results ... 21
2.3.2 Random Vibration Test Results ... 22
2.3.3 Combined Loading Test Results ... 23
2.3.4 Failure Analysis ... 24
2.4 Summary ... 26

Chapter 3: Modified Incremental Damage Superposition Approach ... 28

3.1 Thermal Cycling Simulation ... 30
3.1.1 Damage Calculation Due to Thermal Cycling ... 30
3.1.2 Mean Stress History Calculation ... 34
3.2 Vibration Loading Simulation ... 35
3.2.1 Solder Joint Strain Calculation ... 35
3.2.2 Solder Joint Damage Calculation Due to Vibration Loading ... 37
3.3 Total Damage Superposition ... 40
3.4 Comparison of Simulation and Test Results ... 40
3.5 Summary ... 42

Chapter 4: Rapid Life Prediction Approach 43

4.1 Temperature Cycling Simulation 45
4.1.1 Interconnect Stress/Strain Analysis 45
4.1.2 Interconnect Damage Analysis 47
4.1.3 Means Stress Predictive Models 49
4.2 Vibration Simulation 61
4.2.1 PCB Deformation Calculation 62
4.2.2 Interconnect Stress/Strain Analysis 66
4.2.3 Interconnect Damage Analysis 70
4.3 Damage Superposition 71
4.4 Comparison Between Test Results, LDSA, IDSA and RLPA............ 72
4.5 Summary 73

Chapter 5: Contributions and Suggestions for Future Work 74

5.1 Contributions of the Dissertation 75
5.2 Suggestions for Future Work 77
5.2.1 Vibration Effect on Thermal Cycling 78
5.2.2 Solder Joint Mean Stress History Simulation 78
5.2.3 Experimental Verification and Constants Calibration 79

Appendices 80

Bibliography 122

Chapter 1: Introduction

1.1 Problem Statement and Objectives

Concurrent vibration and thermal environment is commonly encountered in the service life of electronic equipment, including those used in automotive, avionic, and military products. Accelerated testing under combined environments makes the accelerated tests more realistic and should address all relevant failure mechanisms as in the use environment. Conducting accelerated tests under multiple environments is also expected to increase the rate of damage accumulation and therefore decreasing the associated time and costs. However, the complex interactions between combined stresses increase the confusion regarding the most cost-effective and rational way to conduct accelerated tests and to extrapolate results to use environments. Also different loading frequency such as low frequency loads thermal cycling and high frequency loads vibration also contribute the process complexity. Therefore, innovative test methodologies and damage analysis approach are required for reliability prediction, qualification, and accelerated testing design.

The objectives of this dissertation are: 1) to design accelerated testing to assess the effects of combined temperature cycling and vibration loading conditions on plastic ball grid array (PBGA) solder joints reliability; 2) to verify the applicability of traditional Miner's rules to assess PBGA solder joint fatigue damage under combined loading conditions; 3) to apply an incremental damage superposition approach (IDSA) to predict PBGA solder joint fatigue life; 4) to develop an integrated rapid

solder joint fatigue life prediction simulation approach for PBGA under combined temperature cycling and vibration loading condition with considering the interactions between loads.

1.2 Background and Literature Review

For solder joint fatigue, it can be categorized to two basic kinds: low cycle fatigue (LCF) and high cycle fatigue (HCF). Life cycle for LCF is general below 10^3 cycles and for HCF is between 10^4 and 10^8 cycles [Barker, et. al., 1990]. The deformation caused by thermal cycling is considered to be inelastic and belongs to LCF. For SnPb solder, creep deformation has been considered dominant. For lead-free solder, plastic deformation is also as critical as creep. Strain based equations are generally used to predict fatigue life. On the other hand, the deformation caused by mechanical vibrations is considered to be elastic and belongs to HCF. Stress based equations are generally used to predict fatigue life. For combined loading which includes LCF and HCF, low cycle fatigue has been considered the primary cause for failure and high cycle fatigue is the secondary cause for fatigue life. Linear superposition methodology (Miner's rule) has been used to predict fatigue life [Barker, et. al., 1990]. In this section, the commonly life prediction methods and damage superposition techniques for solder are summarized.

1.2.1 Life Prediction Approaches for Solder

There is no a particular methodology or model to be the "cure-all" for failure prediction due to the different failure mechanisms. Therefore it is necessary to

classify the models or methods according to their potential applications. The methods are generally classified into three categories:

1) Stress based approach: The stress-life approach, also called Basquin damage model, relates the stress amplitude to cycles-to-failure in a power law form with the help of two temperature-dependent material constants (fatigue strength coefficient and fatigue damage exponent) that are usually determined empirically [Basquin, 1910; Steinberg, 2000]. The Equation is listed as following:

$$N_1 \sigma_1^{\ b} = C \qquad \text{(Eqn. 1.1)}$$

   where C is the fatigue strength coefficient, b is the fatigue damage exponent.

   Stress approach works well for products or design with high cycle fatigue and involving constant amplitude, completely reversed cyclic loading. The analysis and estimation of material constants for this approach are quite simple and allow for quick "back of the envelope" life calculations. The approach is not suitable for solder life predictions under thermal cycling loads wherein solder experiences elastic and inelastic deformations (including time-independent "plastic deformation", and time-dependent "creep" deformation) and exhibits shorter lives (typically referred to as low cycle fatigue).

2) Strain based approach: Strain Approach, also called Coffin-Manson model, can be expressed as Equation 1.2. The plastic strain-life [Coffin, 1954; Manson, 1965] relates the completely reversed plastic strain range to cycles-to-failure in power law form with the help of two temperature-dependent

material constants (fatigue ductility coefficient and fatigue ductility exponent) that are determined empirically.

$$N_f = \frac{1}{2}\left(\frac{\Delta\gamma_p}{2\varepsilon_f}\right)^{\frac{1}{c}} \qquad \text{(Eqn. 1.2)}$$

where c is the fatigue ductility exponent, ε_f is the fatigue ductility coefficient. Combining the elastic strain-life (Basquin's model) and plastic-strain life (Coffin-Manson model) results in the generalized strain-life model that relates the total strain range (sum of elastic and plastic components) to cycles to failure. Equation 1.3 gives the formula for this approach.

$$\frac{\Delta\gamma}{2} = \frac{\Delta\gamma_e}{2} + \frac{\Delta\gamma_p}{2} = \frac{\sigma_f}{E}(2N_f)^b + \varepsilon_f(2N_f)^c \qquad \text{(Eqn. 1.3)}$$

where

$\Delta\gamma$ is the total strain range,

$\Delta\gamma_e$ is the elastic strain range,

$\Delta\gamma_p$ is the plastic strain range,

E is the modulus of elasticity,

σ_f is stress strength coefficient,

b is the fatigue strength exponent,

c is the fatigue ductility exponent, and

ε_f is the fatigue ductility coefficient.

At large strain amplitudes the strain-life model reduces to Coffin-Manson model and at small strains reduces to Basquins' model.

Further modifications have enabled the strain-life model to be sensitive to means stresses when the loading is not completely reversed and is shown as Equation 1.4.

$$\frac{\Delta\gamma}{2} = \frac{\Delta\gamma_e}{2} + \frac{\Delta\gamma_p}{2} = \frac{(\sigma_f - \sigma_o)}{E}\left(2N_f\right)^b + \varepsilon_f\left(2N_f\right)^c \qquad \text{(Eqn. 1.4)}$$

where σ_o is mean stress

The main limitation of the strain based approach is its inadequacy to account for time-dependent effects (i.e. different ramp rates, strain rates, frequency of loading, hold times etc,) especially at elevated temperatures. However, the simplicity and availability of extensive experimental data for solder makes this approach very attractive.

3) Energy based approach: Energy life approach correlates the fatigue life to the mechanical hysteresis energy in a power law form [Morrow, 1965; Solomon, 1986; Vaynman, 1991; Darveaux et. al., 1995]. The energy based approach recognizes the need for the presence of a stress field to move the dislocations necessary for causing irreversible plastic deformation. Analogous to the strain range partitioning model, the need for strain rate (or failure mechanism) dependent energy life curves resulted in the development of the energy

partitioning model [Dasgupta et. al., 1992]. The energy partitioning model is a generalized creep-fatigue model that partitions the area under the stress-strain hysteresis loop into three components – elastic energy, plastic work and creep work. The total energy per cycle is defined as the sum of the stored elastic energy, the plastic work dissipated, and the creep work dissipated. Each quantity is related to fatigue life by a power law relationship and total damage is obtained by linear superposition of individual damages. Equation 1.5 shows the energy partitioning model and Equation 1.6 gives the calculation formula for the fatigue life. However none of the energy-based models are sensitive to mean stress effects when the loading is not completely reversed. This is particularly important for creep deformations where hydrostatic mean stresses can play a significant role in damage accumulation.

$$Energy = U_e + W_p + W_{cr} = U_o N_{fe}^{b'} + W_{po} N_{fp}^{c'} + W_{co} N_{fc}^{d'} \quad \text{(Eqn. 1.5)}$$

$$\frac{1}{N_f} = \frac{1}{N_{fe}} + \frac{1}{N_{fp}} + \frac{1}{N_{fc}} \quad \text{(Eqn. 1.6)}$$

where

U_{eo} is the elastic coefficient,

b' is the elastic exponent,

W_{po} is the plastic exponent,

c' is the plastic exponent,

W_{co} is the creep coefficient, and

d' is the creep exponent.

Darveaux's methodology [Darveaux, 1992, 1995, 200] links laboratory measurements of low-cycle fatigue crack initiation and crack growth rates to the inelastic work of the solder. It is a strain energy based approach, where work term consists of time-dependent creep and time-independent plasticity. The inelastic behavior is captured in ANSYS using Anand's constitutive model. Equation 1.7-1.9 gives the formula for this approach. However, the methodology is sensitive to the finite element modeling procedure. First, care must be taken in controlling the element thickness at the interface between the eutectic solder and copper pad. Second, element volumetric averaging of the stabilized change in plastic work within this controlled eutectic solder element thickness must be used.

$$N_0 = K_1 (\Delta W_{ave})^{K_2} \qquad \text{(Eqn. 1.7)}$$

$$\frac{da}{dN} = K_3 (\Delta W_{ave})^{K_4} \qquad \text{(Eqn. 1.8)}$$

$$\alpha = N_0 + \frac{a}{da/dN} \qquad \text{(Eqn. 1.9)}$$

where

N_0 is the thermal cycles to crack initiation

a is the entire solder joint equivalent length (e.g. diameter)

da/dN is crack propagation rate

K_i are crack growth correlation constants

ΔW_{ave} is the average viscoplastic strain energy per cycle

α is the characteristic solder joint fatigue life

In summary, there are a variety of approaches (stress, strain, and energy) can be used to analyze the damage caused by different environmental loading conditions. There is no the "cure-all" approach and people need to find an appropriate one based on the application and failure mechanism of interest. When loads become random or are in the presence of multiple loading, the complexity will arise. The current complied solution is to accumulate damage throughout the life cycle using an appropriate damage superposition scheme. In the following section, a brief review of cumulative damage approach applied to solder joint is presented.

1.2.2 Review of Cumulative Damage Approaches

Palmgren [Palmgren, 1924] first proposed the linear damage model and Miner [Miner, 1945] further developed it. It is commonly referred as Miner's rule. The hypothesis of Miner's rule is that damage can be superposed linearly and that failure occurs when the cumulative damage fraction (defined as the fraction of life used up by an event or a series of events) equals unity. Two main shortcomings of linear damage superposition are that: 1) it does not consider load sequence effects. The hypothesis assumes the damage caused by a stress cycle is independent of where it

occurs in the load history; 2) it does not capture the influence of stress level on the rate of damage accumulation.

Barker *et. al.* [1990, 1992] modified the linear damage supposition approach (LDSA) to consider the different frequency loading effects and applied it to solder joint reliability assessment under combined temperature cycling and vibration loading. The damage was calculated independently due to vibration and thermal loads and superposed in a linear fashion with consideration different loading frequency. Equation 1.9 and Equation 1.10 shows the formula to calculate the damage and life.

$$D_{total} = D_v + D_{th} = n_{th}\left(\frac{f_v / f_{th}}{N_v} + \frac{1}{N_{th}} \right) \qquad \text{(Eqn. 1.9)}$$

$$N_f = \frac{1}{D_{total}} \qquad \text{(Eqn. 1.10)}$$

where

D stands for damage;

n is the cycles experienced;

f stands for the frequency of loading;

Subscripts "*th*" for thermal and "*v*" for vibration;

N_f is defined as solder joint fatigue life

Though this approach takes account the different loading frequency effect, it neglects the interactions between loads and loading sequence effects.

Upadhyayula and Dasgupta [1997] proposed an incremental damage superposition approach (IDSA) to calculate the damages based on the hypothesis that random vibration excitation is function of temperature and varying thermomechanical mean stresses affects vibration induced fatigue. Constitutive properties of solder was also hypothesized as a function of temperature and reflected by changes in curvature-strain response curves. This approach has been only demonstrated on leaded packages (J leaded plastic chip carrier and gull winged quad flat pack). Simulation work was based on detailed finite element analysis, which is complex and time-consuming.

Basaran and Chandaroy [2002] developed a unified constitutive model for Pb40/Sn60 solder joints in leadless ceramic chip carrier (LCCC) and implemented in a thermo-viscoplastic-dynamic finite element procedure. In this proposed model a damage criterion based on the second law of thermodynamics and statistical continuum mechanics is used to establish the connection between disorder and entropy. This constitutive model was verified using a series of other researchers' laboratory test data [Adams, 1986; Mcdwoell *et. al.*, 1994; Busso *et. al.*, 1992]. The results indicate that using Miner's rule to calculate accumulative damage by means of two separate analyses, namely dynamic and thermo-mechanical, significantly underestimates the accumulative total damage. It is also shown that a simultaneous application of thermal and dynamic loads significantly shortens the fatigue life of the solder joint.

However they did not provide the experimental verification on their simulation approach.

1.3 Overview of the Dissertation

Chapter 2 presents the accelerated life tests conducted on plastic ball grid array (PBGA) assemblies under multiple environmental loading conditions. Test matrix identification, accelerated load selection, failure detection and response monitoring schemes, and data post-processing schemes are discussed in details. Test results are also summarized.

The modified incremental damage superposition approach (IDSA) is presented in Chapter 3. The tools, methods and procedures used in IDSA such as cycle counting technique, stress analysis and incremental damage assessment are discussed and illustrated for PBGA solder joint study.

Chapter 4 presents a rapid life prediction approach (RLPA) for PBGA solder joint based on the IDSA concept. This approach included a thermomechanical stress model and a vibration stress model to analyze the interconnect stress under thermal cycling and vibration loading conditions. The damage due to two different loadings was then calculated using the generalized strain approach and superposed. This approach was also validated using experimental data.

Contributions of the dissertation and suggestions for future work are presented in Chapter 5.

Chapter 2: Accelerated Testing

Temperature cycling, random vibration, and combined temperature cycling and vibration accelerated fatigue damage caused in PBGA solder joint is investigated experimentally. Section 2.1 outlines the accelerated tests design. In Section 2.2, the vibration response at different temperature levels are characterized. In Section 2.3 results of the accelerated life tests are presented for each test loading condition. Testing was conducted at Motorola and Honeywell facilities. Failure and statistical analysis were conducted by CALCE EPSC.

2.1 Design of Accelerated Stress Test

To successfully design and conduct accelerated testing, it is necessary to understand the failure types and the underlying failure mechanisms [Pecht, 1990, 1994, 1995; Dasgupta, 1991; Lall, 1993]. An overstress failure is defined as the failure due to a single occurrence of a stress event exceeds the intrinsic strength of a material. In contrast, a failure due to accumulation of incremental damage in excess of the material endurance limit is termed as a wearout failure. Accelerated testing for overstress determination is usually not useful to predict product field life. In this study, accelerated stress test is designed to focus on wearout failure mechanism.

2.1.1 Test Loads and Test Matrix

The primary objective in this thesis is to understand the effect of temperature cycling and vibration interactions on solder durability in the accelerated stress condition. Therefore combined temperature cycling and vibration loading were selected for the

test environment. To better understand the difference between combined loading and one single stress loading, pure temperature cycling and vibration loading were selected as well. Test matrix is shown in Table 1.

Table 2.0.1 Accelerated Test Matrix

Tests	Stress Loading	Notes
Temperature Cycling	-50/150 °C	24 minutes ramp and 15 minutes dwell
Vibration	0.1 G^2/Hz	Frequency from 100 to 1000 Hz
Combined Loading	-50/150 °C & 0.1 G^2/Hz	Concurrently

2.1.2 Test Vehicle

The test vehicle consisted of 15 commercially available daisy-chained 272 PBGAs [Motorola] mounted onto a FR-4 PCB. The packages have 272 balls in a partially depopulated array (4 perimeter ball rows and a 4x4 thermal ball area), with a ball pitch of 1.27 mm. The package itself is 27x27 mm^2 in size with non-solder mask defined ball pads of 0.635 mm diameter. Figure 2.1 shows the test board with the packages numbered.

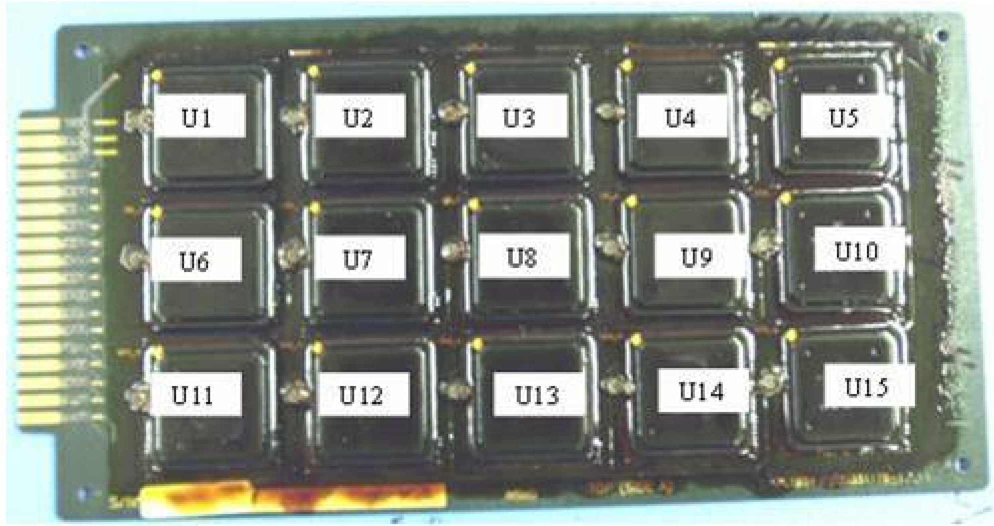

Figure 2.1 Layout of test vehicle

2.1.3 Test Setup

The loads in this study, temperature cycling and vibration, were applied in an accelerated stress test chamber (Manufacturer: Bemco; model number: JT-32L500). Temperature profiles were achieved by convection heating and liquid nitrogen through helical dispersion nozzles providing cooling to the test vehicle. Vibration was performed by a vibration table, which was driven electro-dynamically to produce the vibrations at frequencies. Frequencies are randomly swept across the range of 100 to 1000 Hz. The test boards were clamped along the long edges using wedge locks during tests. Figure 2.2 shows the vibration table with PCBs mounted in place. Three accelerometers (numbered) can be seen attached to the fixture. One each on the PCBs and then one on the vibration table plate. The manufacturer for accelerometers is Unholtz-Dickie with model no. 10B10T. The strain gage (CEA-13-125LN-120) was also attached at the backside of PCB under package U6 to measure the PCB deformation.

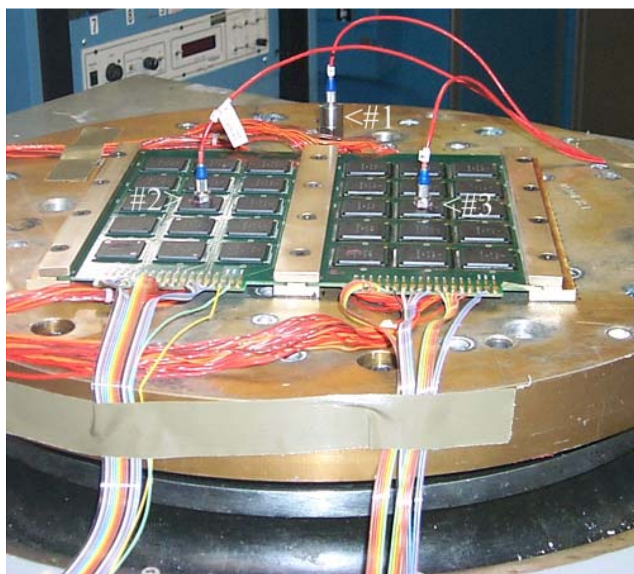

Figure 2.2 Vibration table with PCBs

2.1.4 Failure Monitoring and Detection

Monitoring of daisy chain nets in the chamber is accomplished using a commercial event detector (Anatech® event detector). The event detector monitors the resistance through the daisy chain net and is set to a threshold of 300 ohms [IPC_785, 1992]. Once a daisy chain net has failed 10 times, it is recorded by the event detector as a failed net and a printout is made of the net number. Since the cycles are counted, a failed net is known at which cycle it failed at. The failures are collected for later use in statistical analysis. Auxiliary electrical instrumentation like multimeters were used to confirm interconnect failure by performing static electrical tests with probes attached to the particular daisy-chained interconnects. This exercise confirmed failures in interconnects that were electrically open. Further destructive failure analysis is performed to find the failure site and mode and confirm the failure mechanism.

2.2 Vibration Response Characterization

To consider temperature cycling effects on vibration response, PCB strain history was collected using the strain gage at potential failure site of interest at three discrete temperature levels: -50 °C, 25 °C and 125 °C. The reason to choose these three temperature levels to represent the whole thermal cycle is that the vibration response of the specimen in any two given temperature regions is significantly different.

Figure 2.3 to Figure 2.5 shows the time domain deformation histories. They confirmed that the deformation increased while the temperature was increasing. However, it can be also observed the random vibration loads generate the complex (or irregular) deformation histories. To convert those into a number of events which can be compared to the available constant amplitude data, some cycle counting process [ASTM, 1996; Bannantine, 1993; Downing and Socie, 1982; Dowling, 1972;] are needed for this conversion. The output from a cycle counting analysis is a two dimensional array (or plot) of blocks of constant amplitude events versus the frequency (number of occurrences per unit time) of an event of a given amplitude and in this dissertation, such a plot is referred to as a Range Distribution Function (RDF). Over the years, rainflow counting has become a generic term that describes any cycle counting method that attempts to identify closed hysteresis loops in a material subjected to cyclic loading. In this dissertation, the simplified rainflow counting technique was used to summarize complex and irregular deformation histories (filtered strain-time load histories) collected from strain gages. Cycle counting procedures are based on the identification of local maxima and minima of the load amplitudes experienced. The positions of local maximum (peak) and local minimum

(valley) load values are tabulated. Range-pair counting techniques are then employed to identify hysteresis loops. The identified hysteresis loops can be used for further fatigue analysis. For example, the most damaging hysteresis loop is obtained by combining the largest peak and largest valley. The second largest cycle is obtained by combining the largest peak and valley of the remaining counts. The process is continued until all counts have been exhausted [Upadhyayula, 1999]. Figure 2.6-2.8 shows the temperature dependent strain RDFs. These RDFs were used for damage calculation and discussed later.

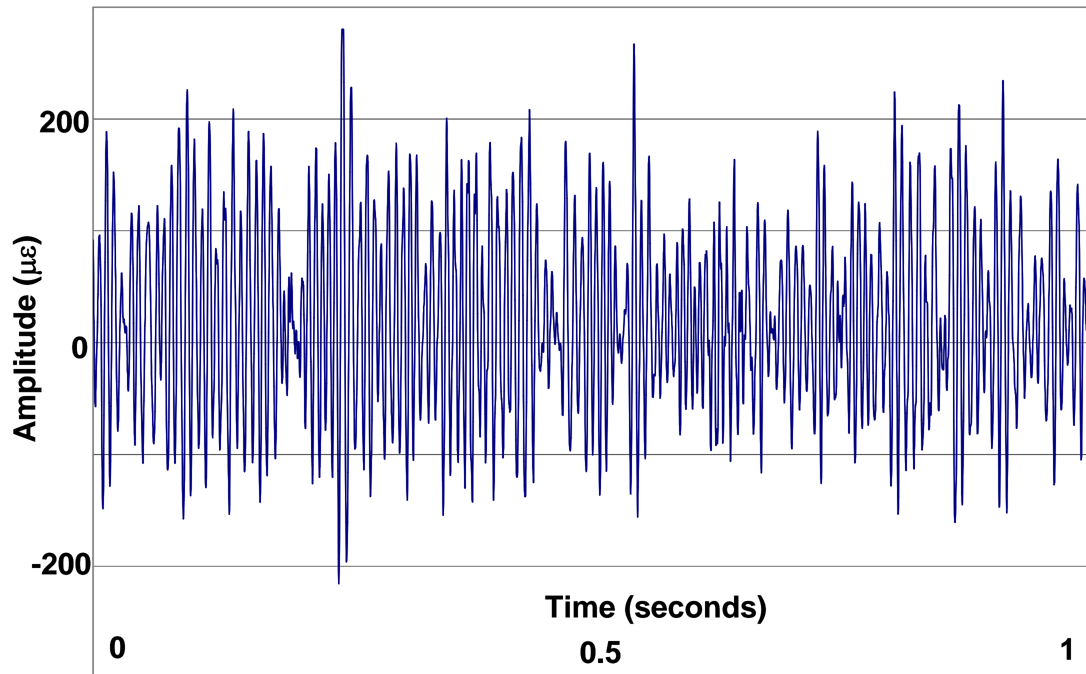

Figure 2.3 PCB strain history under PBGA location at 150 °C

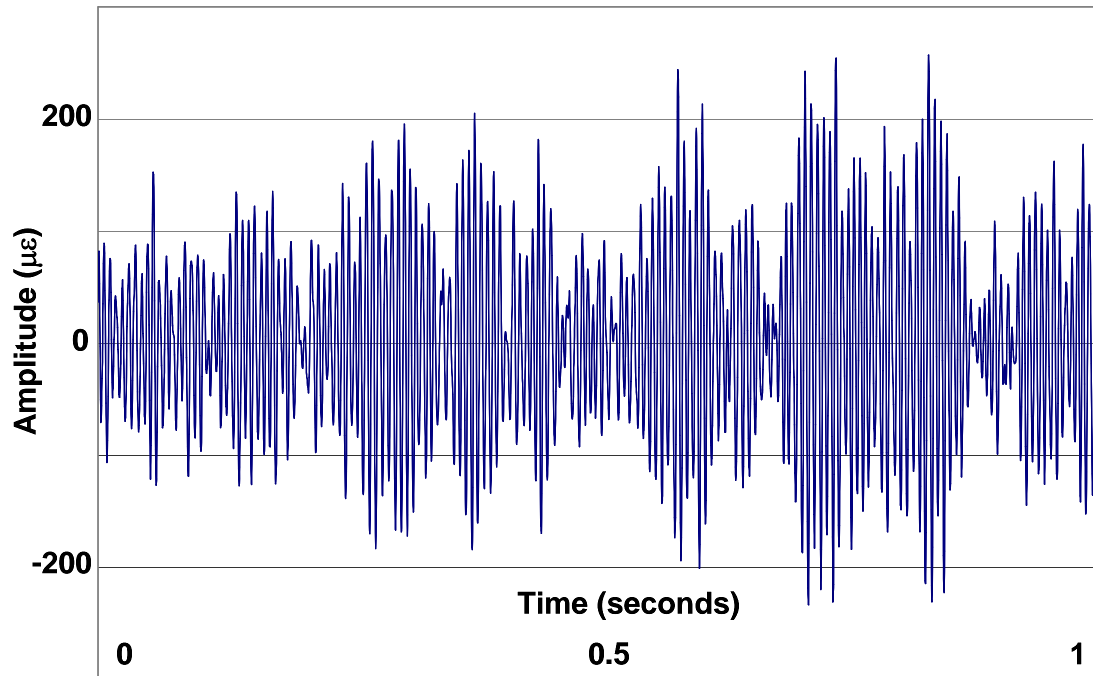

Figure 2.4 PCB strain history under PBGA location at 25 °C

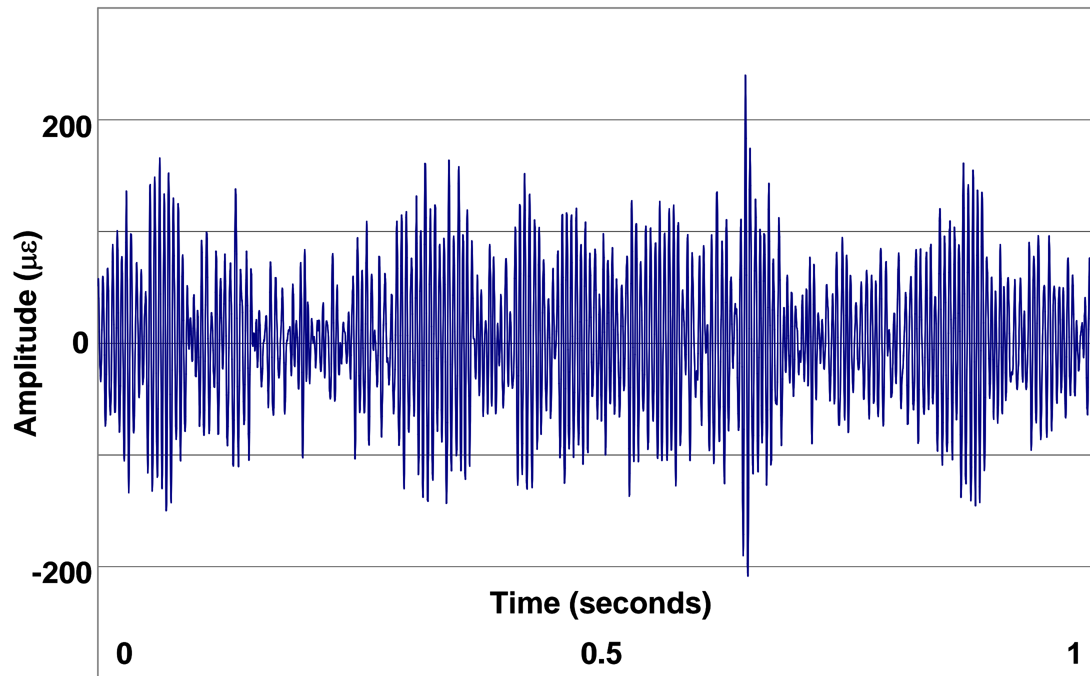

Figure 2.5. PCB strain history under PBGA location at -50 °C

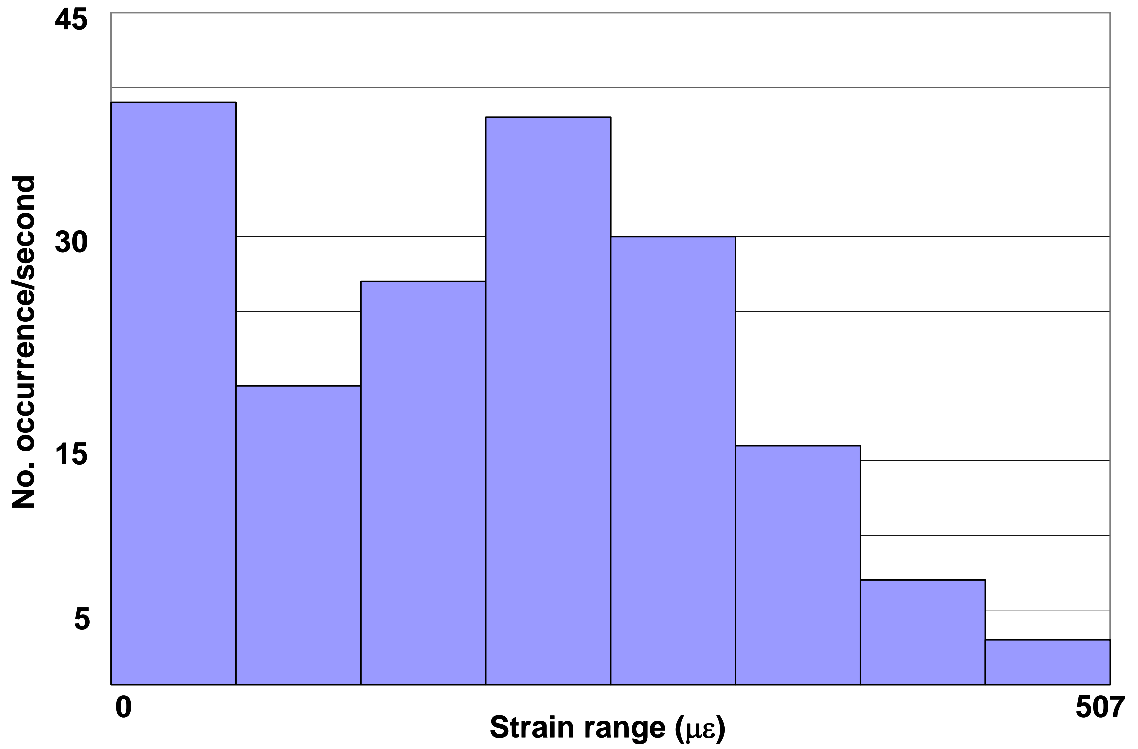

Figure 2.6 PCB strain RDFs under PBGA location at 150 °C

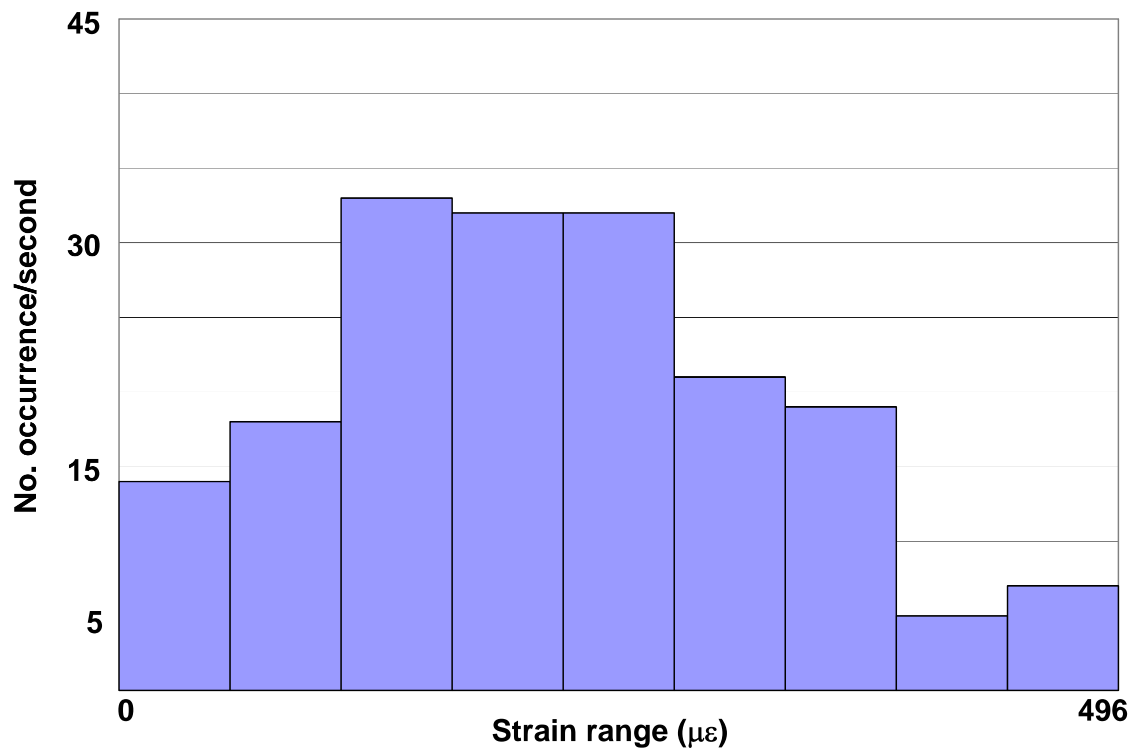

Figure 2.7 PCB strain RDFs under PBGA location at 25 °C

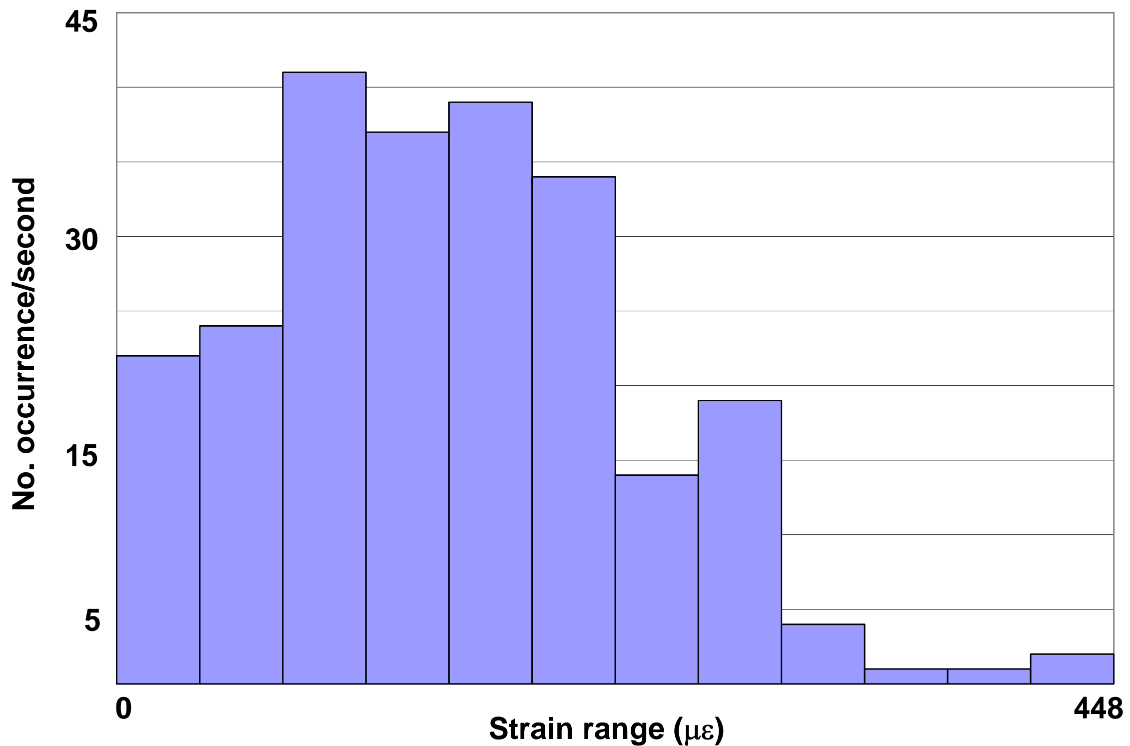

Figure 2.7 PCB strain RDFs under PBGA location at -50 °C

2. 3 Accelerated Life Test Results

In this study, accelerated life tests were conducted to evaluate the solder joint vulnerability to applied loads due to wearout failure mechanisms. The loads include temperature cycling, random vibration and combined temperature cycling and vibration loading. The main purpose is to explore the interactions between temperature and vibration environments in precipitating solder interconnect failures. The tasks in this step included implementation of accelerated tests and verification of observed failures.

2.3.1 Temperature Cycling Test Results

Temperature profile has been shown in Table 2.1. Temperature cycling test was stopped after 4002 cycles with nine components failed and six survived. Two-parameter Weibull distribution was used to as the best fit distribution for test results. Figure 2.6 shows temperature cycling test results with the shape factor (β= 8.61), and characteristic life (η= 2611 cycles). Based on this distribution, the mean fatigue life of the PBGA solder joint was 2467 cycles (3207 hours) under this temperature cycling condition.

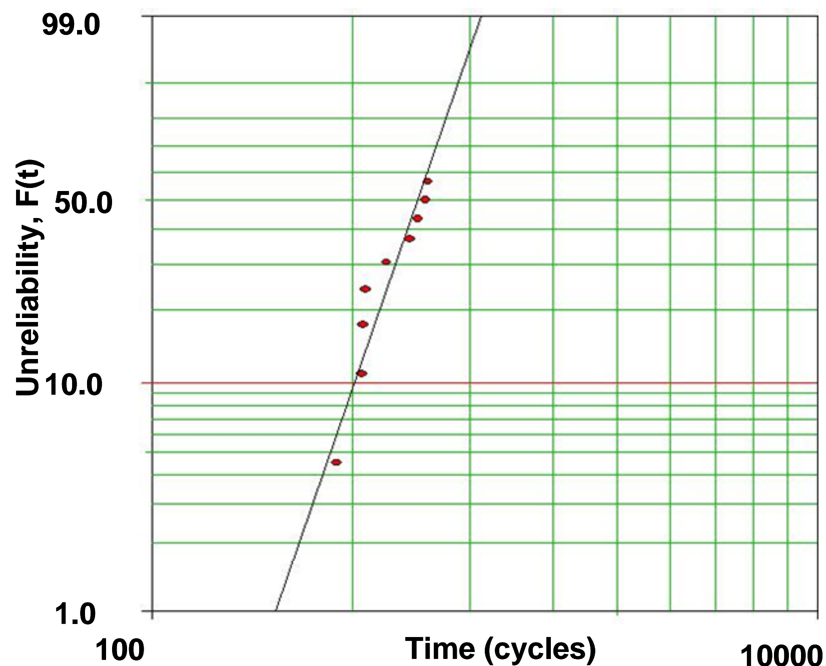

Figure 2.6 2-Parameter Weibull distribution of thermal cycling test results (β= 8.61, η= 2611, ρ= 0.95)

2.3.2 Random Vibration Test Results

Random vibration loading has been also shown in Table 2.1. Vibration test was stopped after 2237 hours exposure. Six components failed and nine survived. Since the packages locate at different position on the board, time to failure of each package was normalized based on unit 6 curvature information. The curvature information is obtained from quick FEA simulation using a commercial software calcePWA®. Two-parameter Weibull distribution was used to as the best fit distribution for test results. Figure 2.7 shows vibration test results with shape factor (β= 1.48) and characteristic life (η= 3232 hrs). The mean life of the PBGA solder joint was calculated to 2922 hours under this vibration loading condition. It was noticed, the shape parameter of vibration test results is much lower than the one in thermal cycling test. It indicates the vibration fatigue is quite different than temperature cycling fatigue. Therefore, simply linear superposition may be not appropriate for combined these two loadings. Combined loading experiment is then performed to verify it.

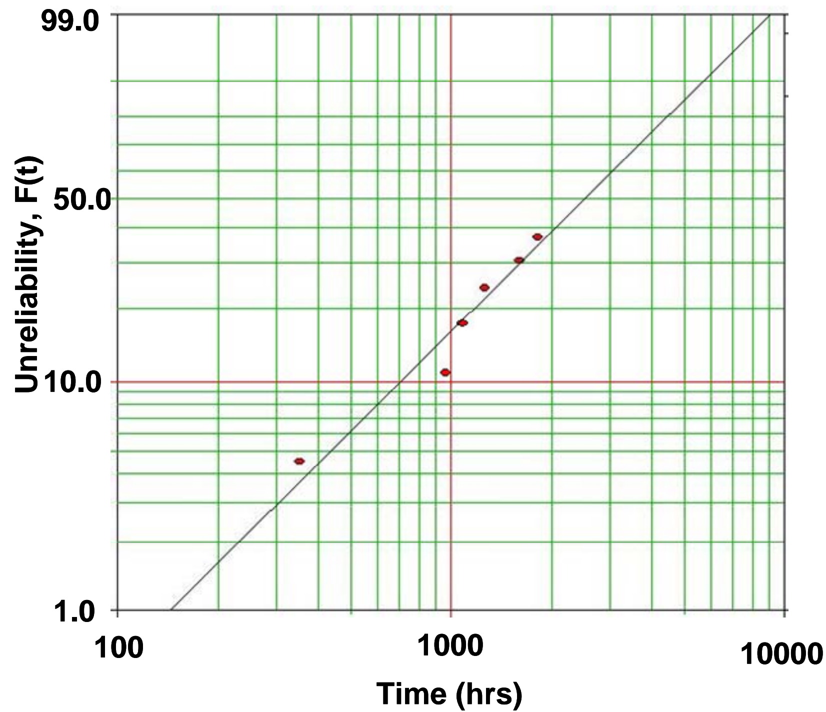

Figure 2.7 Two-parameter Weibull distribution of normalized vibration test results (β= 1.48, η= 3232, ρ= 0.97)

2.3.3 Combined Loading Test Results

Combined temperature cycling and vibration test was completed after 2953 hours exposure with all components failed. Time to failure of each package was also normalized based on unit 6. Two-parameter Weibull distribution was also used to as the best fit distribution for test results. Figure 2.8 shows combined loading test results with shape factor (β= 1.2) and characteristic life (η= 193 hrs). The mean life of the PBGA solder joint was calculated to 192 hours under combined loading.

The experimental results show the time to failure of components significantly shorter under the combined loading compared to test results under temperature cycling alone and vibration alone. The earlier failure phenomena indicate the interaction exists

between temperature cycling and vibration loading. That interaction may change the vibration response of board, the stress state in solder, and the fatigue properties.

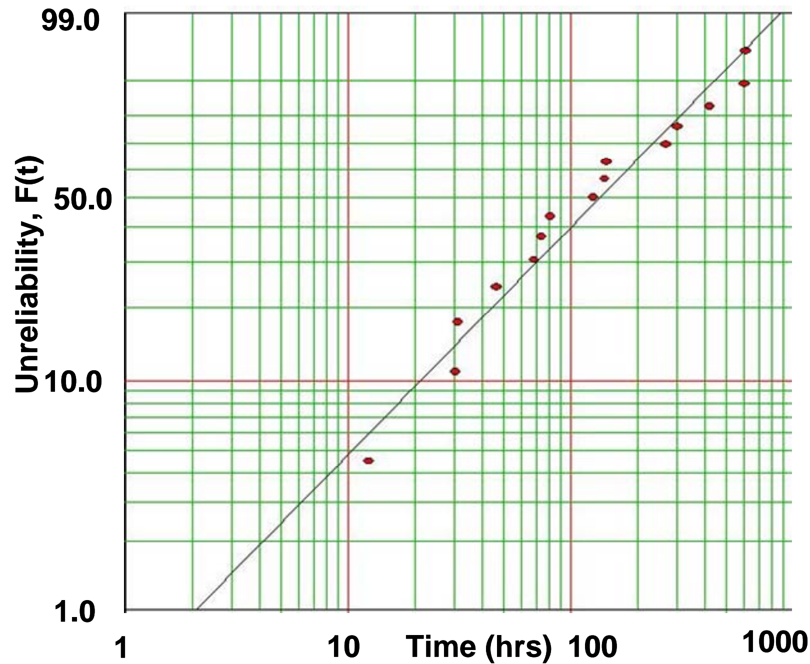

Figure 2.8 Two-parameter Weibull distribution of combined loading test results (β= 1.2, η= 193, ρ= 0.98)

2.3.4 Failure Analysis

Failure analysis is the key component in physics of failure (PoF) methodology. The failure site, mode and mechanism can be identified through appropriate failure analysis. In this study, non-destructive and destructive failure analyses were performed to identify the failure on the solder joint. First, multimeters were used to confirm interconnect failure by performing static electrical tests with probes attached to the particular daisy-chained interconnects. Then visual inspections were performed

on failed packages before they were removed from boards. Figure 2.9 shows a possible crack at a solder joint through visual inspection after the combined loading test. The failed specimen was then cross-sectioned to determine the failure site. Figure 2.10 shows the cross-section of the solder joint ball shown in Figure 2.9. The failures were identified to be due to fatigue cracks on the solder joint.

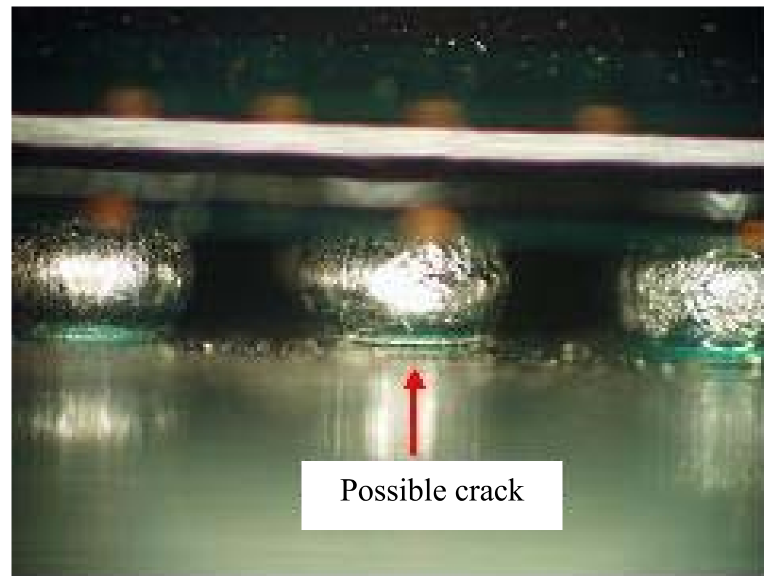

Figure 2.9 A perimeter visual inspection image from one package with a possible cracked solder joint

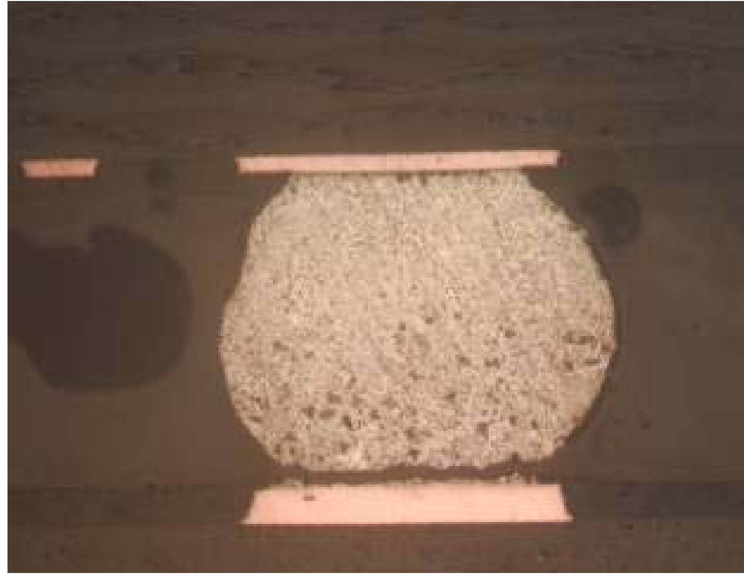

Figure 2.10 A cross-section image of the solder joint in Figure 2.9

2.4 Summary

Results from temperature cycling, random vibration loading and combined temperature and vibration accelerated life tests of PBGA assemblies were presented in this chapter. Section 2.1 outlined the design of accelerated test, such as test matrix, test setup, and failure detection schemes. In Section 2.2, the vibration response characterization results were presented. The characterization involved understanding the test specimen response to the selected test loads. The important observation made in Section 2.2 was that increasing the temperature increased the observed specimen response to random vibration excitation. In Section 2.3 experimental results were presented for PBGA assemblies under different environmental loading conditions. The primary conclusion from the experiments is that there exists a strong dependence of solder damage on load interactions (thermal cycling + vibration loads versus thermal cycling load alone versus vibration load alone). These phenomena cannot be

quantified by a linear damage superposition approach such as the Palmgren-Miner hypothesis. The experimental observation calls for a detailed non-linear damage superposition scheme to understand and quantify the effects of temperature-vibration interactions on solder joint durability.

Chapter 3: Modified Incremental Damage Superposition Approach

This incremental damage superposition approach (IDSA) was first proposed by Upadhyayula and Dasgupta [Upadhyayula, 1999] and applied to leaded packages. This approach uses a variant of Miner's hypothesis, but in an incremental piece-wise linear sense at each stress level, to track nonlinear interactions between different load types of varying frequencies (temperature cycling and vibration). The original IDSA consists of four steps: Step 1) Thermal response characterization; Step 2) Vibration response characterization; Step 3) Interconnect stress analysis for combined temperature and vibration loads; Step 4) Creep-fatigue damage superposition.

In this dissertation, this approach is applied to PBGA packages with some modifications. The modifications include the method to obtain strain relationship between PCB and solder joint, and strain approach to obtain solder joint damage. The details will be discussed in following sections.

Instead of four steps organized as Upadhyayula [1999], this work is described to two major parts: thermal cycling simulation and vibration simulation. Figure 3.1 shows the flowchart for this work. Each box will be explained in details later.

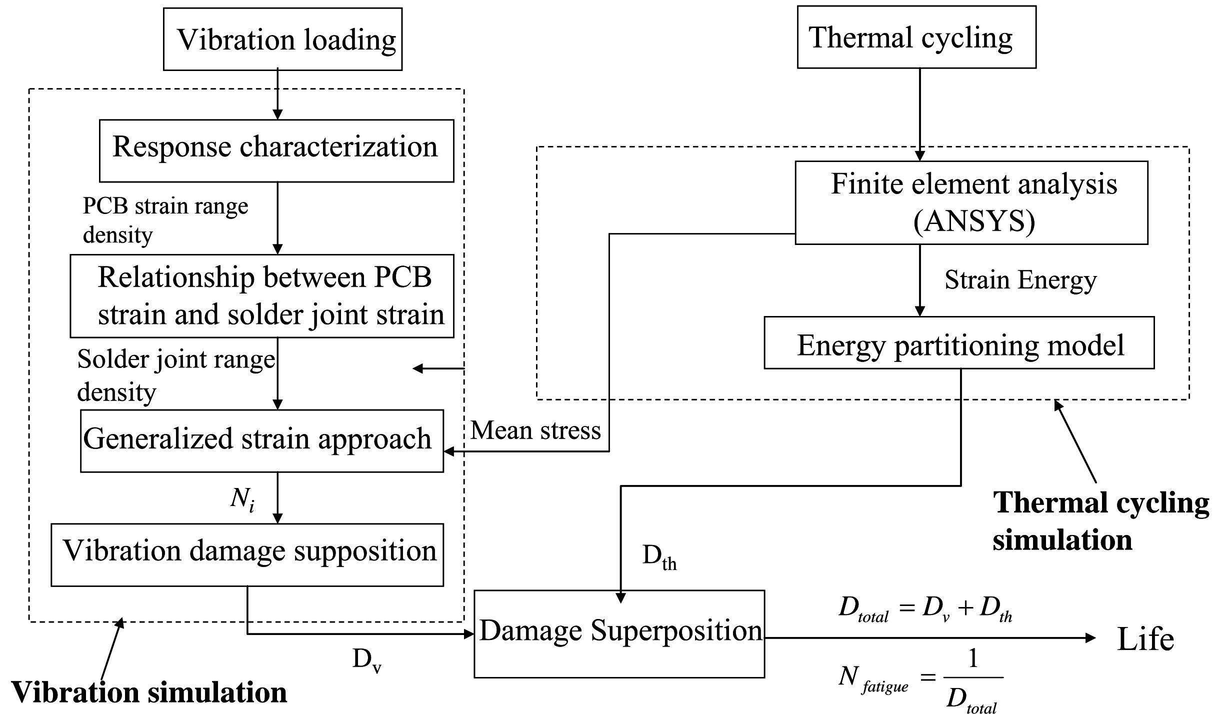

Figure 3.1 Flowchart of incremental damage superposition approach on PBGA solder joint reliability assessment under combined temperature cycling and vibration loading

3.1 Thermal Cycling Simulation

Thermal cycling simulation includes two parts: damage calculation due to thermal cycling loading and means stress history calculation. This work is done using finite element analysis (FEA). Details are described as following.

3.1.1 Damage Calculation Due to Thermal Cycling

Finite element analysis (FEA) was used to simulate the temperature cycling test. A strip 3-dimenstion PBGA assembly model was developed using a commercial software ANSYS®. Figure 3.2 shows the whole model with zoom in on the solder ball. Thermal loading profile was the same as the one in temperature cycling test and combined loading test. The geometric parameters and mechanical properties are listed in Tables 3.1 and 3.2. Temperature-dependent elastic properties were used for all materials except for the eutectic solders. The property data of the 63Sn37Pb eutectic solder was directly measured in the CALCE EPSC laboratory and used for simulation. Table 3.3 and 3.4 are linear isotropic material properties and creep properties for 63Sn37Pb eutectic solder. The CTE of solder is 21 ppm/°C at 25 °C. The nonlinear stress vs. plastic strain curves of eutectic solder is shown in Figure 10 [Qi, 2004].

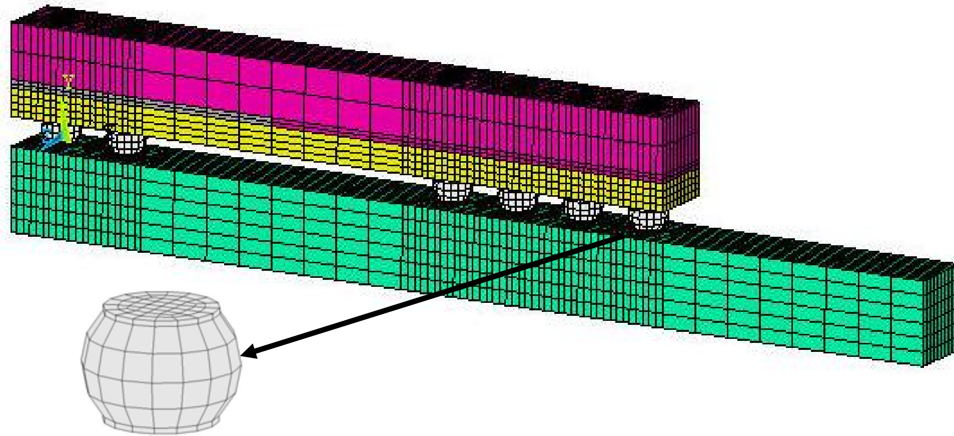

Figure 3.2 A strip 3D FEA model for PBGA272 assembly

Table 3.1 Geometry parameters used in the FEA model

Name	Dimension (mm)
272 PBGA package dimension (x X y)	27 X 27
Overmold thickness	1.15
Substrate thickness	0.5
Pitch	1.27
Die dimension (x X y X z)	10.16 X 10.16 X 0.15
Board thickness	1.5
Solder ball collapse height	0.45
Solder joint width	0.635
Pad thickness	0.015
Ball layout	Peripheral array

Table 3.2 Material properties in the model

Material	E (GPa)	CTE (ppm)	Poisson's ration
Die	303.46	5.26	0.22
FR4 (board)	17.2	15.7	0.28
Overmold	15.86	15.0	0.25
Substrate	13.0	13	0.2
Cu (pad)	121	17	0.3

Table 3.3 Linear isotropic material properties for 63sn37pb eutectic solder [Qi, 2004]

	T1	T2	T3	T4	T5	T6	T7
Temp (K)	193	208	218	273	298	338	378
Elastic Modulus (MPa), x	54497	50994	48658	35812	29973	20629	12455
Poisson Ratio, xy	0.35	0.35	0.35	0.35	0.35	0.35	0.35

Table 3.4 Creep table--generalized garofalo (secondary) [Qi, 2004]

	T1	T2
Temperature (K)	218	398
C1	1239.5	255.95
C2	0.053523	0.14197
C3	3.3	3.3
C4	6359.5	6359.5

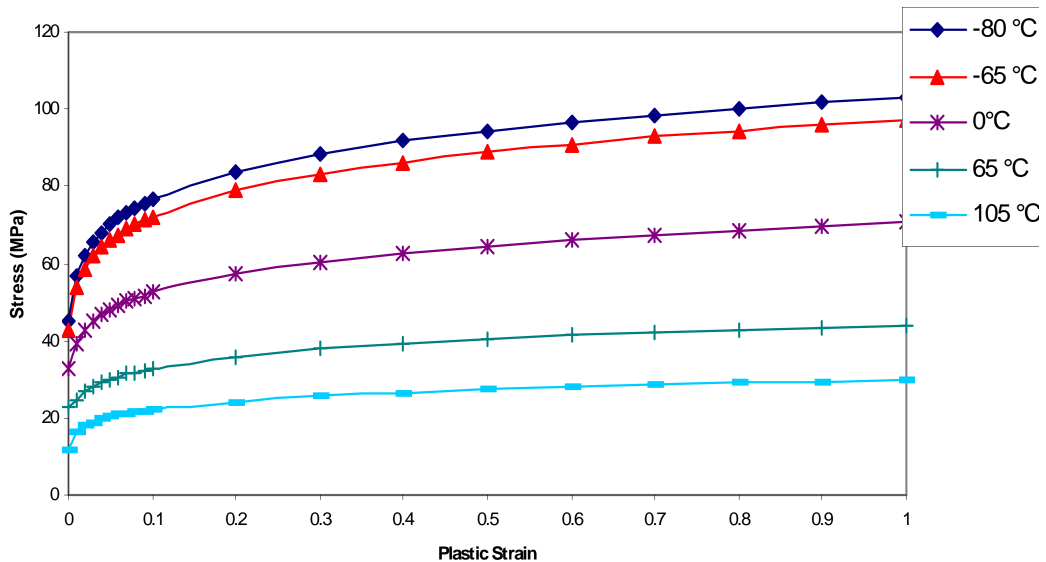

Figure 3.3 Nonlinear Stress vs. Plastic Strain Curve for Solder Material [Qi, 2004]

The outmost ball was chosen for stress/strain calculation due to the maximum stress/strain location. Strain energy was averaged along the bottom layer of solder joints where the maximum strain locates. The energy partitioning approach [Dasgupta, *et. al.*, 1992] was used to compute the damage due to temperature cycling

loading. This approach has been experimentally verified in previous studies [Barker, et. al., 1993; Rothman, et. al., 1996]. The primary feature of the energy-partitioning approach is to partition the area under the stress-strain curve into three components-elastic, plastic and creep energy. The total energy per cycle (U_{total}) is defined as the sum of the stored elastic energy, the plastic work dissipated, and the creep work dissipated

$$U_{total} = U_e + W_p + W_{cr} = U_{eo} N_{fe}^{b'} + W_{po} N_{fp}^{c'} + W_{co} N_{fc}^{d'} \qquad \text{(Eqn. 3.1)}$$

where U_{eo} is the elastic coefficient, b' is the elastic exponent, W_{po} is the plastic exponent, c' is the plastic exponent, W_{co} is the creep coefficient, and d' is the creep exponent. Table 3.5 lists these constants value [Rothman, 1995].

Table 3.5 Energy partitioning damage model constants for eutectic solder [Rothman, 1995]

Energy Partitioning Model Constant	Value
b'	-0.18
c'	-0.6
d'	-1
U_{eo} (MPa/cycle$^{b'}$)	0.698
W_{po} (MPa/cycle$^{b'}$)	165
W_{co} (MPa/cycle$^{b'}$)	94

Damage contribution from thermal cycling load (D_{th}) is given by

$$D_{th} = D_{el} + D_{pl} + D_{cr} = \frac{1}{N_{fe}} + \frac{1}{N_{fp}} + \frac{1}{N_{fc}} = \frac{1}{N_{th}} \qquad \text{(Eqn. 3.2)}$$

where, N_{fe}, N_{fp}, N_{fc} are cycles to failure for corresponding elastic, plastic and creep damaged and N_{th} is total cycles to failure under thermal cycling loading.

3.1.2 Mean Stress History Calculation

Another key output from FEA thermal simulation is mean stress history. It has been experimentally observed and verified that if cyclic loading is not completely reversed, then the mean stresses can affect the fatigue life [Dowling, 1993]. A tensile mean stress decreases the fatigue life while a compressive mean stresses can enhance the fatigue life. Figure 11 shows the mean stress history in one thermal cycle. It illustrates that the mean stress during the hot dwell was compressive in nature and during the cold dwell was tensile in nature. This mean stress history was used for damage calculation in vibration simulation and discussed as following.

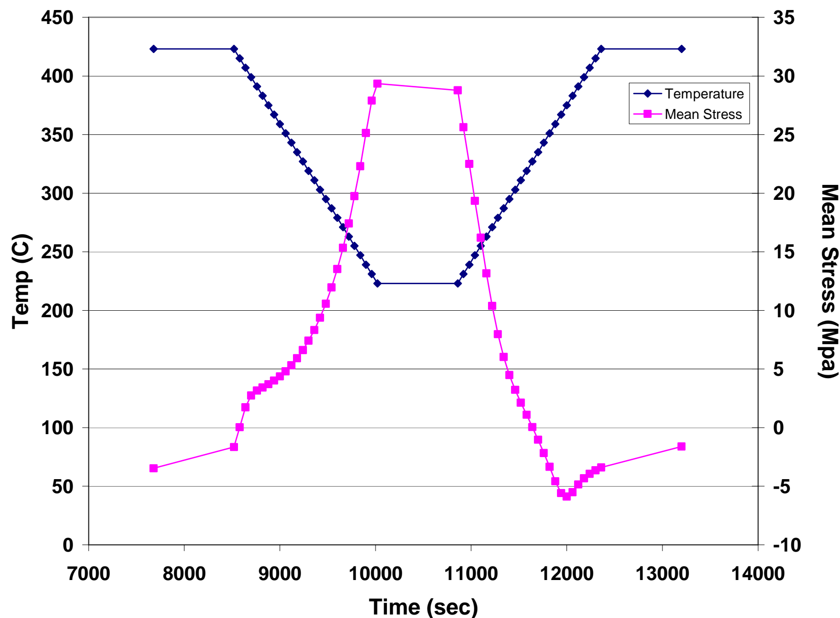

Figure 3.4 Mean stress history from the thermomechanical analysis of PBGA272

3.2 Vibration Loading Simulation

Vibration loading simulation also involves two parts: solder joint strain calculation and damage calculation due to vibration loading. The first part is done using FEA and the second part is done using a strain range approach. Details are described as following.

3.2.1 Solder Joint Strain Calculation

The PCB strain information under different temperature levels were already obtained from the experimental measurement and described in Chapter 2. The main purpose of this experiment measurement is to get solder joint strain information for damage calculation later. Therefore it is necessary to build a relationship between the PCB strain information and solder joint strain information. To different from the original IDSA [Upadhyayula, 1999], the relationship was built in this study through running FEA models under static bending loadings at three temperature levels (150 °C, 25 °C, and -50 °C). The advantage of this method is to fully reuse the models built for thermal cycling simulation and quickly obtain accurate results. Figure 3.5 shows the deform shape when bending loading was applied on the edge of PCB. The PCB strain was averaged along the bottom layer elements based on the strain gage size. The solder joint strain was averaged along the 2% elements around the maximum strain element. The relationships between PCB strain and solder joint strain at different temperature levels were built using power law relationship and shown in Figure 3.6. Using these response curves, the solder joint strain range RDFs at different

temperatures were then obtained from the PCB strain histories. These information are used for damage analysis in next section.

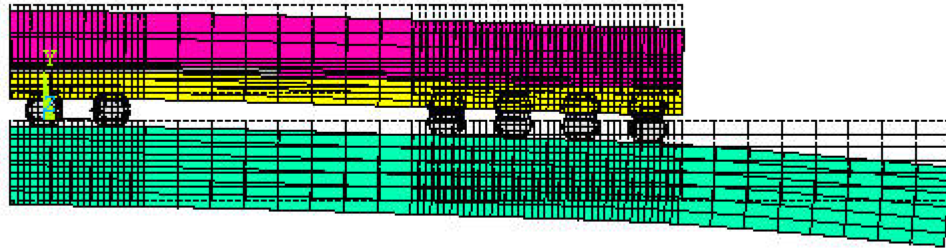

Figure 3.5 Deformed shape of PBGA assembly under bending loading

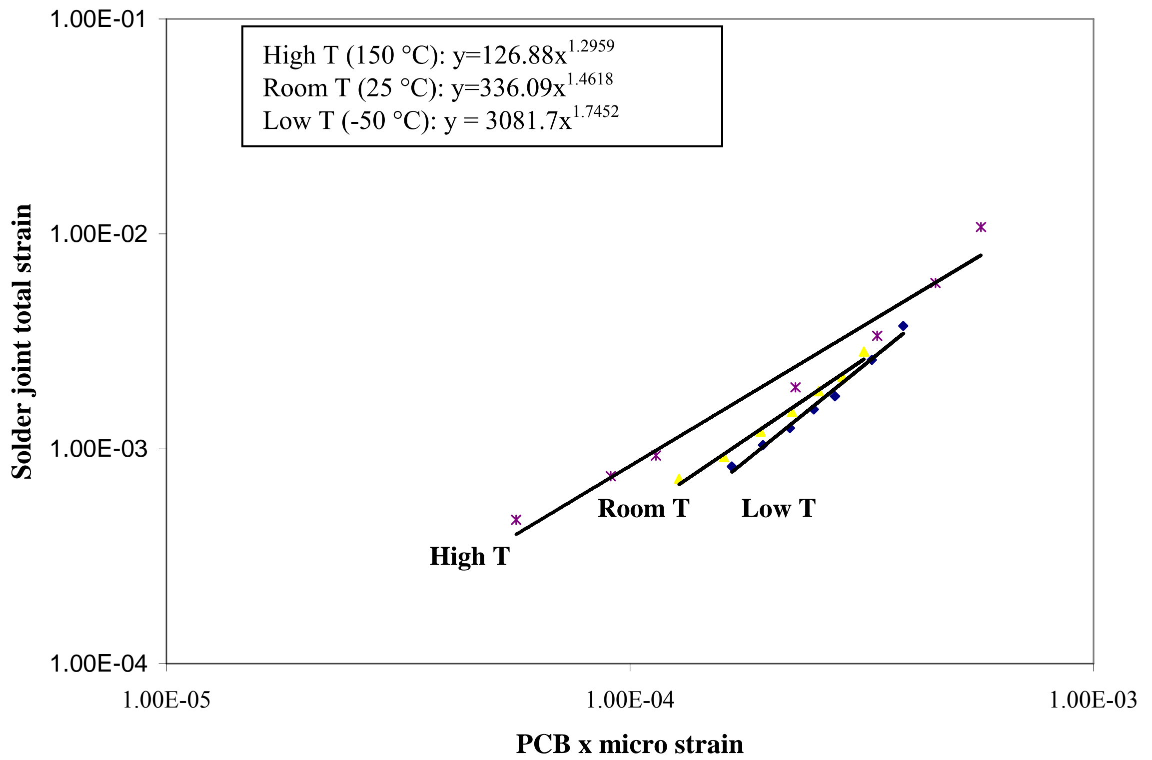

Figure 3.6 Temperature dependent PCB strain-solder joint strain response curves for PBGA272

3.2.2 Solder Joint Damage Calculation Due to Vibration Loading

In Chapter 1, a generalized strain range approach with considering of the mean stress in the elastic term [Morrow, 1965] was described for solder joint life predictions:

$$\frac{\Delta\varepsilon}{2} = \frac{\Delta\varepsilon_e}{2} + \frac{\Delta\varepsilon_p}{2} = \frac{(\sigma_f - \sigma_o)}{E}\left(2N_f\right)^b + \varepsilon_f\left(2N_f\right)^c \qquad \text{(Eqn. 3.3)}$$

where

$\Delta\varepsilon$ = the total strain range,

$\Delta\varepsilon_e$ = the elastic strain range,

$\Delta\varepsilon_p$ = the plastic strain range,

E = the modulus of elasticity,

σ_f = stress strength coefficient,

σ_o = mean stress,

b = the fatigue strength exponent,

c = the fatigue ductility exponent,

ε_f = the fatigue ductility coefficient.

Considering the temperature effect on the strain range, mean stress and coefficients, Equation 3.3 can be modified to Equation 3.4:

$$\frac{\Delta\varepsilon(T)}{2} = \frac{(\sigma_{f(T)} - \sigma_{o(T)})}{E(T)}\left(2N_f\right)^b + \varepsilon_{f(T)}\left(2N_f\right)^c \qquad \text{(Eqn. 3.4)}$$

The strain range in Equation 3.4 was obtained from the strain RDF described in previous Section 3.2.1. The mean stress history was obtained from thermal cycling

simulation 3.1.2. In the original IDSA approach, the damage constants—fatigue coefficient and ductility coefficient are temperature independent. Upadhyayula [1999] suggested considering these damage constants are temperature dependent in future work and gave the constants values. In this study, this suggestion is taken and constants at different temperature levels are used in Equation 3.4 as listed in Table 3.6. Since there are no vibration test results under extreme temperature levels, the constant values are not validated for this study. The variation between simulation and test results are expected.

Table 3.6 Temperature dependent damage constants [Upadhyayula, 1999]

Damage constants	Low T	Room T	High T
Fatigue coefficient σ_f	215 MPa	155 MPa	45 MPa
Ductility coefficient ε_f	0.4	0.62	1.3

By numerically solving Equation 3.4, the life response to each strain range at different temperature levels can be obtained. The damage accumulated in the solder joint was then computed by incrementally adding the damage due to vibration loads (with mean stresses included) at each discrete temperature level:

$$D_v = \sum_j \left(\sum_i \left(\frac{n_i}{N_i} \right)_{T_j} \right) t_j = \frac{1}{N_v} \qquad \text{(Eqn. 3.5)}$$

where

n_i = number of occurrences from strain RDF,

T_j = discretized temperature levels,

t_j = fraction of total time spend at the discretized temperature level,

N_i = life predictions from generalized strain life model for each increment (in presence of mean stresses),

D_v = accumulated vibration induced damage,

N_v = accumulated solder joint fatigue life under vibrational loading.

Equation 3.5 gives the solder joint damage caused by vibration loading with effect of thermal cycling along one thermal cycle. This damage is then superposed with the damage due to thermal cycling and discussed in next section.

3.3 Total Damage Superposition

The overall damage per thermal cycle was calculated by superposing the damage due to temperature cycling loading and the damage due to vibration loading:

$$D_{total} = D_{th} + D_{v} \qquad \text{(Eqn. 3.6)}$$

where

D_{th} = damage caused by temperature cycling (from Eqn. 3.2)

D_{v} = damage caused by vibration loading (from Eqn. 3.5)

and the fatigue life was the reverse of the total damage :

$$N_f = \frac{1}{D_{total}} \qquad \text{(Eqn. 3.7)}$$

3.4 Comparison of Simulation and Test Results

In this section, the simulation results are compared with test results under combined temperature cycling and vibration loading conditions. Solder joint fatigue life was normalized based on the life under random vibration loading at room temperature. Figure 3.10 shows the solder joint life under thermal cycling loading is close to the life under vibration loading at room temperature. While two different loadings combined together, the solder joint life dramatically decreases to approximately 7%

of the life under pure vibration loading condition. The experimental results show the strong dependence of load combinations on solder joint durability.

The first simulation effort is to apply linear superposition damage approach (LDSA) to estimate the solder joint life under combined loading condition. As described in Chapter 1, by solving Equation 1.9 and 1.0, the solder joint life can be obtained. For this case, the vibration natural frequency, f_v, is 270 Hz, and thermal cycling frequency, f_{th}, is calculated as the reciprocal of total cycle time (78 minutes). The life under thermal cycling is 2467 cycles and 2922 hours for vibration loading. To calculate one thermal cycle damage and converted to total life expected, Figure 3.10 shows there is about 7 times difference between LDSA prediction and experimental results. Therefore in applications where load interactions are significant, damage superposition approaches that add damages due to individual loads in a linear fashion are not suitable and more detailed damage superposition schemes are required to systematically account for non-linear load interactions.

The second simulation effort is to apply the incremental damage superposition approach (IDSA) on this PBGA solder joint life prediction. As described in 3.1 and 3.2, through thermal cycling simulation, vibration simulation and damage superposition, Figure 3.10 shows the IDSA prediction within two times range of experimental results, which is generally acceptable for simulation accuracy. This simulation result proves this modified IDSA approach reflects the damage trend by considering the temperature effects on vibration and the interactions between combined loads.

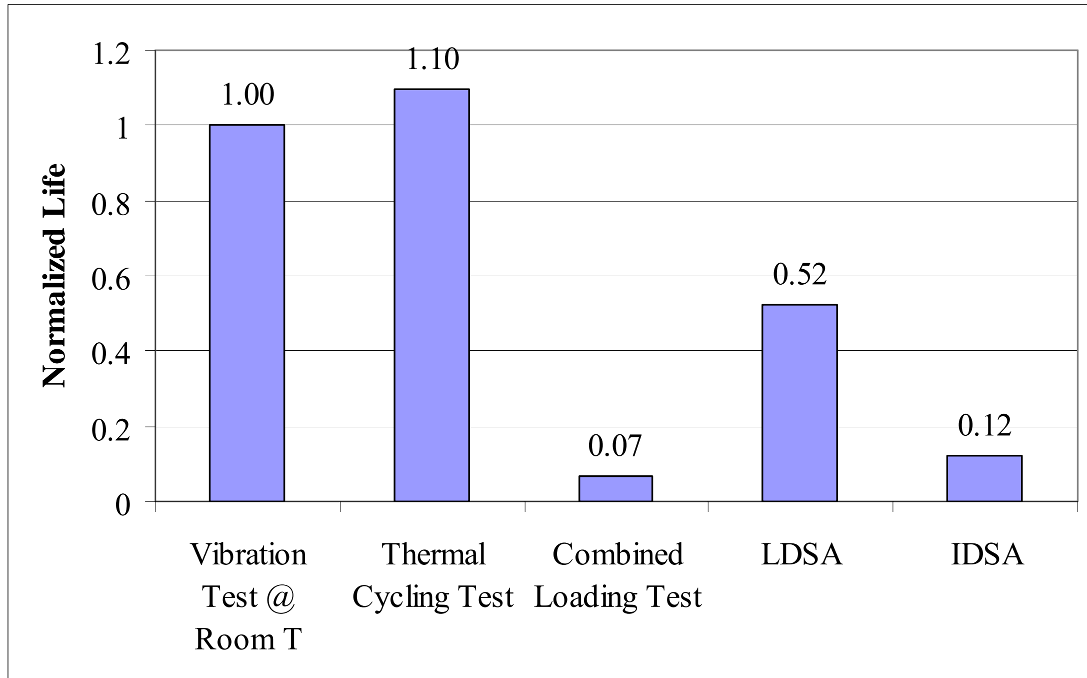

Figure 3.10 Comparison of the IDSA damage prediction for PBGA272 with the LDSA prediction and experimental results

3.5 Summary

A more detailed damage superposition scheme that systematically accounts for non-linear load interactions was applied to simulate solder joint fatigue life. The interactions that have been systematically captured in this modified IDSA include: changes of vibration response under random vibration loading at different temperatures, temperature dependent PCB strain-solder joint strain response curves due to changes in constitutive properties of solder, effects of thermomechanical mean stresses on vibration induced fatigue, and incremental damage accumulation instead of linearly superposing independent damages due to vibration and thermal loads. The simulation results showed the trend fits experimental results well. It indicates this incremental damage superposition approach can catch the possible interaction between two loads.

Chapter 4: Rapid Life Prediction Approach

Chapter 3 already demonstrated the modified IDSA applicability on PBGA solder joint durability assessment under combined environmental loading conditions. However, this approach is based on detailed finite element analysis and experimental strain measurement, which is costly and time consuming. Based on this incremental damage superposition concept, a rapid solder joint fatigue life prediction simulation approach for PBGA was also developed for combined temperature cycling and vibration loading conditions.

This approach includes a thermomechanical stress model and a vibration stress model to analyze the interconnect stress under thermal cycling and vibration loading conditions. The mean stress during thermal cycling was obtained from pre-built predictive models. The damage due to two different loadings was then calculated using the generalized strain approach and superposed. The flow chart is shown in Figure 4.1 and details for each part are described in the following sections.

Compared to the detail FEA approach, the major advantage of this approach is quick reliability assessment within acceptable accuracy. Therefore, it can be used as a rapid tool for qualification and accelerated testing design and approximate life prediction.

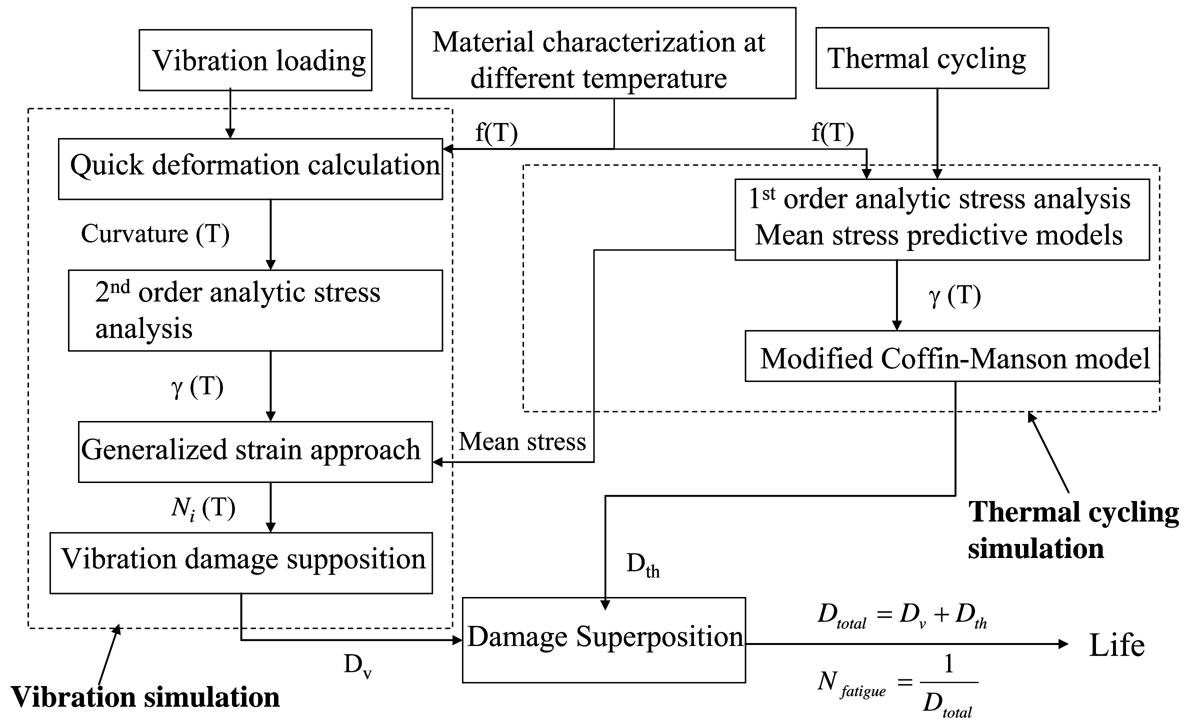

Figure 4.1 The flowchart of rapid life prediction approach (RLPA)

4.1 Temperature Cycling Simulation

Temperature cycling simulation involves three parts: interconnect stress/strain analysis, interconnect damage analysis, and mean stress response curve generation. The backbone of this work is the similar as previous discussion 3.1 but with the purpose to replace the detail finite element analysis with some rapid models and methods.

4.1.1 Interconnect Stress/Strain Analysis

To analyze the solder joint damage, the interconnect stress should be analyzed first. The stress analysis model chosen in this study is a 1st order Analytic Stress Analysis Model [Engelmaier, 1991; CALCE, 2004]. This model assumes the cyclic strain is caused by the differences in expansion between the PBGA and the PCB. The solder joint is approximately considered as a simple pillar of solder that is subjected to in plane shear stresses. The thermally induced cyclic strain was calculated by considering only in-plane deformations due to a very stiff component and PCB acting on a simple column of solder. Creep fatigue was assumed as dominates damage mechanism, and local CTE mismatch was ignored. Equation 4.1 gives the strain calculation formula

$$\Delta\gamma_p = F\frac{L_D}{h}\Delta\alpha\Delta T_e \qquad \text{(Eqn. 4.1)}$$

where

$\Delta\gamma$ is solder strain range,

h is nominal height of solder joint,

$\Delta\alpha\Delta T_e = \alpha_c\Delta T_c - \alpha_s\Delta T_s$ = equivalent, cyclic, in-plane thermal expansion mismatch,

α_c, α_s are coefficients of linear thermal expansion for component and PCB, respectively,

ΔT_c, ΔT_s are cyclic temperature swing of component and substrate (beneath component), respectively,

F is empirical correction factor to account for idealized assumptions, (F varies from 0.5 to 1.5, typical values are around 1.0 and are determined by fitting fatigue life results to predicted life)

L_D is component length, = 0.707 * interconnect span length for the outer corner

In this study, the input parameter value for this model is listed in Table 4.1.

Table 4.1 The input parameters for 1st order stress analysis model

Parameter	Value
L_D	19.1 mm
h	0.45 mm
$\Delta\alpha$	2.7 ppm/°C
ΔT	200 °C
F	1.0

4.1.2 Interconnect Damage Analysis

After the stress/strain analysis, interconnect damage analysis is performed. The starting point of the methodology is the well known Coffin-Manson plastic strain fatigue life relationship.

$$N_{f,th} = \frac{1}{2}\left(\frac{\Delta\gamma_p}{2\varepsilon_f}\right)^{\frac{1}{c}} \qquad \text{(Eqn. 4.2)}$$

In the above equation, it is difficult to determine the time and temperature dependent plastic shear strain range, $\Delta\gamma_p$. A modified Coffin-Manson equation (Engelmaier, 1991; CALCE, 2004] was developed to use the maximum available displacement shear and accounting for the incomplete degree of stress relaxation/creep with a time and temperature dependent exponent. The modified Coffin-Manson strain fatigue life relationship is then

$$N_{f,th} = \frac{1}{2}\left(\frac{\Delta\gamma}{2\varepsilon_f}\right)^{\frac{1}{c}} \qquad \text{(Eqn. 4.3)}$$

where

N_f = median cycles to component failure (number of cycles to 50% of component population failure)

$\Delta\gamma$ = solder cyclic shear strain range

$2\varepsilon_f$ = fatigue ductility coefficient

c = fatigue ductility exponent

Using isothermal experimental data developed by R. Wild [1973], the approximate values for the fatigue ductility constants for eutectic solder were determined to

$2\varepsilon_f = 0.65$ for near eutectic solders

$c = -0.442-(6 \times 10^{-4})T_{SJ}+1.74 \times 10^{-2} \ln(1+360/t_d)$ for near eutectic solders

where

$T_{SJ} = 0.25(T_c+T_s+2T_o)$ = mean cyclic solder joint temperature

T_s, T_c = steady state operating temperature for substrate and component

T_o = temperature during off half-cycle

t_d = half-cycle dwell time at high temperature

The key assumptions in this model include:

1) Failure obeys a power law relation;
2) Fatigue exponent was evaluated from Wild's early solder data;
3) $\Delta\gamma$ is the total average strain range and not the average plastic strain range;
4) $\Delta\gamma$ as calculated in the 1st order stress analysis model (not valid for more sophisticated stress or strain analysis results).

This model has been validated on BGA through extensive test results from literatures [CALCE, 2002]. Out of the 58 comparisons only 5 were outside of the 2x band. For these five (5) the software estimate was conservative as Figure 4.2 shows.

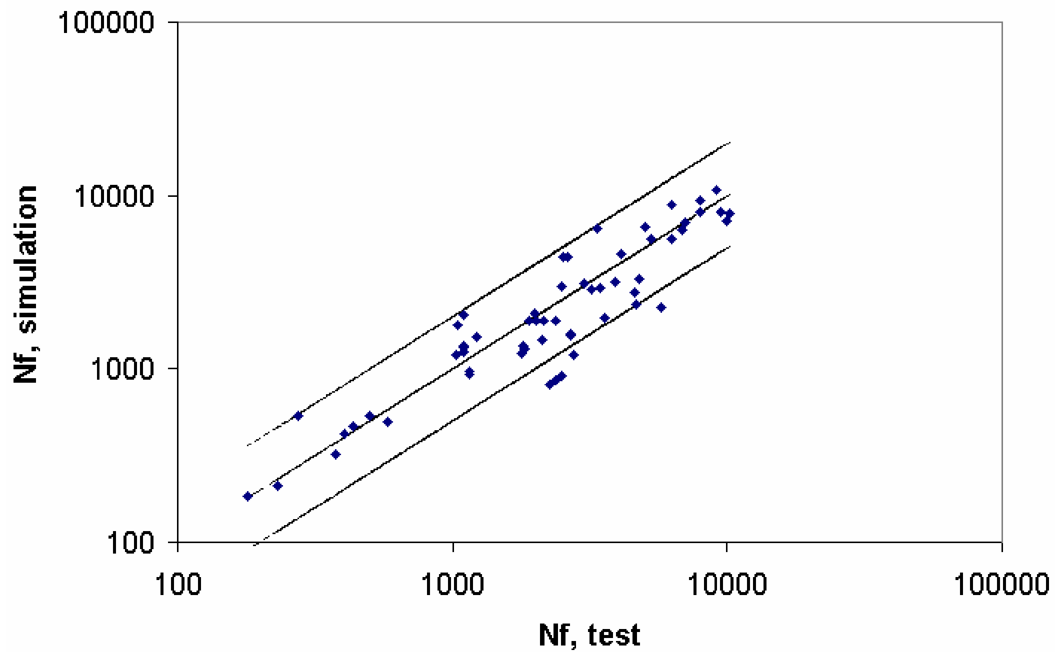

Figure 4.2 Validation of 1st order thermal fatigue model for BGA

Then the damage due to thermal cycling load can be calculated using Equation 4.4

$$D_{th} = \frac{1}{N_{f,th}} \qquad \text{(Eqn. 4.4)}$$

This damage caused by temperature cycling will be superposed with the damage caused by vibration loading later.

4.1.3 Means Stress Predictive Models

As described in Chapter 3, mean stress history under thermal cycling loading can be determined by creating a finite element model. However, it requires user to master the FEA techniques and spend time and cost to finish this modeling work. Therefore, there is a need to a method that does not require the user to perform a detailed finite element analysis and that can be used quick what-if design analysis. In this study, the effects of factors such as ball pitch (A), solder joint height (B), temperature range (C)

and CTE mismatch (D) on mean stress history were studied. These four factors are chosen since they are also reflected in 1st order stress analysis model. The ball pitch does not explicitly show up in 1st order stress analysis model, but it relates to component length. For example with smaller pitch, the component length will decrease with the same number of balls. Thus, the final predictive equation will be of the form:

$$Mean_Stress = f(A, B, C, D) \quad \text{(Eqn. 4.5)}$$

4.1.3.1 Design of Simulation (DOS)

As shown in Table 4.1, a full 2-level, 4 factor design of simulation (DOS) were performed. As seen, ball pitch (A) was varied from 1 to 1.27 mm, solder joint height (B) was varied from 0.45 to 0.55 mm, temperature range (C) was varied from 105 °C to 200 °C, and CTE mismatch (D) was varied from 1.4 ppm/°C to 2.7 ppm/°C.

Table 4.1 2-level 4-factor DOS

Run	A (mm)	B (mm)	C (°C)	D (ppm/°C)	Mean Stress (MPa) @ -55 °C	Mean Stress (MPa) @ 25 °C	Mean Stress (MPa) @ 150 °C
1	1.27	0.45	105	1.8	20.2	4.6	-2.21
2	1.27	0.45	105	2.7	19.99	4.5	-2.2
3	1.27	0.45	200	1.8	29.03	3.3	-1.62

4	1.27	0.45	200	2.7	28.77	4	-1.62
5	1.27	0.55	105	1.8	23.42	6.96	-2.55
6	1.27	0.55	105	2.7	23.36	6.73	-2.55
7	1.27	0.55	200	1.8	33.72	6.4	-1.8
8	1.27	0.55	200	2.7	33.87	6.5	-1.8
9	1	0.45	105	1.8	20.45	6.36	-2.21
10	1	0.45	105	2.7	20.52	6.25	-2.22
11	1	0.45	200	1.8	28.84	5.6	-1.66
12	1	0.45	200	2.7	28.9	5.6	-1.66
13	1	0.55	105	1.8	22.32	7.78	-2.53
14	1	0.55	105	2.7	22.55	7.8	-2.54
15	1	0.55	200	1.8	32.16	7.5	-1.85
16	1	0.55	200	2.7	32.31	7.5	-1.84

For each case, a finite element simulation was performed. As described in Chapter 3, mean stresses at three different temperature levels are the keys for damage calculation. Therefore three response mean stress at three different temperatures are listed in Table 4.1.

4.1.3.2 Main Effects and Interaction Analysis

Main effects and interaction analysis will help determine the predictors and the combination of predictors that have a significant effect on the response. Mean stress will be the response and the predictors are the A, B, C, and D. Minitab® version 14 was used for all analysis. First of all, mean stress at low temperature was chosen for analysis.

Figure 4.3 shows a normal probability plot of the effects of a confidential interval of 95%. The most influential predictors are found to be in the order of importance: C, B, BC, AB, A, and AC.

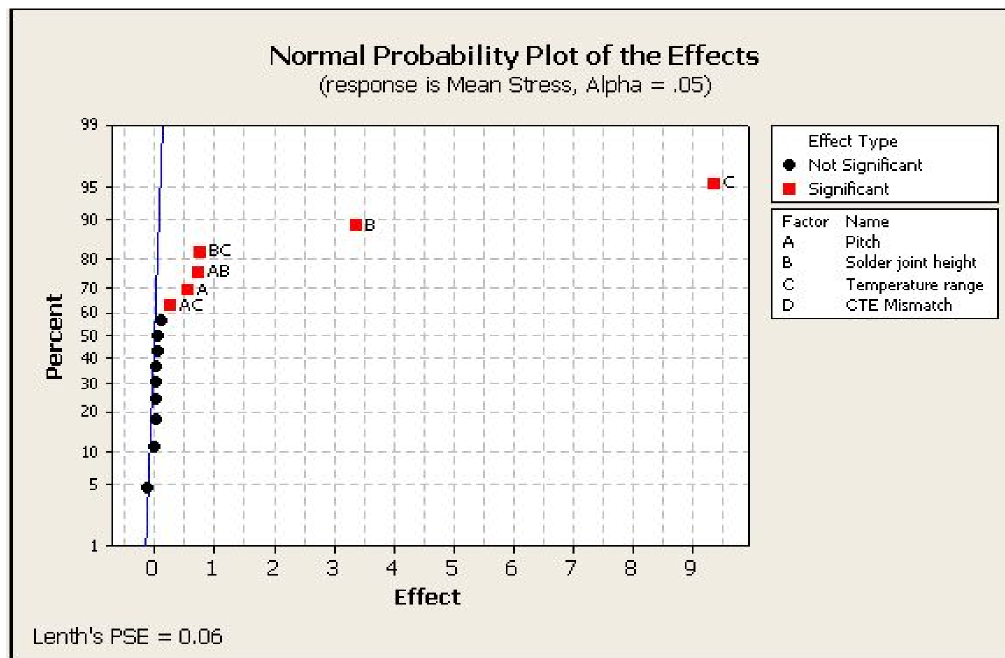

Figure 4.3 Normal probability plot of the effects

It is observed that predictor D, the CTE mismatch, is not considered a significant factor. This can be seen by looking at the main effects plot shown in Figure 4.4 and the interaction effects plot shown in Figure 4.5. Figure 4.5 shows the interaction

terms BC, AB and AC to be most significant as shown by the nonparallel lines in the interaction plot matrix. One possible reason for CTE mismatch insignificancy is the variation is too small. The values were chosen in this study is from the CTE experimental measurement between PBGA and two different types FR4 boards. These two types FR4 boards were chosen is because their CTE are different but with similar modulus. CTE mismatch may be a significant factor if it varies in a large range, such as ceramic and PCB. However, the modulus should be also considered as a factor then. This part work is discussed as suggestion on future work in Chapter 5 and beyond this study scope.

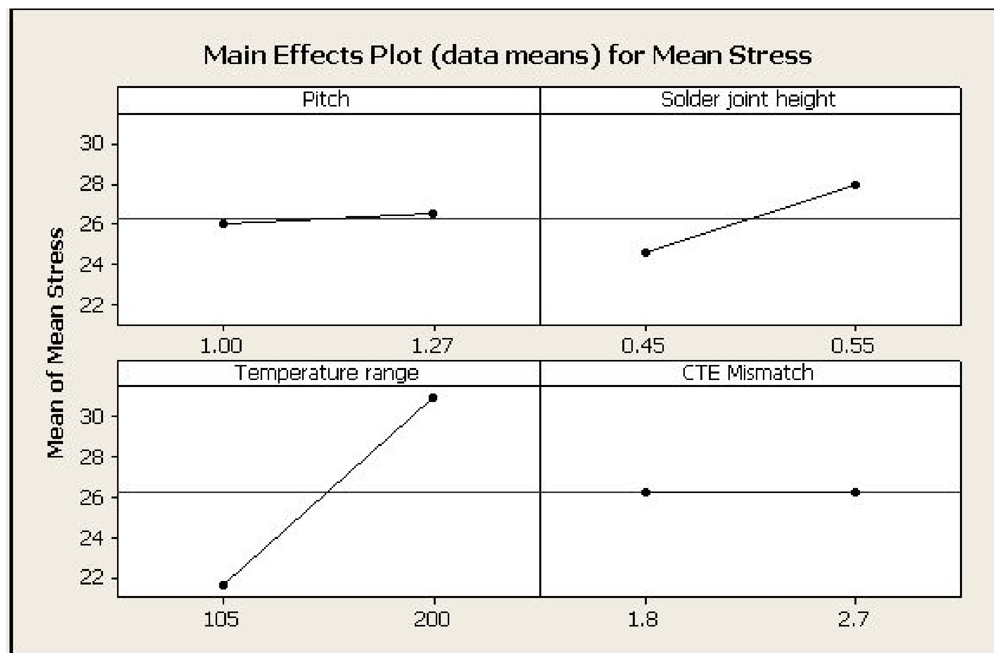

Figure 4.4 Main effects

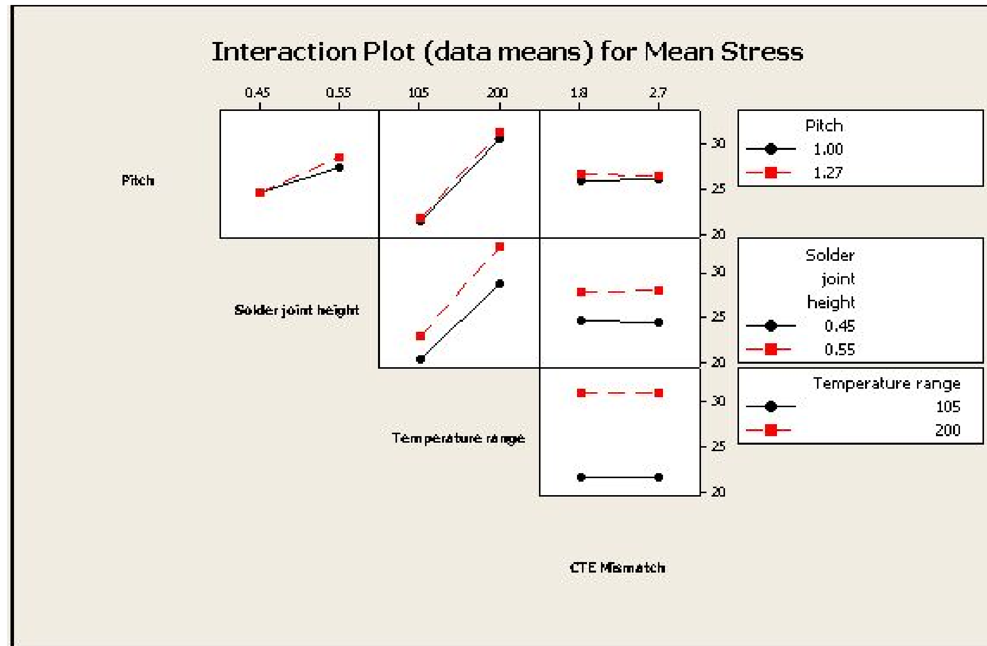

Figure 4.5 Interaction effects

4.1.3.3 Linear Regression Analysis

The next step is to perform regression analysis based on A, B, C, AB, AC, and BC. The stepwise regression was chosen using both forward method and backward method to check the consistence. Alpha was chosen 0.05 for 95% confidence level. The results are shown in Figure 4.6 and Figure 4.7. Both of Figures indicate the solder joint height (B), temperature range (C) and ball pitch*temperature range (AC) are the significant ones. Therefore another two interaction term, AB and BC, will neglected in the final regression model. On the other hand, since ball pitch (A) and CTE mismatch (D) have real physical means and the final model should include these two items.

Stepwise Regression: Mean Stress versus Pitch, Solder joint height, ...

```
Forward selection.  Alpha-to-Enter: 0.05


Response is Mean Stress on 6 predictors, with N = 16


Step                      1       2        3
Constant             11.268  -5.613   -5.773

Temperature range    0.0984  0.0984   0.0974
T-Value                9.75   27.80    32.75
P-Value               0.000   0.000    0.000

Solder joint height            33.8     36.7
T-Value                       10.04    12.13
P-Value                       0.000    0.000

AC                                   -0.0068
T-Value                                -2.59
P-Value                                0.024

S                      1.92   0.673    0.561
R-Sq                  87.16   98.53    99.06
R-Sq(adj)             86.25   98.31    98.82
Mallows C-p           111.5     4.1      1.1
```

Figure 4.6 Forward stepwise regression analysis

Stepwise Regression: Mean Stress versus Pitch, Solder joint height, ...

```
Backward elimination.  Alpha-to-Remove: 0.05


Response is Mean Stress on 6 predictors, with N = 16


Step                       1        2        3        4
Constant              -5.649   -5.826   -5.763   -5.773

Pitch                   -0.2
T-Value                -0.07
P-Value                0.946

Solder joint height     36.7     36.6     36.7     36.7
T-Value                 9.01    10.57    11.60    12.13
P-Value                0.000    0.000    0.000    0.000

Temperature range     0.0977   0.0977   0.0977   0.0974
T-Value                26.72    28.18    29.85    32.75
P-Value                0.000    0.000    0.000    0.000

AC                   -0.0057  -0.0057  -0.0056  -0.0068
T-Value                -0.89    -0.94    -0.98    -2.59
P-Value                0.398    0.370    0.349    0.024

AB                       0.2      0.2
T-Value                 0.08     0.10
P-Value                0.935    0.919

BC                    -0.004   -0.003   -0.003
T-Value                -0.20    -0.21    -0.23
P-Value                0.843    0.836    0.825

S                      0.646    0.613    0.584    0.561
R-Sq                   99.06    99.06    99.06    99.06
R-Sq(adj)              98.44    98.60    98.72    98.82
Mallows C-p              7.0      5.0      3.0      1.1
```

Figure 4.7 Backward stepwise regression analysis

The results of a regression analysis based on A, B, C, D, and AC is shown in Figure 4.8. As seen, this model includes all predictor terms and the interaction effect of ball pitch and temperature range. This model is adequate based on the R-Sq(adj) of 98.6% and the standard deviation, $\sigma = 0.61$ MPa. Many other models are possible, however this model fits the criteria and is of the simple form, as shown in Equation 4.6.

$$Mean_Stress_{lowT} = -5.62 + 0.03A + 36.7B + 0.0974C - 0.085D - 0.00684AC$$

(Eqn. 4.6)

```
Regression Analysis: Mean Stress versus Pitch, Solder joint height, ...

The regression equation is
Mean Stress = - 5.62 + 0.03 A + 36.7 B + 0.0974 C - 0.085 D - 0.00684 AC


Predictor                 Coef   SE Coef      T      P
Constant                -5.616     2.627  -2.14  0.058
Pitch                    0.029     1.668   0.02  0.987
Solder joint height     36.748     3.581  10.26  0.000
Temperature range     0.097436  0.003279  29.71  0.000
CTE Mismatch           -0.0845    0.3462  -0.24  0.812
AC                   -0.006838  0.004253  -1.61  0.139


S = 0.612410   R-Sq = 99.1%   R-Sq(adj) = 98.6%


Analysis of Variance

Source          DF       SS      MS       F      P
Regression       5  397.324  79.465  211.88  0.000
Residual Error  10    3.750   0.375
Total           15  401.075
```

Figure 4.8 Regression analysis on A, B, C, D, and AC

For the high temperature and room temperature, the same effect and regression analysis were performed using Minitab® 14. Figure 4.9–4.11 show the effects analysis for high temperature means stress. The most influential predictors are found to be in the order of importance: C, B, BC, AB, and A, which are similar as the trend for low temperature. Through regression analysis, it was found no interaction term is significant and CTE mismatch, D, is excluded since insignificancy. The predictive model is given in Equation 4.7.

$$Mean_Stress_{highT} = -1.89 + 0.0741A - 2.57B + 0.00679C \quad \text{(Eqn. 4.7)}$$

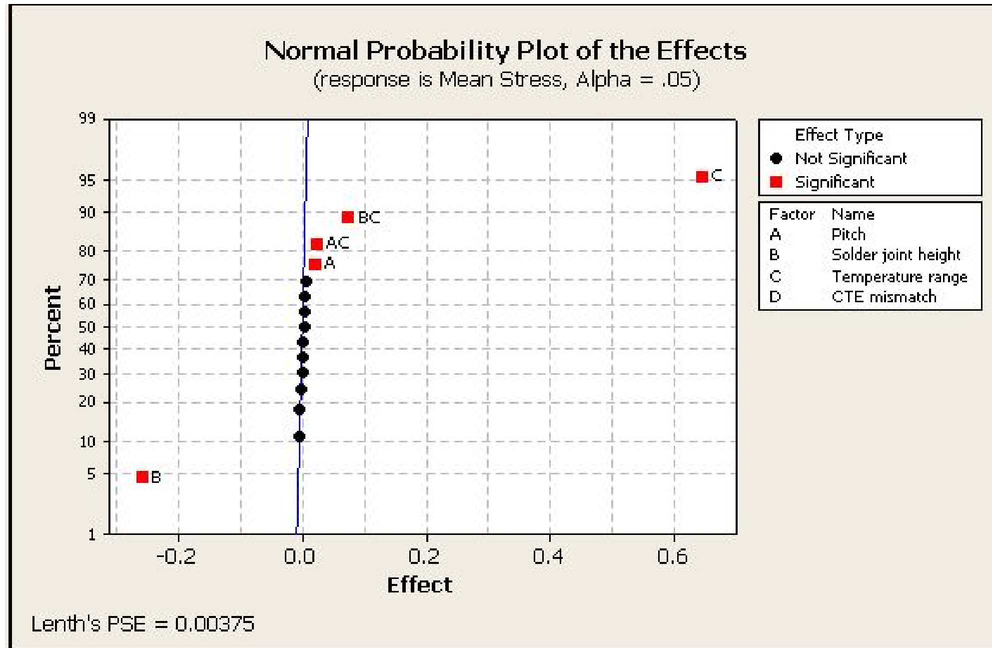

Figure 4.9 Normal probability plot of the effects on means stress at high temperature

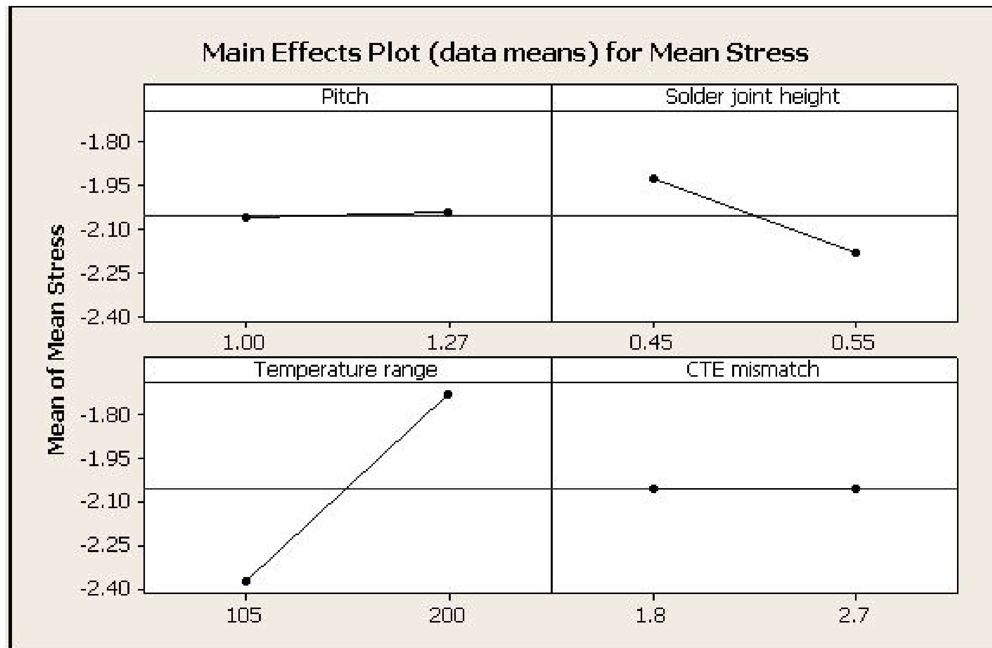

Figure 4.10 Main effects on mean stress at high temperature

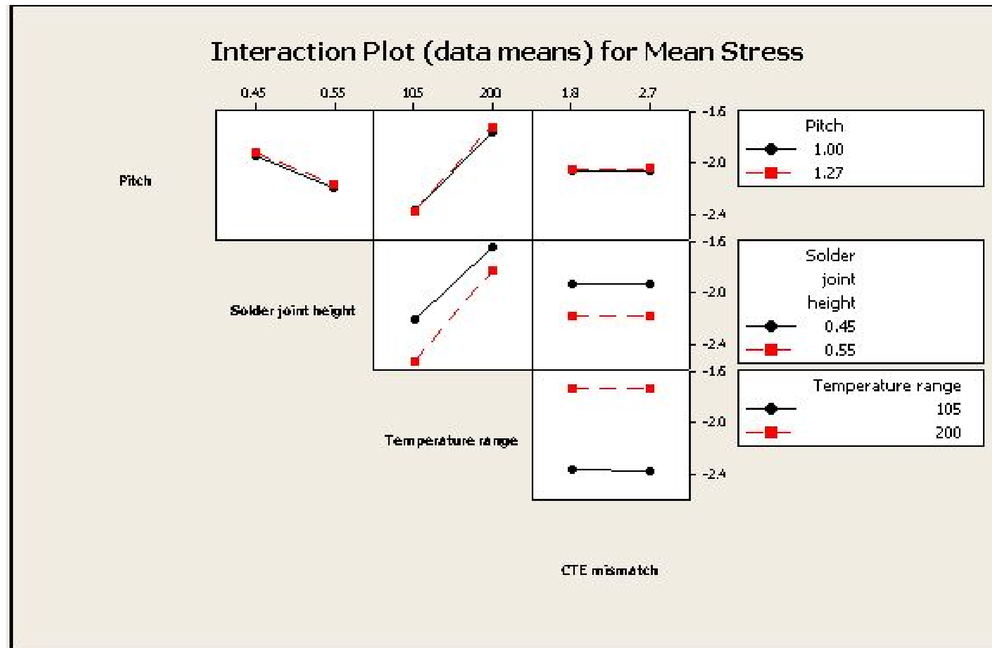

Figure 4.11 Interaction effects on means stress at high temperature

For room temperature, the most influential predictors are found to be in the order of importance: B, A, C and AB. Through regression analysis, it was observed the interaction term AB is not significant. Figure 4.12–14 for effects analysis on room temperature mean stress. Therefore, the final predictive model in terms of A, B, C, and D is given in Equation 4.8.

$$Mean_Stress_{roomT} = 2.28 - 5.28A + 21.2B - 0.00603C + 0.053D \quad \text{(Eqn. 4.8)}$$

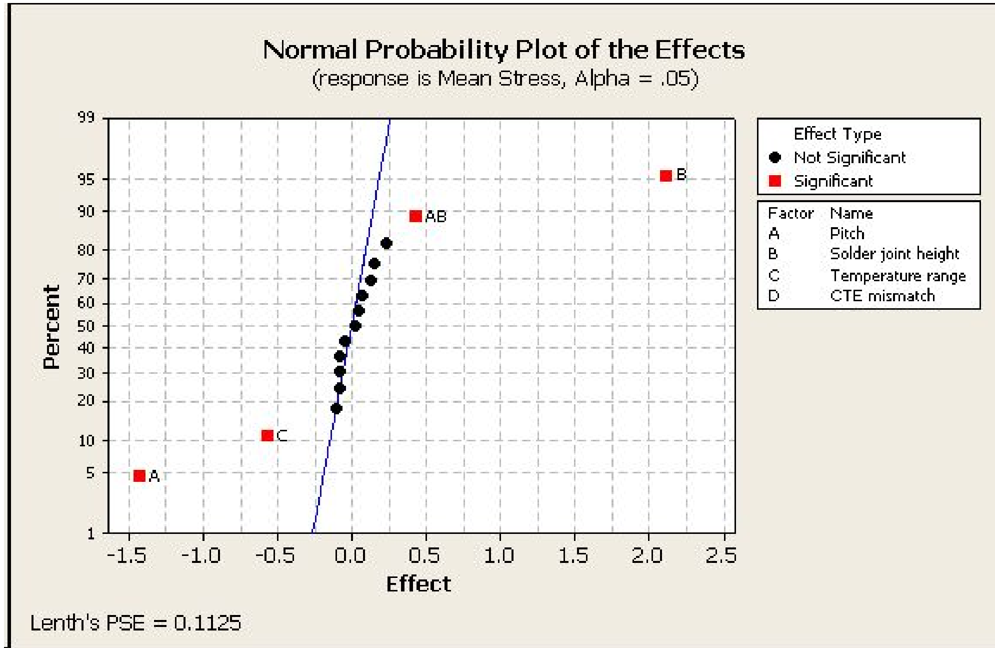

Figure 4.12 Normal probability plot of the effects on means stress at room temperature

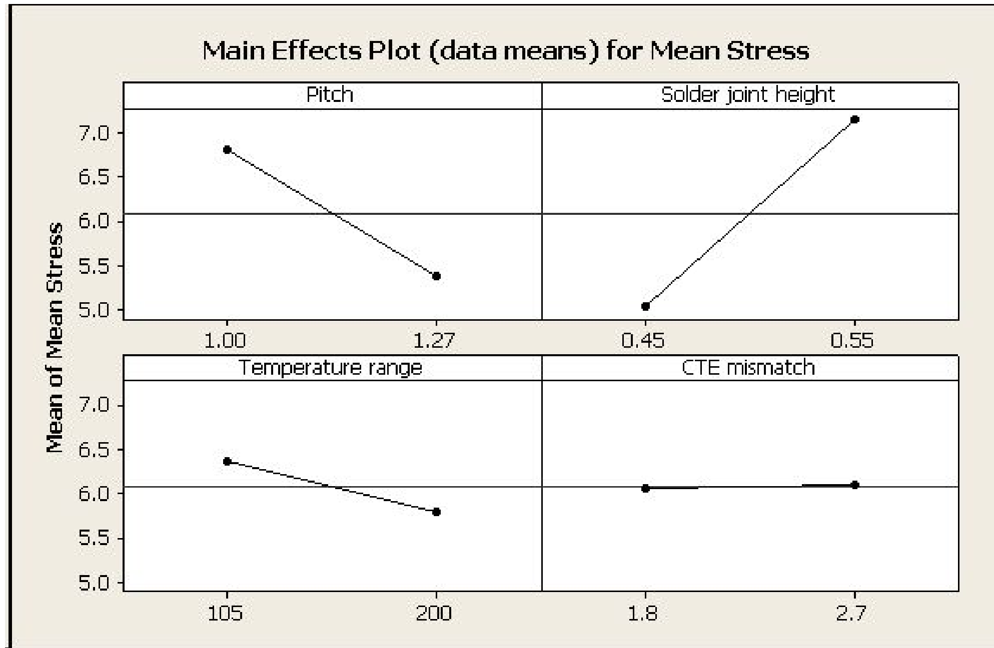

Figure 4.13 Main effect on mean stress at room temperature

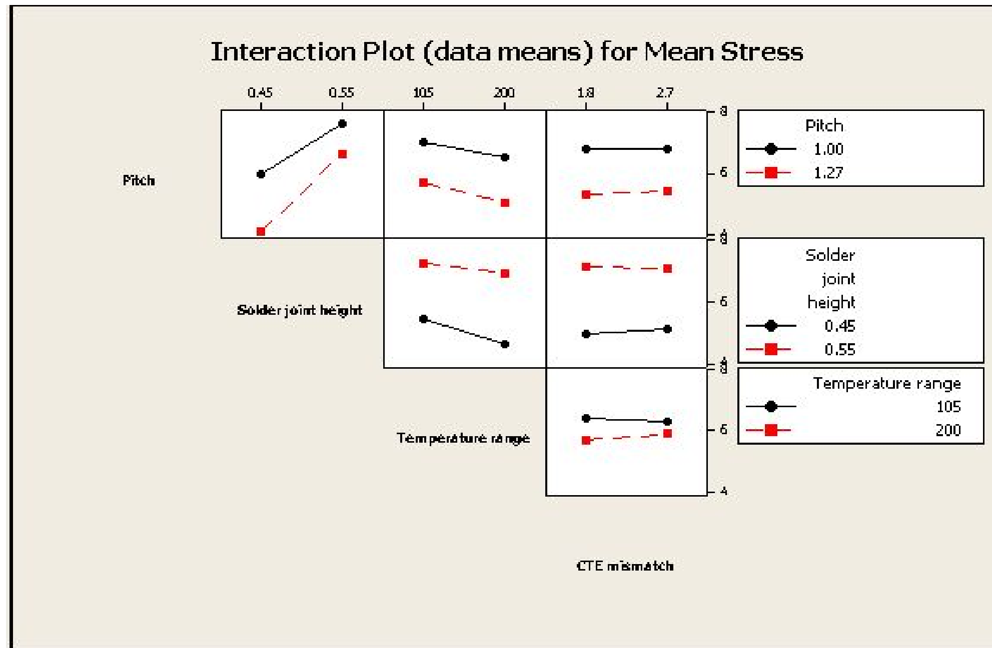

Figure 4.14 Interaction plot on effects on mean stress at room temperature

For this study, the mean stresses at three different temperature levels (-50 °C, 25 °C, and 150 °C) can be solved using Equation 4.6-4.8 as 28.90 MPa, 4.05 MPa, and -1.59 MPa. These information will be used for vibration damage analysis and discussed later.

4.2 Vibration Simulation

Vibration simulation involves three steps: deformation calculation, interconnect stress/strain analysis and interconnect damage analysis. In this part, instead of using experimental strain measurement, interconnect stress/strain are calculated using curvature information and bending moment. The generalized strain approach is applied for damage assessment. Finally the damage is incrementally superposed for the discretized temperature levels.

4.2.1 PCB Deformation Calculation

Experimental measurement is an accurate way to obtain PCB deformation. However, it is costly to setup the measurement and time consuming to post process the data. It is necessary to find a way to quickly estimate PCB and interconnect deformation. In this study, PCB deformation under random vibration loading was quickly assessed using a commercial software calcePWA®. The assessment process is described as following.

First, the whole assembly including PBGAs and PCB was modeled with correct boundary conditions, as Figure 4.15 shows. The geometry and material properties are described in Chapter 3. Then the assembly was automatically meshed to generate a FEA model, which is shown in Figure 4.16. Figure 4.17 gives random vibration loading as PSD plot. The frequency range is 100-1000Hz and PSD level is 0.10 G^2/Hz. Using the software built-in FEA analysis function, the assembly vibration mode, natural frequency, and curvature information can be quickly obtained. Figure 4.18–4.20 shows the first three modes and responded natural frequency.

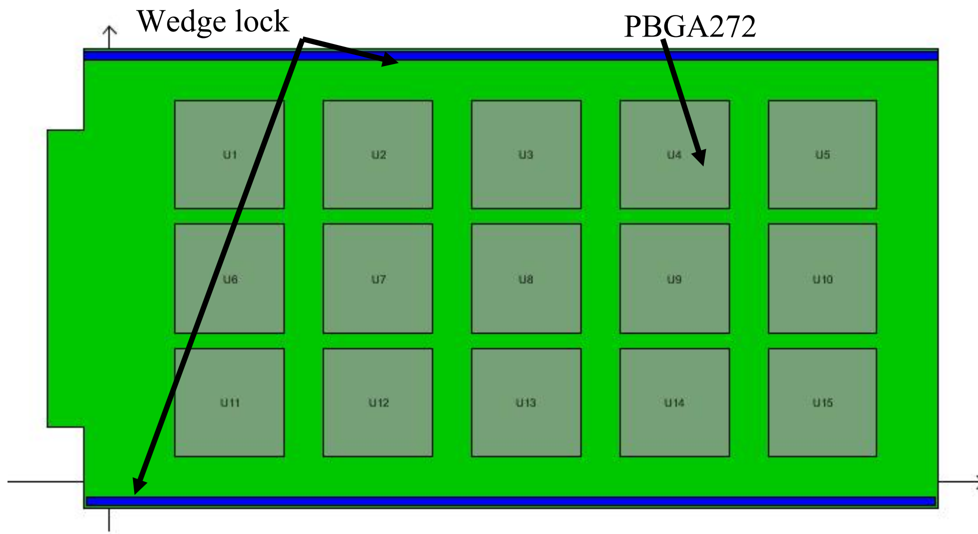

Figure 4.15 PBGA assembly model in calcePWA®

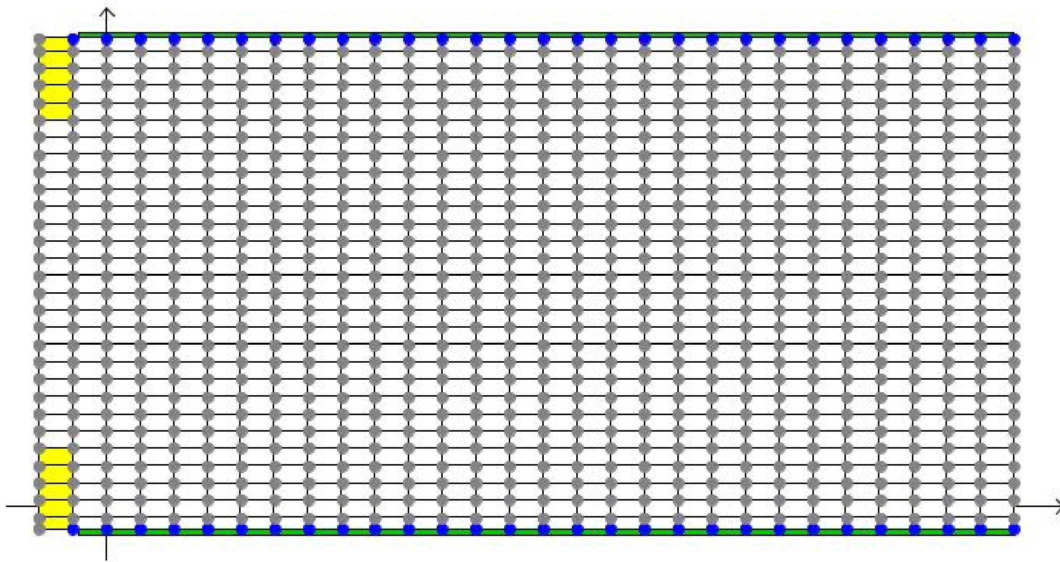

Figure 4.16 FEM for the PBGA assembly

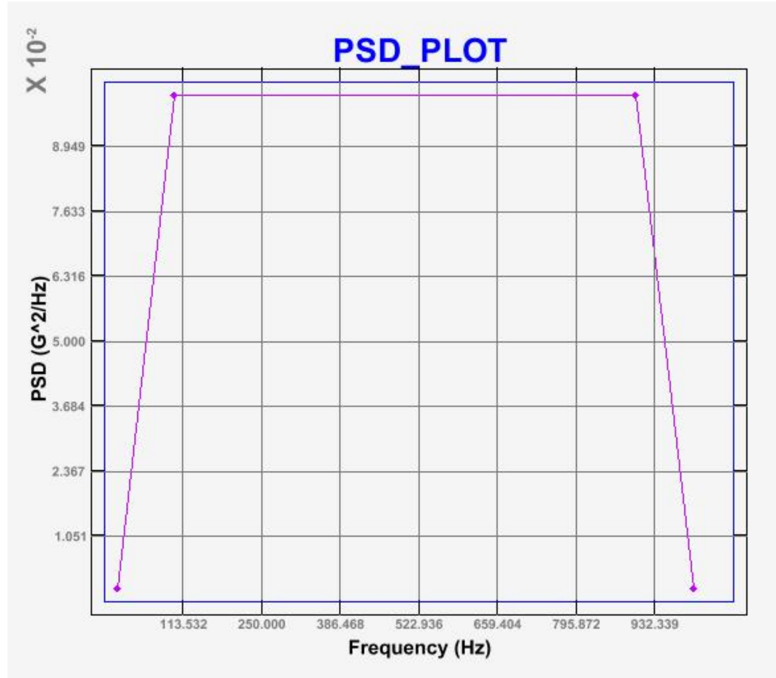

Figure 4.17 Random vibration PSD plot

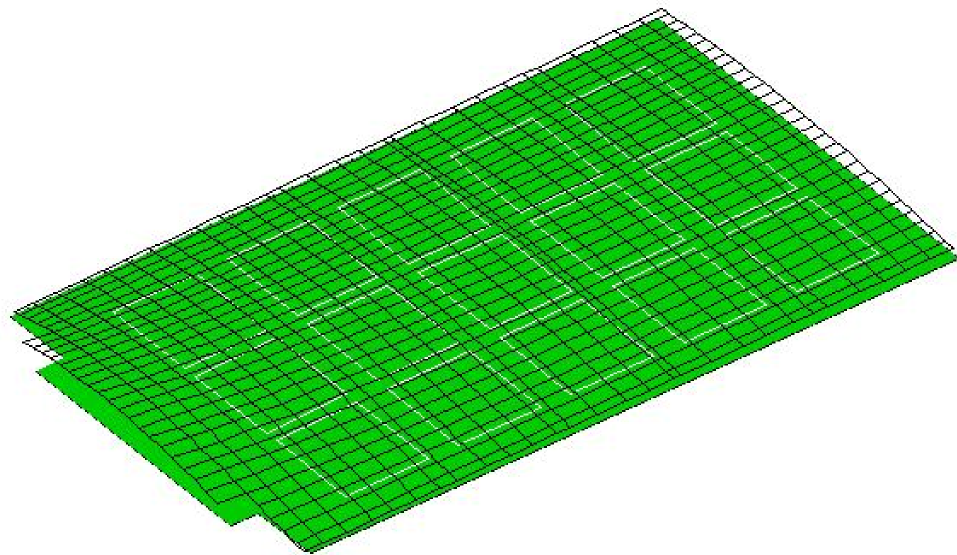

Figure 4.18 First mode of PBGA assembly with natural frequency, 277 Hz

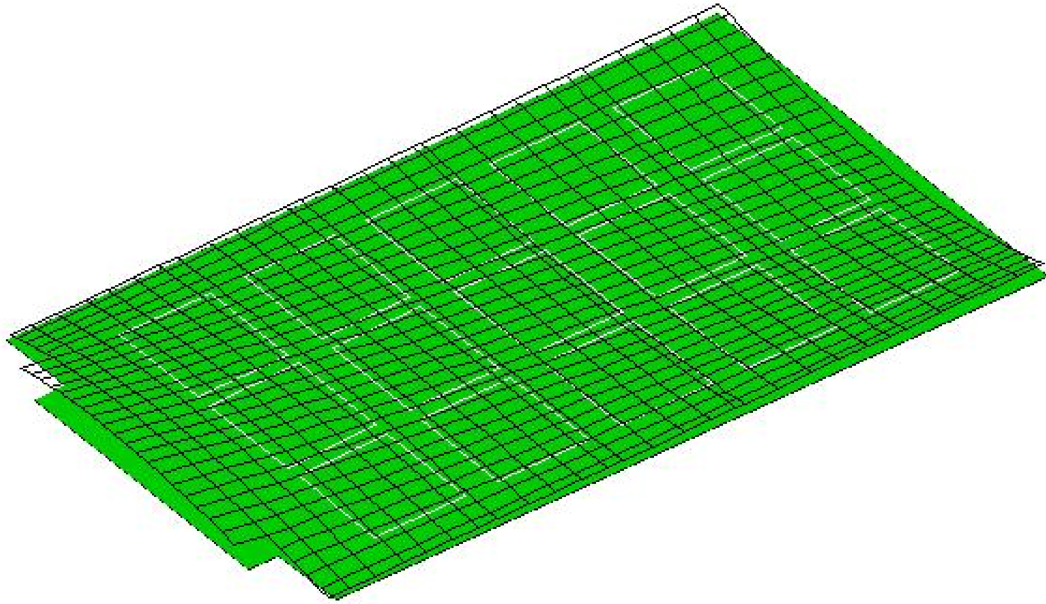

Figure 4.19 Second mode of PBGA assembly with natural frequency, 329 Hz

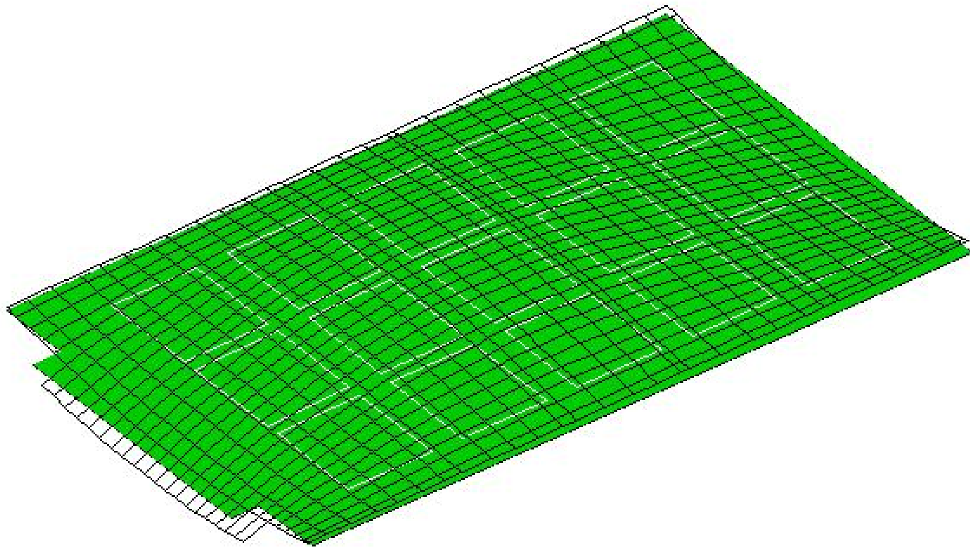

Figure 4.20 Third mode of PBGA assembly with natural frequency, 491 Hz

The board curvature distribution at room temperature is schematically shown in Figure 4.21. Considering the temperature effects, the PCB curvature was also

calculated at high temperature, 150 °C, and low temperature, -50 °C. This curvature information will be used to for load input for local component model.

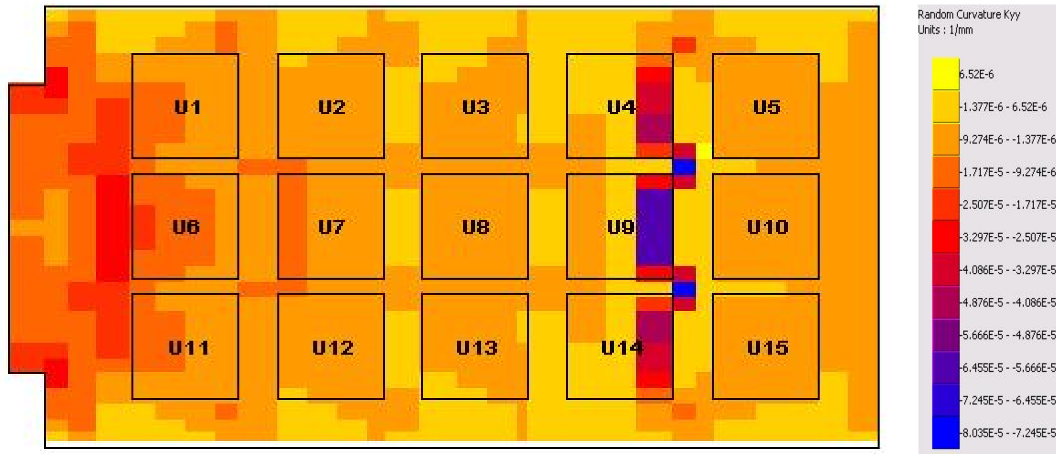

Figure 4.21 The board random curvature at room temperature

4.2.2 Interconnect Stress/Strain Analysis

Though detailed FEA may accurately determine interconnect stress/strain under vibration loading, it is not satisfied the rapid assessment requirement for most users. Therefore it is necessary to develop a simple analytic model to approximately analyze the interconnect stress/strain within acceptable accuracy range.

Siddharth [1995] proposed a rapid stress analysis model to calculates the deformations induced in the leaded component-PWB assembly due to external bending moments applied to the PWB. The primary purpose of developing the model was for evaluating the maximum stress in the leads. This model is applicable to problems associated with either a static deformation of the component/PWB assembly or vibration. There are several major assumptions in his study:

(a) Lead-solder attachment is treated as a continuous elastic attachment. This assumption is valid for the number of leads in the package is sufficiently large compared to the length of the component. For high density area array package, such as PBGA272, this assumption is also valid.

(b) Lead-solder attachment is assumed to transmit axial forces to the component in the direction perpendicular to the plane of PWB.

(c) The component and the board are modeled as rectangular beams with enhanced rigidity. The governing equations of the model are based on beam theory and therefore account for warpage or bending only in one in-plane direction.

(d) Rotational stiffness of the lead-solder attachment assumed to have negligible effect on board and component curvatures.

Using Euler-Bernoulli beam theory [Timoshenko, 1971; Boresi and Sidebottom, 1993] the deflections in the component and the PWB are given by the following expressions:

$$D_1 w_1^{iv}(x) = q(x) = k[w_2(x) - w_1(x)] \qquad \text{(Eqn. 4.9)}$$

$$D_2 w_2^{iv}(x) = -\frac{b_1}{b_2} q(x) = -\frac{b_1}{b_2} k[w_2(x) - w_1(x)] \qquad \text{(Eqn. 4.10)}$$

where

$w_1(x)$ = deflections of the component as a function of position x,

$w_2(x)$ = deflections of the PWB as a function of position x,

D_1 = flexural rigidities of component,

D_2 = flexural rigidities of PWB,

b_1, b_2 are the thickness of the component and PWB respectively,

k = spring constant of the elastic attachment.

The spring constant, k, of the elastic attachment is related to the spring constant K of an individual lead-solder assembly by the expression

$$k = \frac{mK}{2lb_1} \qquad \text{(Eqn. 4.11)}$$

where l is the half-length of the component-PWB assembly (shown in Figure 4.16); m is the total number of interconnects (lead-solder I/Os) in the package. Combining Equations 4.10 and Equation 4.11 and using the boundary conditions in Equation 4.12 a fourth order differential equation is obtained.

$$w_1^{'}(0) = w_2^{'}(0) = w_1^{''}(l) = w_1^{'''}(l) = w_2^{'''}(l) = 0; w_2^{''}(l) = \frac{M}{b_2 D_2} \qquad \text{(Eqn. 4.12)}$$

The details on the solution of the differential equations are presented elsewhere [Suhir, 1988 and Siddharth, 1995] and the final deflections in the component and the PWB are presented in Equations 4.13 and 4.14

$$w_1(x) = \frac{Ml^2 b_1}{2b_1 D_1(1+\eta)}\left[\left\{\frac{x}{l}\right\}^2 + \frac{\chi_1(u)}{3}V_o(\alpha x) - \frac{\phi_1(u)}{u^2}V_2(\alpha x)\right] \qquad \text{(Eqn. 4.13)}$$

$$w_2(x) = \frac{Ml^2 b_1}{2b_1 D_1(1+\eta)}\left[\left\{\frac{x}{l}\right\}^2 - \frac{1}{\eta}\left\{\frac{\chi_1(u)}{3}V_o(\alpha x) - \frac{\phi_1(u)}{u^2}V_2(\alpha x)\right\}\right] \qquad \text{(Eqn. 4.14)}$$

where

$V_o(\alpha x) = \cosh(\alpha x)\cos(\alpha x)$

$V_1(\alpha x)$ = [cosh(αx)sin(αx) + sinh(αx)cos(αx)]/sqrt(2)

$V_2(\alpha x)$ = sinh(αx)sin(αx)

$V_4(\alpha x)$ = [cosh(αx)sin(αx) - sinh(αx)cos(αx)]/sqrt(2)

$u = \alpha l = [Km(1+\eta)/(8\ b_2\ D_2\ l)]^{1/4}$

$\chi_1(u) = (6/u^2)$ {[cosh(u) sin (u) – sinh(u) cos (u)]/[sinh(2u) +sin (2u))]}

$\phi_1(u) = (2)$ {[cosh(u) sin (u) + sinh(u) cos (u)]/[sinh(2u) +sin (2u))]}

The force in the lead at a position x is given by

$$F_L = K[w_1(x) - w_2(x)] \quad \text{(Eqn. 4.15)}$$

The stress in the lead due to axial force:

$$\sigma = \frac{F_L}{A_L} \quad \text{(Eqn. 4.16)}$$

where,

F_L = force experienced in the lead

A_L = area of cross-section of the lead

In this study, solder joints are the replacement for the lead-solder attachment in his model. The bending moment was first calculated using well known plate moment-curvature relations for small deformation theory as Equation. 4.17 shows:

$$M = \frac{1}{12} Eh^3 / (1 - \nu^2) \kappa \quad \text{(Eqn. 4.17)}$$

where,

E is modulus,

ν is Poisson’s ratio,

κ is curvature,

h is thickness of plate.

The curvature information was obtained from PCB deformation analysis as described in previous section. For different curvatures at different temperature levels, the bending moments are separately calculated. For this study, the temperature levels are high temperature (150 °C), room temperature (25 °C), and low temperature (-50 °C). Then the stress in solder joint can be obtained by solving Equations 4.13-4.16. Since it is assumed solder joints as elastic attachment under vibration loading condition, the strain can be obtained using the simple elastic stress and strain relationship.

4.2.3 Interconnect Damage Analysis

Interconnect damage analysis is performed after interconnect stress/strain analysis done. A generalized strain range approach was used to for solder joint damage assessment. This approach has been discussed in Chapter 3. It is aware the difference between here and Chapter 3 is that: 1) strain range is obtained through the curvature and stress/strain analysis using quick methods; 2) mean stress is obtained from the predictive models which were built based on the DOS. The Equation 4.18shows the calculation again

$$\frac{\Delta\varepsilon(T)}{2} = \frac{(\sigma_{f(T)} - \sigma_{o(T)})}{E(T)}\left(2N_f\right)^b + \varepsilon_{f(T)}\left(2N_f\right)^c \qquad \text{(Eqn. 4.18)}$$

Then the fatigue life responded to the strain ranges at different temperature levels can be obtained by numerically solving this equation. The damage accumulated in the solder joint was computed by incrementally adding the damage due to vibration loads (with mean stresses included) at each discrete temperature level as Equation 4.19 shows

$$D_{v(total)} = \sum_{T} D_v(T) f_j = \sum_{T} \frac{f_j}{N_{f(T)}} \qquad \text{(Eqn. 4.19)}$$

where

D_v = accumulated vibration induced damage

N_f = accumulated solder joint fatigue life under vibrational loading

f_j = fraction of vibration damage at the discretized temperature level

4.3 Damage Superposition

The overall damage was a superposition of the damage due to thermal cycling loading and the damage due to vibration loading. The fatigue life is then the reversal of the overall damage.

$$D_{total} = D_{th} + D_v \qquad \text{(Eqn. 4.20)}$$

$$N_f = \frac{1}{D_{total}} \qquad \text{(Eqn. 4.21)}$$

4.4 Comparison Between Test Results, LDSA, IDSA and RLPA

Figure 4.17 compares RLPA predictions for PBGA272 with experimental results and linear damage superposition predictions and IDSA predictions. It indicates RLPA can reflect the experimental trend better than the traditional linear damage superposition approach. As expected, RLPA is not accurate as IDSA due to much simplification. However, considering its rapidness and easy to use, it is still can be used as a design tool for PBGA solder joint reliability assessment at the beginning stage.

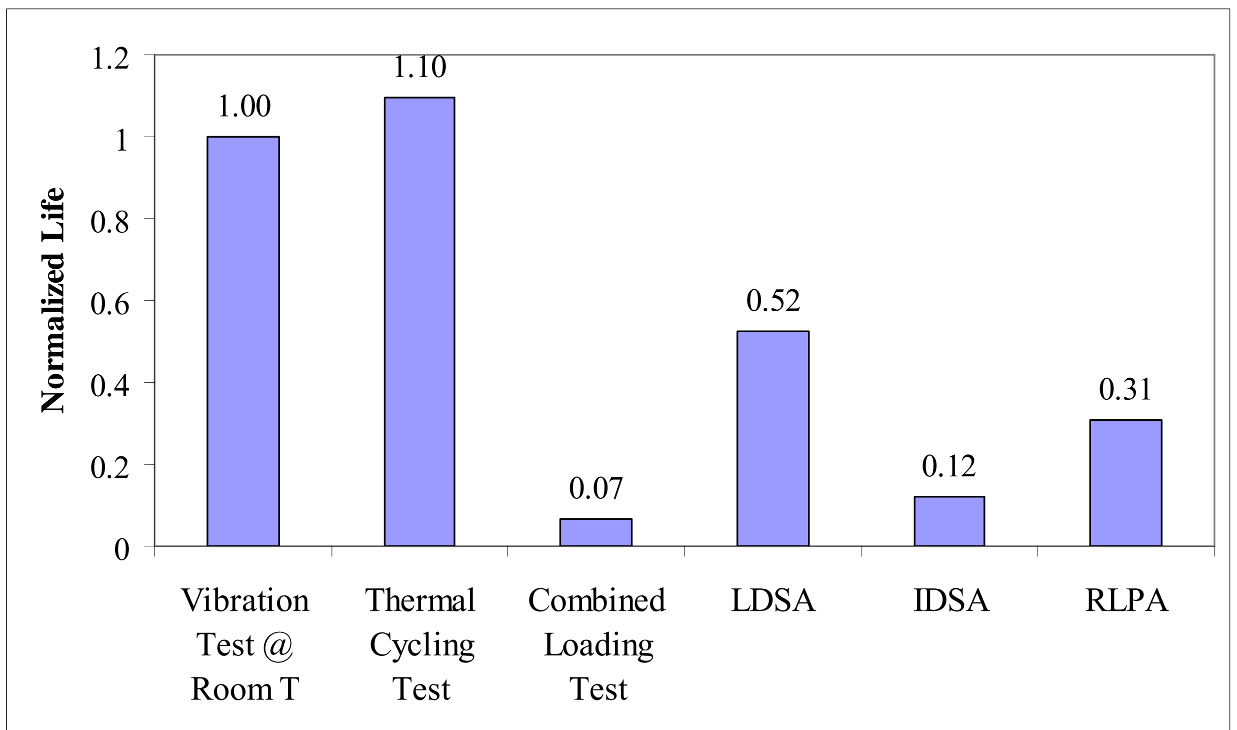

Figure 4.17 Comparison between experimental results and simulation results

4.5 Summary

Based on the incremental damage superposition concept, a rapid solder joint fatigue life prediction approach for PBGA was also developed for combined temperature cycling and vibration loading conditions. This approach replace the detail FEA models with a thermomechanical stress model and a vibration stress model to analyze the interconnect stress under thermal cycling and vibration loading conditions. The mean stress during thermal cycling was obtained from a pre-built response curve. The damage due to two different loadings was then calculated using the generalized strain approach and superposed.

The simulation results showed the prediction trend fits experimental results better than the traditional Miner's rule. It indicates this rapid approach can capture the interaction between two environmental loadings and can be used as the approximate design tool for qualification and accelerated tests and quick reliability assessment.

Chapter 5: Contributions and Suggestions for Future Work

Concurrent vibration and thermal environment is commonly encountered in the service life of electronic equipment, including those used in automotive, avionic, and military products. Combined temperature cycling and vibration loading tests are expected to reflect the real use environments and enhance the test time compression by increasing the rate of damage accumulation and therefore decreasing the associated time and costs. On the other hand, use of combined test environments is complicated by the presence of multiple competing failure mechanisms that are influenced by various factors such as applied loads, test configuration, material behavior, microstructural influences etc. Though extensive research exists in literature for solder joint failures due to thermal cycling, limited research has been conducted on investigating solder joint failures due to a combination of vibration and thermal cycling. It is required a systematic study through experiments, stress/strain analysis and damage estimation to ensure accurate extrapolation of damage accumulation rates from test environment to use environment.

This dissertation provides the first systematic experimental study where significant interactions between combined temperature cycling and vibration loads resulted in quicker damage accumulation in solder joints as compared to the damage accumulation due to temperature cycling alone and vibration alone. The dissertation

also applies an incremental damage superposition approach on PBGA solder joint to quantify the complex interactions between temperature cycling and vibration loads.

Based on this incremental damage superposition approach concept, this study further provides a rapid solder joint fatigue life prediction simulation approach for PBGA solder joint under combined temperature cycling and vibration loading conditions. The results of this study enable one to

(i) design qualification and accelerated tests appropriately;

(ii) predict product field life by extrapolating laboratory results quickly and accurately.

Section 5.1 summarized the primary contributions of the dissertation while Section 5.2 presents suggestions for future work.

5.1 Contributions of the Dissertation

1) This study first systemically studied the PBGA solder joint damage under multiple environmental loading conditions (thermal cycling alone, vibration loading alone, and combined thermal cycling + vibration loads) and explores the clear dependence of solder damage on load interactions. Specifically, for the load histories employed in this dissertation, solder joints are found to be more vulnerable to the combined application of random vibration and thermal cycling than to random vibration excitation at room temperature and thermal cycling alone. Therefore traditional linear damage superposition approaches that add damages due to individual loads in a linear fashion are not suitable for those applications where load interactions are significant.

2) An modified incremental damage superposition approach (IDSA) using finite element analysis was applied to PBGA solder joint reliability assessment. This approach can model the nonlinear interactions between vibration loading and thermal cycling. It considers the temperature effect on vibration response and constitutive properties of solder, and the vibration fatigue damage affected by thermomechanical mean stress affects. The total damage is incrementally superposed along the whole thermal cycle instead of linearly superposing damages due to vibration and thermal loads acting independently. This approach was validated through experiments and reflects the actual damage trends.

3) A rapid solder joint fatigue life prediction simulation approach for PBGA solder joint was also developed for combined temperature cycling and vibration loading conditions. This approach included a thermomechanical stress model and a vibration stress model to analyze the interconnect stress under thermal cycling and vibration loading conditions. The mean stress during thermal cycling was obtained from the response curve. The damage due to two different loadings was then calculated using the generalized strain approach and superposed. This approach was also validated using experimental data and can quickly predict solder joint life in an acceptable range.

In conclusion, this dissertation first systematically studied the interactions effects on PBGA solder joint fatigue through experiments and simulation. Experimental results clearly showed much earlier PBGA solder joint failure under combined loading compared with either thermal cycling or vibration loading alone. It was found that traditional linear superposition can overpredict the solder joint fatigue life since it

neglects the interaction of the vibration and thermal cyclic loadings. The dissertation also demonstrates an incremental damage superposition approach using finite element analysis can adequately captures the interactions between temperature and vibration loads and accurately predict PBGA solder joint fatigue life. Further, a rapid solder joint fatigue life prediction simulation approach for PBGA solder joint was also developed to quickly calculate the damage caused by combined temperature cycling and vibration loading conditions and assess solder joint reliability. This study provides the conceptual framework for quantifying the interactions between temperature and vibrations on solder durability. However, further studies are required to verify, enhance and improvise the techniques that were presented in this study. Suggestions for further improvements are provided in Section 5.2.

5.2 Suggestions for Future Work

This dissertation provides a detail and a rapid modeling approaches to quantify temperature and vibration interactions on solder joint durability. The damage methodology developed in this study can be used to design meaningful and faster accelerated and qualification tests. For example, the damage methodology can potentially be used to guide the short combined loading tests to replace long duration pure loading tests. The damage methodology can also be used to extrapolate test results to use environment conditions. However, for this complex combined loading phenomenon, there are still some further work needs to do. In this section, suggestions are provided for future improvements of the tools, approaches and procedures presented in this dissertation.

5.2.1 Vibration Effect on Thermal Cycling

In this study, only the effect of thermal cycling on vibration loading was considered and calculated. Zhao et. al. [2000] used moiré interferometry (MI) to measure the inelastic deformation field of solder joints of an actual ball grid array (BGA) package under concurrent vibration (in-plain) and thermal cycling loading. Measurements showed vibration has significant effects on the inelastic behavior of solder joints, especially coupled with thermal cycling. However, no reliability tests were performed to obtain the solder joint fatigue life under combined loading conditions and no damage model were proposed to take account for the combined loading in their study. Therefore, the methodology to consider both thermal cycling effects and vibration effects on each other should capture more realistic physics and give more accurate results.

5.2.2 Solder Joint Mean Stress History Simulation

The mean stress history response curves were developed through design of simulation using finite element analysis in this study. This predictive response curve based on four physical meaning factors is easy to use, time-effective, and does not require advanced mechanics and finite-element knowledge, and thus can be used by any designer in the early stages of design. It was observed the CTE mismatch is not significant among these factors due to small variation. With material change, huge CTE mismatch is expected to contribute to the model more. Then the modulus of material should also be considered one of key factors in the new model built-up. Meanwhile, the predictive models are based on 2 levels of each factor. They can not

accurately predict if there is nonlinearity of the response. A 3 level DOS is advised to determine nonlinearity for the future study.

On the other hand, the predictive models for mean stress are only applicable between the ranges of each respective factor. Use of the model far outside these ranges may lead to unrealistic results. Therefore, an analytic close-formula to calculate solder joint mean stress history, which can safely extrapolate outside test parameter ranges, will greatly benefit for designers if available.

5.2.3 Experimental Verification and Constants Calibration

The models developed in this study were validated with comprehensive experimental data. Successful verification will definitely enhance the confidence in using these models as proactive tools for designing meaningful and faster accelerated wearout tests. Therefore, one of the future tasks should experimentally verify the modified IDSA predictions and RLPA predictions and calibrate the constants in the models. The tests should include vibration durability test under extreme temperatures, sequentialtemperature cycling and vibration loading tests, etc.

Appendices

Appendices A Related to Chapter 2

A.1 Normalized experimental data procedure

In the Chapter 2, Figure 2.1 shows the fifteen components locate on the board with different locations. Under vibration conditions, different locations will have different vibration response. That means the components may under different stress conditions. To remove the layout effects on time to failure of components, the normalization technique was applied in this study. The theory hypothesis is that the stress applied to components is proportional to the component curvature and the damage accumulated is also proportional to the component curvature as Equation A.1 shows:

$$D = \frac{1}{N_f} \propto \sigma \propto \kappa \qquad \text{(Eqn. A.1)}$$

The normalized procedure is as following:

1) All components curvatures under vibration loading were calculated using a commercial software calcePWA®.

2) Choose one component curvature as the reference (generally the maximum curvature is chosen as the reference, in this study, U6). All component curvatures were divided by the reference curvature as normalization.

3) The original time to failure of each component was then divided by the normalized curvature as normalization.

Figure A.1–A.2 compare the original time to failure and the normalized time to failure under vibration loading condition in 2-parameter Weibull distribution plots. It shows the normalization removed the layout effect and generated more good fit data. For the combined loading test, the same normalized process has been done. Figure A.3–A.4 show the original test results and the normalized test results under combined loading conditions.

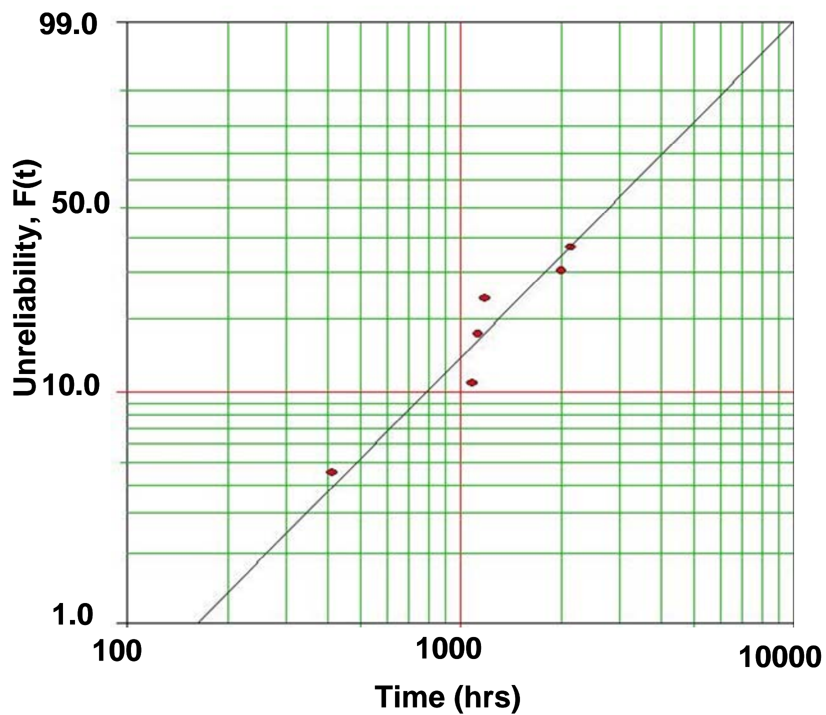

Figure A.1 Two-parameter Weibull distribution of original vibration test results

(β= 1.49, η= 3551, ρ= 0.95)

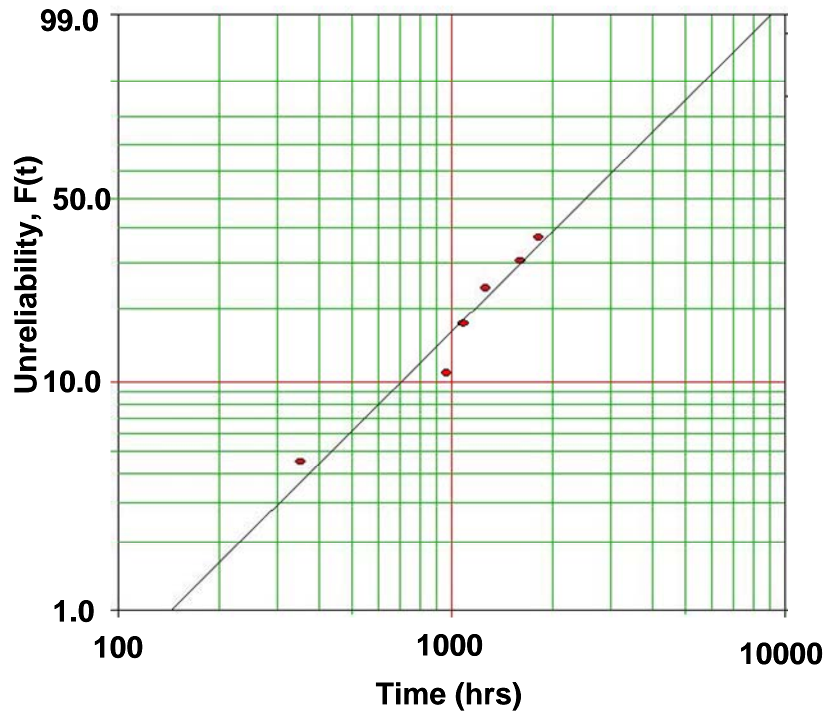

Figure A.2 Two-parameter Weibull distribution of normalized vibration test results (β= 1.48, η= 3232, ρ= 0.97)

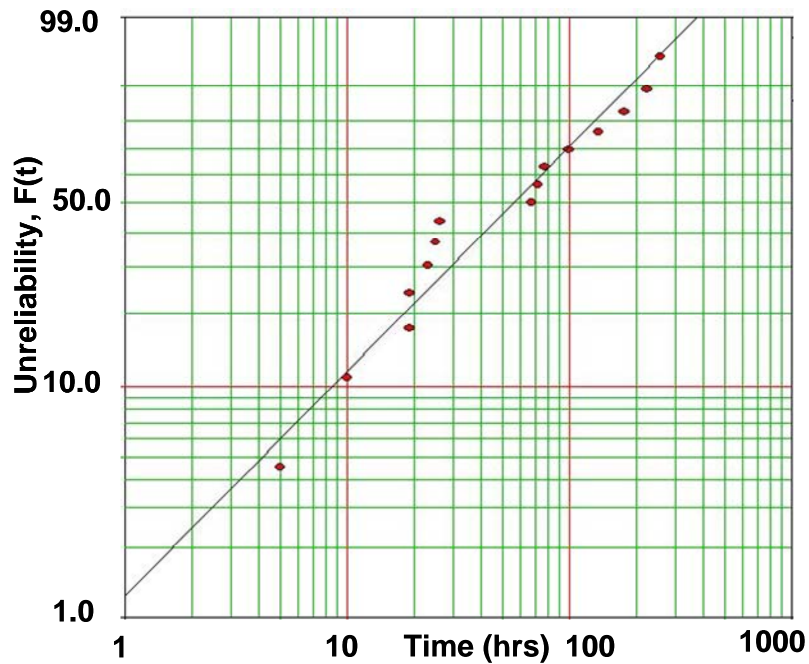

Figure A.3 Two-parameter Weibull distribution of original combined loading test results (β= 1.0, η= 81, ρ= 0.97)

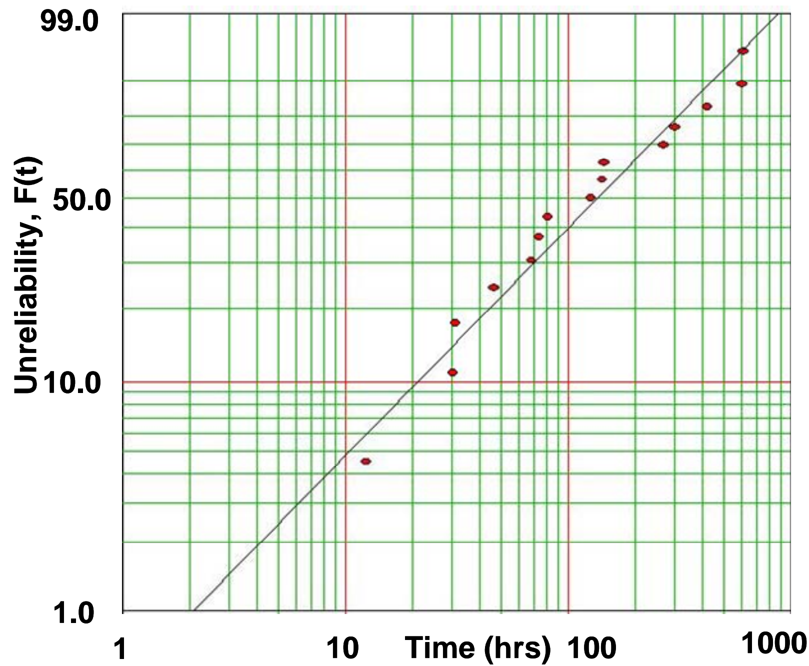

Figure A.4 Two-parameter Weibull distribution of normalized combined loading test results (β= 1.2, η= 193, ρ= 0.98)

A.2 Two-parameter and three-parameter Weibull distribution comparison

To statistically analyze the test results, an appropriate distribution should be chosen. In this study, different distributions (normal, log normal, exponential and two-parameter Weibull) were tested using Weibull++ 6©. Based on the wearout failure mechanism and distribution fit, two-parameter Weibull was chosen as the best fit to analyze the test data.

To further investigate the distribution analysis, three-parameter Weibull distribution was also chosen to analyze the test data. Compared to two-parameter Weibull distribution, there is one more parameter, location parameter, γ, for three-parameter Weibull distribution. If the location parameter is assumed to be zero, then three-parameter Weibull will become two-parameter Weibull distribution.

As the name implies, the location parameter locates the distribution along the abscissa. Change the value of γ has the effect of "sliding" the distribution and its associated function either to the right (if $\gamma > 0$) or to the left (if $\gamma < 0$). γ provides an estimated of the earliest time-to-failure of units under test. γ must be less than or equal to the first time-to-failure. The life period 0 to $+\gamma$ is a failure free operation period. A negative γ may indicate that failures have occurred prior to the beginning of the data collection period of the analysis. For example, failures might have occurred during production, in storage, in transit, during check out prior to the start of a mission, or prior to actual use. γ has the same units as t, such as hours, miles, cycles, actuations, etc. The third parameter of the Weibull distribution, γ, is utilized when the data points do not fall on a straight line, but on a concave up or down curve. The calculation of the value for γ can be done automatically using the Weibull++ 6©. To straighten the original data line, the value of γ must be subtracted from each of the points. Not that when adjusting for γ, the x-axis scale for the straight line become ($t-\gamma$).

Figure A.5 shows the three-parameter weibull distribution for thermal cycling test results. The straight line is adjusted line for γ and the curve line is for unadjusted line for γ. The time to 50% failure was calculated as 2574 cycles. Compared to the calculation from two-parameter distribution, 2502 cycles for time to 50% failure, there is no big difference. For simplicity and consistence, two-parameter Weibull was used in this study as best-fit distribution. For completion, Figure A.6 and Figure A.7 give the three-parameter Weibull distribution for vibration test results and combined

loading test results. The time to 50% failure is 2242 hours under vibration loading and 126 hours under combined loading.

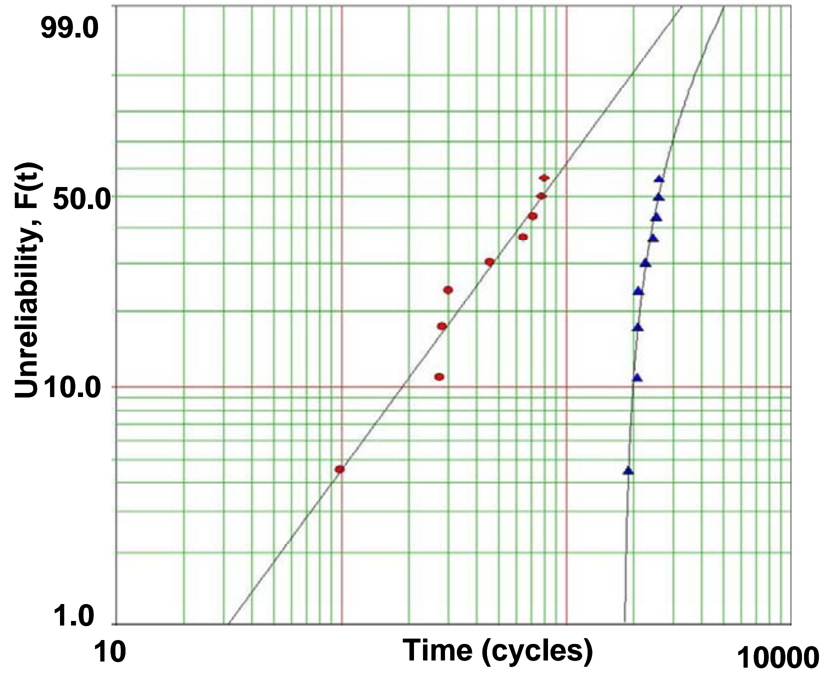

Figure A. 5 Three-parameter Weibull distribution of thermal cycling test results

(β= 1.32, η= 1030, γ=1793, ρ= 0.98)

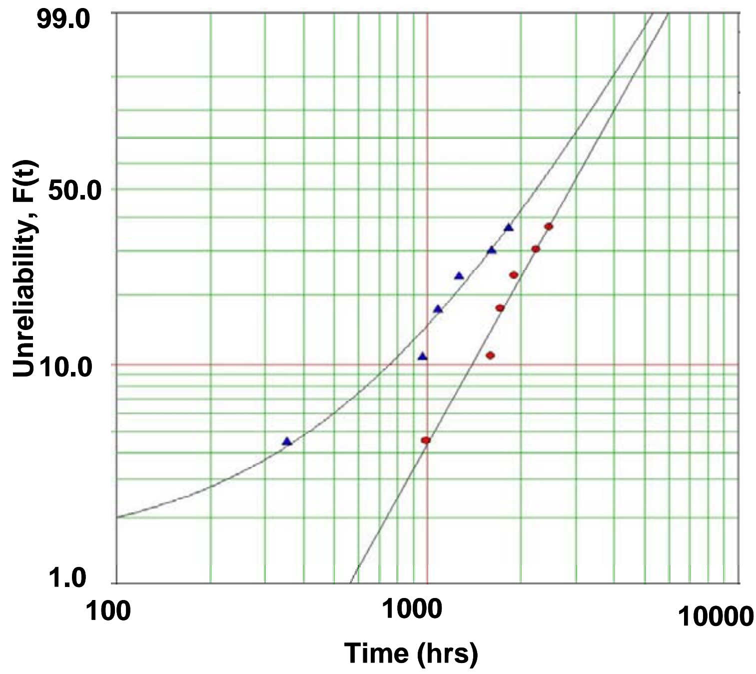

Figure A. 6 Three-parameter Weibull distribution of vibration test results (β= 2.60, η= 3318, γ=639, ρ= 0.99)

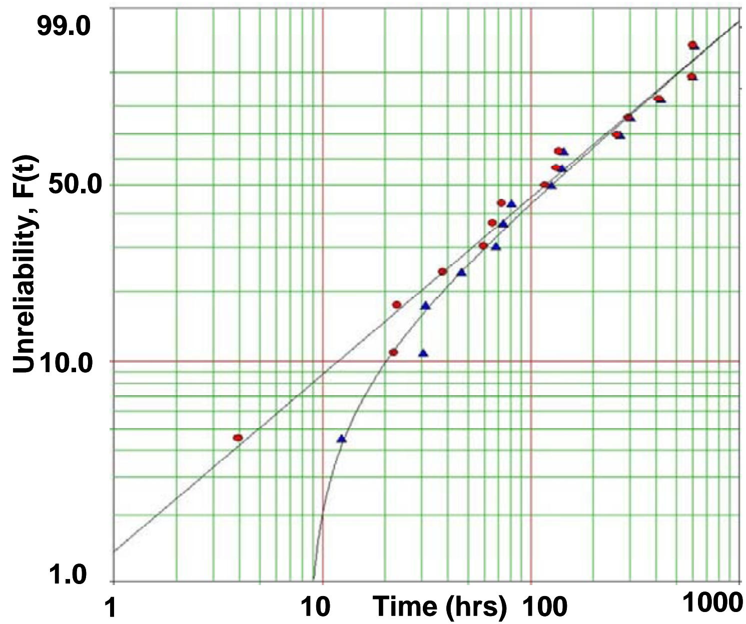

Figure A. 7 Three-parameter Weibull distribution of combined loading test results (β= 0.82, η= 184, γ=8, ρ= 0.99)

Appendices B Related to Chapter 3

B.1 MIDSA detail calculation procedure

The flowchart of MIDSA is shown in Figure 3.1. All steps and equations are already discussed in Chapter 3. In this section, the detail calculations are described to better understand this approach. The calculation sequence and intermediate results are listed as the following:

B.1.1 Damage calculation due to thermal cycling

First, a strip 3-dimenstion PBGA assembly model was developed using a commercial software ANSYS®. There are 15760 elements for the whole assembly; 1,379 elements for the solder ball; and 48 elements for the interface layer. Element was chosen as 3-D 8-node Structural Solid. The boundary conditions are center point of the board fixed in all direction and 3 vertical surfaces are symmetrical. Thermal loading profile was the same as the one in temperature cycling test and combined loading test. Temperature-dependent elastic properties were used for all materials except for the eutectic solders. All the geometric parameters and mechanical properties can be found in Chapter 3.

Solder is modeled as a visco-plastic material. The elastic-plastic behavior of solder is modeled using Ramberg-Osgood power law hardening model [Skipor, 1996].

$$\varepsilon = \varepsilon_{el} + \varepsilon_{pl} = \frac{\sigma}{E} + \left(\frac{\sigma}{K}\right)^{1/n_p} \qquad \text{(Eqn. B.1)}$$

where ε is mechanical strain, ε_{el} is the elastic strain, ε_{pl} is the plastic strain, E is the elastic modulus, σ is the corresponding stress, K is the strength coefficient and n_p is

the work hardening exponent. In this study temperature dependent elastic-plastic constitutive constants are obtained from literature [Skipor, 1996]. The nonlinear stress vs. plastic strain curves of solder at different temperatures are shown in Figure 3.3 in Chapter 2.

Creep, in this study is defined as temperature and time dependent inelastic deformation. A generalized Garofalo steady state model is used to mode steady state creep and the constitutive equation is shown in Equation B.2.

$$\frac{\partial \varepsilon}{\partial t} = C_1 \left[\sinh\left(C_2 \sigma\right)\right]^{C_3} \exp\left(\frac{-C_4}{T}\right) \qquad \text{(Eqn. B.2)}$$

For SnPb solder, the constants are listed in Table B.1. The T is in K unit.

Table B.1 Generalized Garofalo (secondary) creep model constants [Lau, 2003]

	C_1	C_2	C_3	C_4
SnPb	462(508-T)/T	1/(37.78x106-74414T)	3.3	6360

The simulation was performed for three completed thermal cycling cycle for stable purpose. After that, the maximum Von Mises stress/strain of element was first identified for solder balls. In this study, it locates at the outmost ball interface layer. Then the strain energy was averaged along the whole layer where the maximum stress/strain element locates.

When the strain energies were obtained from the last cycle, the values were substituted into Equation 3.1 to solve the life prediction under the thermal cycling.

The constants for the equation can be found in Table 3.5. The predicted life under thermal cycling was calculated as 2630 cycles. The damage was then calculated using Equation 3.2: D_{th} = 1/2630/78/60 = 8.12E-8 (1/s).

B.1.2 Mean stress calculation due to thermal cycling

Mean stresses in general have a volumetric effect on the deformation of a material (analogous to hydrostatic pressure acting on an element) [Mendelson, 1968]. In this study, the output hydrostatic pressure from ANSYS® FEA calculation was used as the mean stress.

Different elements have the different means stress value. Since the bottom layer elements of solder joint were used in thermal cycling damage and vibration damage calculation, the same elements were chosen for mean stress analysis. The mean stress was averaged along the elements on that layer. Figure 3.4 shows the mean stress history along the last thermal cycle. The values at different temperature levels were used for later vibration damage calculation, such as 28.77 MPa at -55 °C, 4.0 MPa at 25 °C, and -1.62 MPa at 150 °C.

B.1.3 PCB vibration response characterization

The PCB strain deformation was collected using the strain gage at potential failure site of interest at three discrete temperature levels: -50 °C, 25 °C and 125 °C. In this study, the strain gage was located on PCB backside under component U6. The reason to choose these three temperature levels to represent the whole thermal cycle is that the vibration response of the specimen in any two given temperature regions is significantly different.

The time domain deformation histories were already shown in Figure 2.3 to Figure 2.5. Then the complex (or irregular) deformation histories were converted into a number of events which can be compared to the available constant amplitude data using rainflow counting process and binning method [Vichare, et. al., 2006], as Figure 2.6-2.8 show. These strain range distribution functions (RDFs) were used to calculate the solder joint strain and discussed later.

B.1.4 Solder joint strain calculation

The solder joint strain vs. PCB strain relationship was built using the developed FEA model. The methodology was described as the following:

1) Set the reference temperature to the desired temperature (e.g. 25 °C) and input correct material properties at this temperature
2) Apply the static bending forces on the end of board
3) Average the x direction strain of the bottom layer of the PCB elements under the component
4) Average the von Mises strain of the elements of the bottom layer of outmost solder ball
5) Use the power law to build the relationship between the solder joint strain and the PCB strain
6) Repeat the Step 1) to Step 5) to different temperatures (e.g. -50 °C and 150 °C)

The deformed shape of PBGA assembly under bending loading and the family strain response curves were shown in Figure 3.5 and Figure 3.6.

Then the solder joint strain range distribution can be obtained using the response curves with the substitution the measured PCB strain range distribution.

Figure B.1—B.3 gives the solder joint strain range distribution functions at different temperatures.

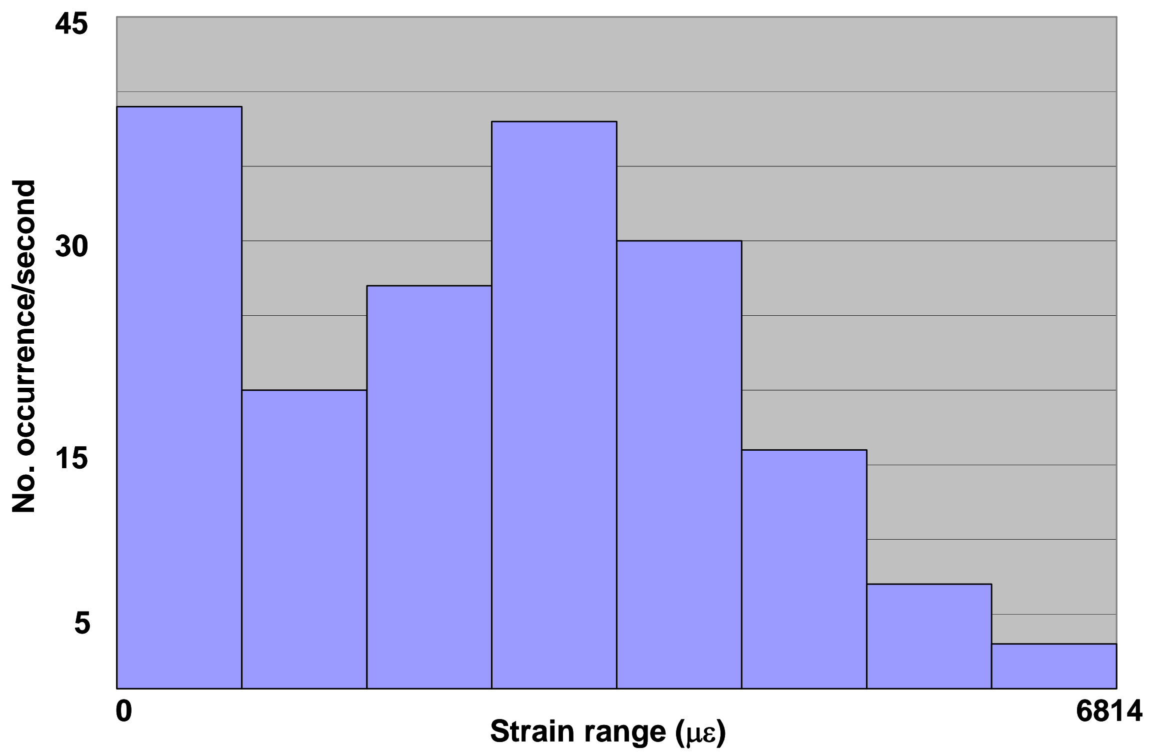

Figure B.1 Solder joint strain range distribution function at 150 °C

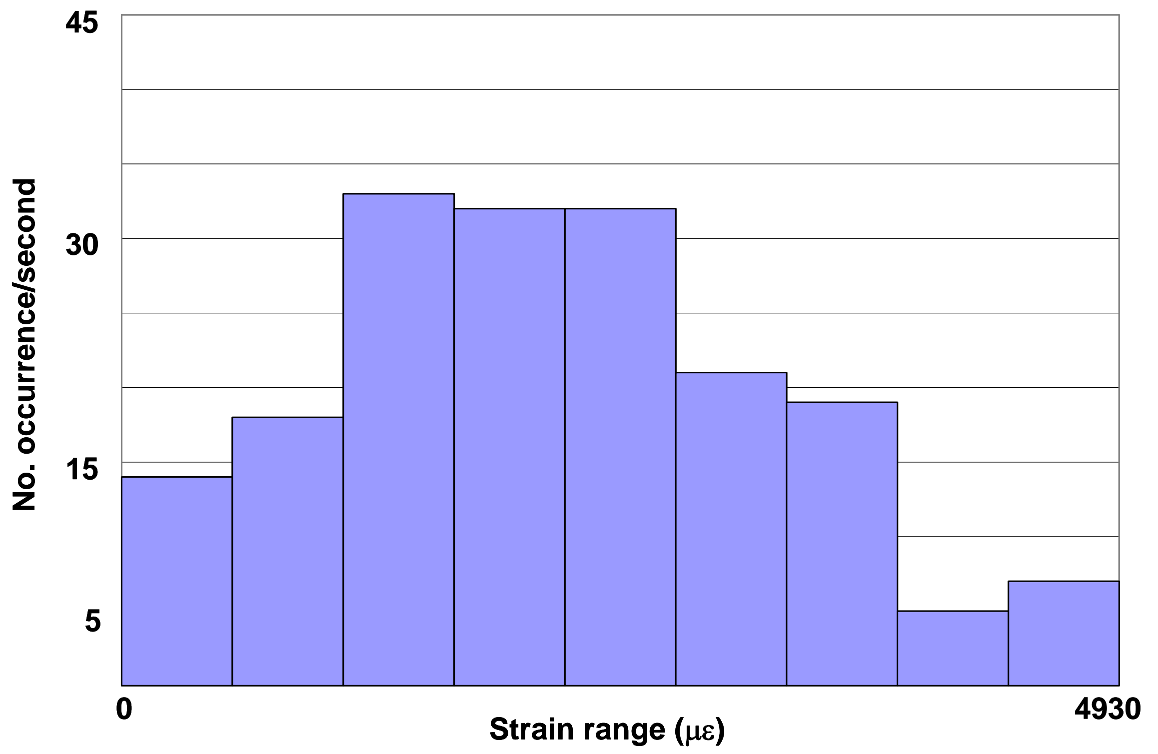

Figure B.2 Solder joint strain range distribution function at 25 °C

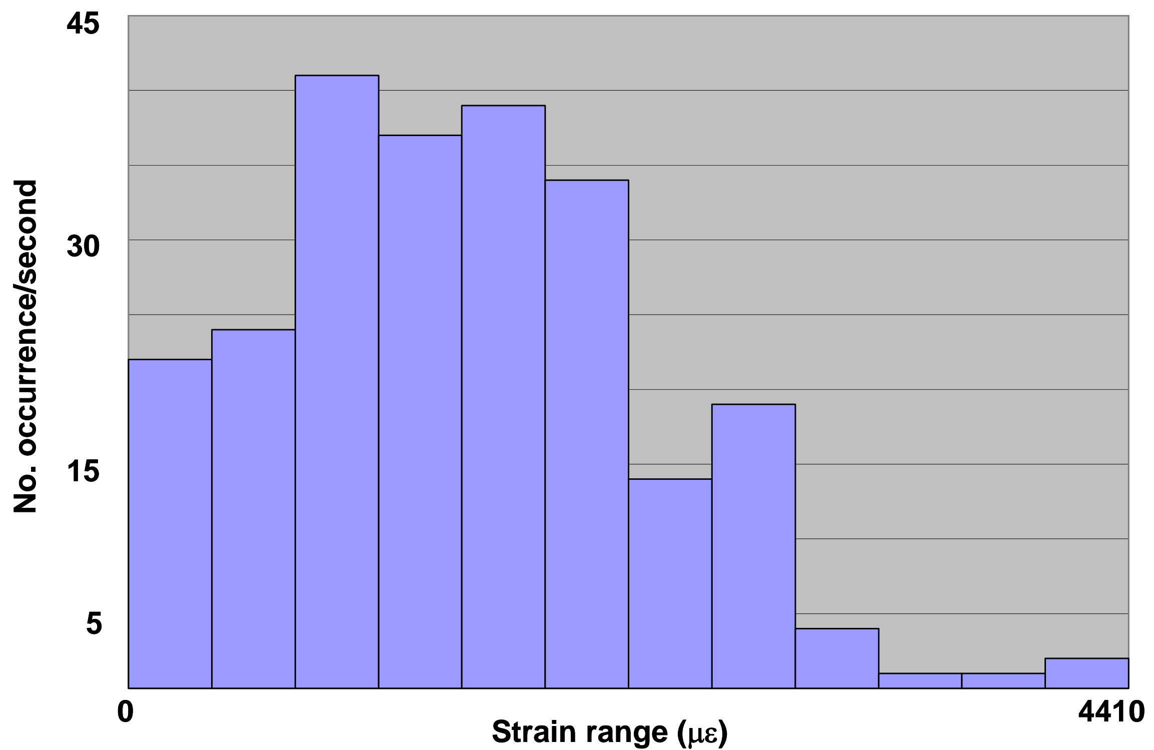

Figure B.3 Solder joint strain range distribution function at -50 °C

B.1.5 The analysis on the response curve significant digits

The response curves were shown in Figure 3.6 and the equations are listed here.

High T (150 C): $y = 126.88x^{1.2959}$ (Eqn. B.3)

Room T (25 C): $y = 336.09x^{1.4618}$ (Eqn. B.4)

Low T (-50 C): $y = 3081.7x^{1.7452}$ (Eqn. B.5)

The coefficients and power constants were obtained from power law regression. Though all of them have five significant digits, it may not be necessary to keep all of significant digits for the results accuracy. Therefore the analysis on significant digits was carried out and steps are listed here:

1) Substitute the maximum PCB strain range 507E-6 as x into the original high temperature responses curve. The output solder joint strain range is 6814E-6.

2) Change the response curve formula to $y = 127x^{1.3}$

3) Repeat the step 1) and get the output as 6612E-6

4) Calculate the relative difference between these two outputs as (6612-6814)/6814*100% = -3%

5) Change the response curve formula to y = 127x1.29

6) Repeat the step 1) and get the output as 7133E-6

7) Repeat the step 4) to get the relative difference as 5%.

8) Therefore, the new response curve for high temperature can be changed to $y = 127x^{1.3}$

Repeat these steps to room temperature and low temperature response curves, we can have a new family temperature dependent solder joint strain response curve:

High T (150 C): $y = 127x^{1.30}$ (3% variation) (Eqn. B.6)

Room T (25 C): $y = 336x^{1.46}$ (2% variation) (Eqn. B.7)

Low T (-50 C): $y = 3081x^{1.75}$ (4% variation) (Eqn. B.8)

B.1.5 Solder joint damage calculation due to vibration loading

In Chapter 3, Equation 3.4 gives the formula to calculate the solder joint damage. The detail calculation procedure is described as the following:

1) Choose the desired temperature level to calculate the damage (e.g. 150 °C)

2) Choose the solder modulus (E) and damage constants (σ_f and ε_f) related to this temperature

3) Find the solder joint strain range distribution at this temperature from the Figure B.1

4) Numerically calculate the life (N_f) for each strain range at this temperature level

5) Summarize the damage based on the occurrences for each life (N_f)

6) Calculate the fraction of total time spend at this temperature level, tj, (e.g. 15 minutes / 78 minutes, for high temperature)

7) Multiply the output from Step 5) and output from Step 6) to obtain the damage at this temperature level

8) Repeat Step 1)—4) for other temperature levels (e.g. 25 °C and -50 °C)

9) Finally summarize all damages at different temperature levels using Equation 3.5.

The Table B.2 gives the damage results for each temperature level. The accumulated damage due to vibration loading was the summary of the damage at each temperature level, 71E-8 (1/s).

Table B.2 Solder joint damage calculation due to vibration loading

	Damage (1/s)	Time fraction	Final damage (1/s)
High temperature (150 °C)	17.1E-7	15/78	32.9E-8

Room temperature (25 °C)	3.27E-7	48/78	20.1E-8
Low temperature (-50 °C)	9.36E-7	15/78	18.0E-8

B.1.6 Total damage superposition

The final step in MIDSA is that superposition of damage due to thermal cycling and damage due to vibration loading. Equation 3.6 gives the formula to calculate. The detail calculation was described as the following:

$D_{total} = D_{th} + D_{vib} = 8.12E\text{-}8 + 71.0\ E\text{-}8 = 79.12\ E\text{-}8$ (1/s)

Therefore, the predicted life N_f = 1/Dtotal = 1/79.12 E-8/3600 = 351 hours

The normalized life based on the life under pure vibration loading was calculated as $N_{normalized} = N_f/N_{vib} = 351/2522 = 0.14$

The comparisons between test results, LDSA results and MIDSA were shown in Figure 3.10.

B.2 Comparison between MIDSA and IDSA

As described in Chapter 3, this study used the modified incremental damage superposition approach to consider the temperature effect on damage constants. To study this consideration efficiency, the solder joint life under combined loading was also calculated using the original IDSA. The calculation steps are the same as described in B.1. The damage due to thermal cycling was not affected. The damage due to vibration loading was changed because the solder modulus and damage constants were considered as temperature independent. In this study, the values for

modulus and damage constants σ_f, ε_f are 17687.2 MPa, 155 MPa, and 0.62, respectively. The new calculation results are listed in Table B.3. The final damage due to vibration loading using the original IDSA was 63.3E-8 (1/s)

Table B.3 Solder joint damage calculation due to vibration loading using IDSA

	Damage (1/s)	Time fraction	Final damage (1/s)
High temperature (150 °C)	10.2E-7	15/78	19.6E-8
Room temperature (25 °C)	3.27E-7	48/78	20.1E-8
Low temperature (-50 °C)	12.36E-7	15/78	23.6E-8

Similar as described in B.1.6, the total damage under combined loading was equal to

$D_{total} = D_{th} + D_{vib}$ = 8.12E-8 + 63.3 E-8 = 71.42 E-8 (1/s)

Then the predicted life was calculated as 1/71.42E-8/3600 = 389 hours.

So the relative difference between the prediction using MIDSA and the original IDSA is (389-351)/351*100% = 11%.

Appendices C Related to Chapter 4

C.1 RLPA detail calculation procedure

The flowchart of RLPA is shown in Figure 4.1. All steps and equations are already discussed in Chapter 4. In this section, the detail calculations are described to better understand this approach. The calculation sequence and intermediate results are listed as the following:

C.1.1 Damage calculation due to thermal cycling

The solder joint damage due to thermal cycling was calculated based on interconnect stress/strain analysis and fatigue damage analysis. Equation 4.1 and 4.3 give the theoretical formula for calculation. The implementation was completed using a commercial software calcePWA®. The details on how to use this software can be found from its manual or Help function. The calculation steps in this study are:

1) Create a PCB with the same dimension and layers as the test vehicle
2) Choose the plastic ball grid array (PBGA) package from the library and specify the dimensions and material properties
3) Locate the PBGAs on the board as the test vehicle layout
4) Apply the thermal cycling profile as the environmental stress loading
5) Run the stress/strain and damage evaluation module and output the predicted life

In this study, the predicted life under thermal cycling is 2630 cycles. Therefore, the damage due to thermal cycling is 1/2832/78/60 = 7.55E-8 (1/s).

C.1.2 Mean stress calculation due to thermal cycling

Next step is to develop a pre-built predictive model for mean stress history. This work was done through a design of simulation (DOS) and implemented by using FEA.

The detail calculation for mean stress history was already discussed in Appendix B.1.2. The only difference here is that sixteen runs were performed, instead of running one thermal cycling loading in MIDSA. The DOS sixteen run profiles were listed in Table 4.1. The reason to choose these four parameters, pitch, solder joint height, temperature range, and CTE mismatch is to include the key factors in interconnect stress/strain model discussed in Chapter 4.1.1 and Appendix C.1.1. The value ranges were chosen based on the possible variation of products.

After mean stresses were calculated, the main effects and interaction analysis were performed to determine the significant factors for predictive models. This work was done using Minitab® 14. The details on how to use this software can be referred to its Manual and Help function. The procedure in this study is described as the following:

1) Generate a 2-level 4-factor factorial DOE based on Table 4.1

2) Input the mean stress response values in the DOE (e.g. mean stress at low temperature)

3) Analyze the factorial design by plotting normal probability plot of the effects of a confidential interval of 95%. The most influential predictors can be found from the plot.

4) Plot main effects and interaction plots to find the significant factors and the significant combination of factors

5) Perform the linear regression analysis to generate the predictive model for mean stress at this temperature level

6) Repeat Step 1) to Step 5) for other two temperature levels (e.g. High temperature, 150 °C and room temperature, 25 °C) to get the predictive models

The developed predictive models for three temperature levels were shown in Equation 4.6–4.8. Then the mean stress history under the test condition can be predicted by these equations. In this study, the mean stresses are 28.90 MPa, 4.05 MPa, and -1.59 MPa for three different temperature levels (-50 °C, 25 °C, and 150 °C). These information will be used for vibration damage analysis and discussed later.

C.1.3 Analysis on factors chosen in DOS

In Chapter 4.1.3.1 and Appendix C. 1.2, the reason to choose the four factors: pitch, solder joint height, temperature range and CTE mismatch is to keep the consistence with the interconnect analytical stress/strain model. It is already observed the CTE mismatch is not significant factor from previous study. One of possible reason is the variation range is too small in the original DOS. It is also observed the pitch is not a significant factor. Therefore, a new 2-level 4-factor DOS designed to replace pitch with solder joint diameter as a new factor and a bigger variation range for CTE mismatch. Table C.1 lists the new DOS with mean stress results.

Table C.1 2-level 4-factor new DOS

Run	Solder joint diameter, A (mm)	Solder joint height, B (mm)	Temperature range, C (°C)	CTE mismatch, D (ppm/°C)	Mean Stress (MPa) @ low T	Mean Stress (MPa) @ High T	Mean Stress (MPa) @ Mean T
1	0.635	0.45	105	5.7	20.61	-2.58	2.76
2	0.635	0.45	105	2.7	20	-2.21	2.24
3	0.635	0.45	200	5.7	31	-1.89	-0.17
4	0.635	0.45	200	2.7	28.77	-1.62	0.57
5	0.635	0.55	105	5.7	24.44	-2.94	3.34
6	0.635	0.55	105	2.7	23.42	-2.55	4.53
7	0.635	0.55	200	5.7	36.52	-2.08	1.26
8	0.635	0.55	200	2.7	33.87	-1.8	1.78
9	0.776	0.45	105	5.7	20.61	-2.58	2.76
10	0.776	0.45	105	2.7	20.52	-2.22	4.3
11	0.776	0.45	200	5.7	30.9	-1.86	-0.57
12	0.776	0.45	200	2.7	28.75	0.5	0.25

13	0.776	0.55	105	5.7	24.37	-2.93	3.3
14	0.776	0.55	105	2.7	22.55	-2.54	5.73
15	0.776	0.55	200	5.7	32.15	-1.89	2.62
16	0.776	0.55	200	2.7	32.31	-1.84	2.62

Then the main effects, interaction analysis and linear regression analysis were performed followed the procedures which were described above. Mean stress response at low temperature were shown in Figure C.1–C.3 as an example. It is observed factor C, temperature range, and factor B, solder joint height are the two most significant factors. This observation is consistent with the previous DOS results. The interaction analysis shows there are interactions exit between solder joint diameter and solder joint height, AB, and solder joint diameter and temperature range, AC. Therefore, these two combination factors were considered when regression analysis were preformed.

The linear regression analyses were performed and the predictive models were generated based on four factors and the combination factors as:

$$Mean_Stress_{lowT} = -15.6 + 10.3A + 35.6B + 0.176C + 0.434D - 0.105AC$$

(Eqn. C.1)

$$Mean_Stress_{highT} = 6.76 - 4.47A - 13.0B - 0.0195C - 1.12D + 0.0427AC + 1.88BD$$

(Eqn. C.2)

$$Mean_Stress_{meanT} = 9.2 - 13.7A - 9.0B - 0.0271C - 0.280D + 35.8AB$$

(Eqn. C.3)

The predictions for mean stress using the new predictive models are 30.0 MPa, 0.50 MPa, and -1.15 MPa for low temperature, mean temperature and high temperature. It is close to previous prediction results. Therefore, either these new DOS predictive models or the original new DOS predictive models work fine for mean stress history simulation.

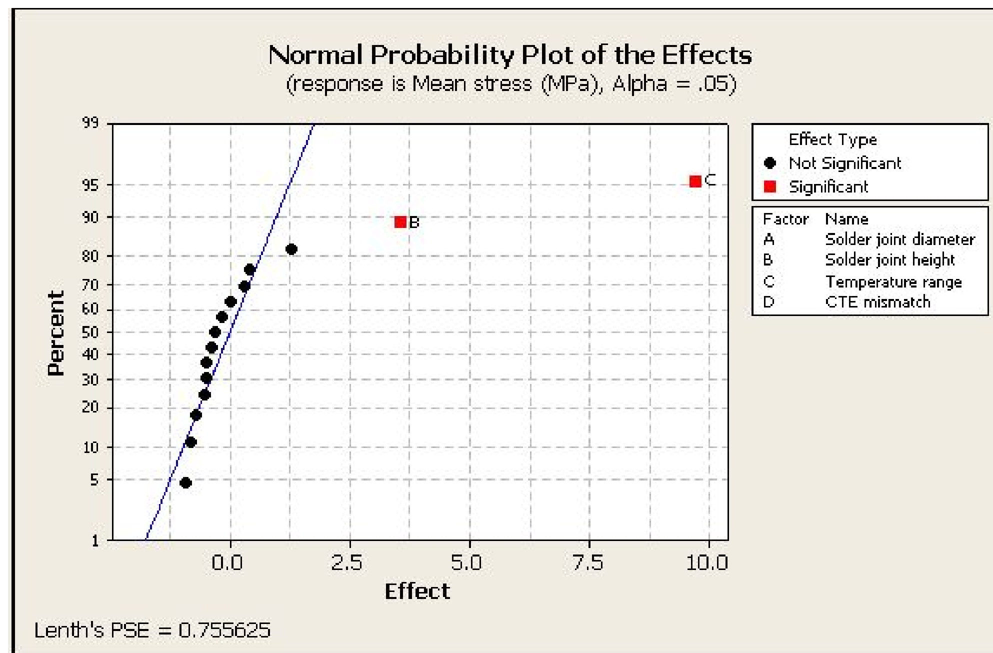

Figure C.1 Normal probability plot of the effects

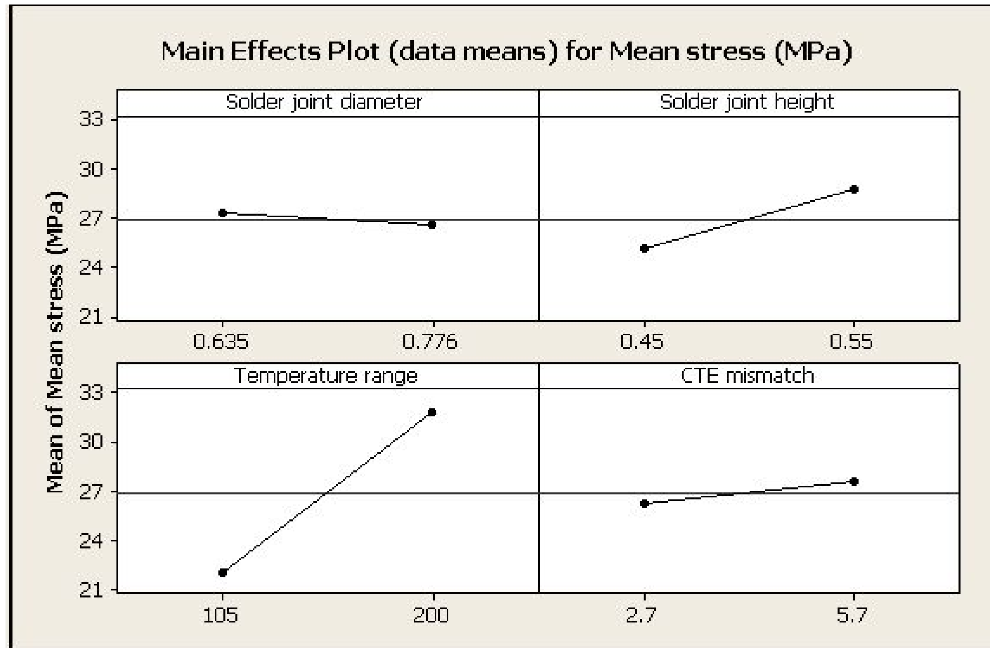

Figure C.2 Main effects

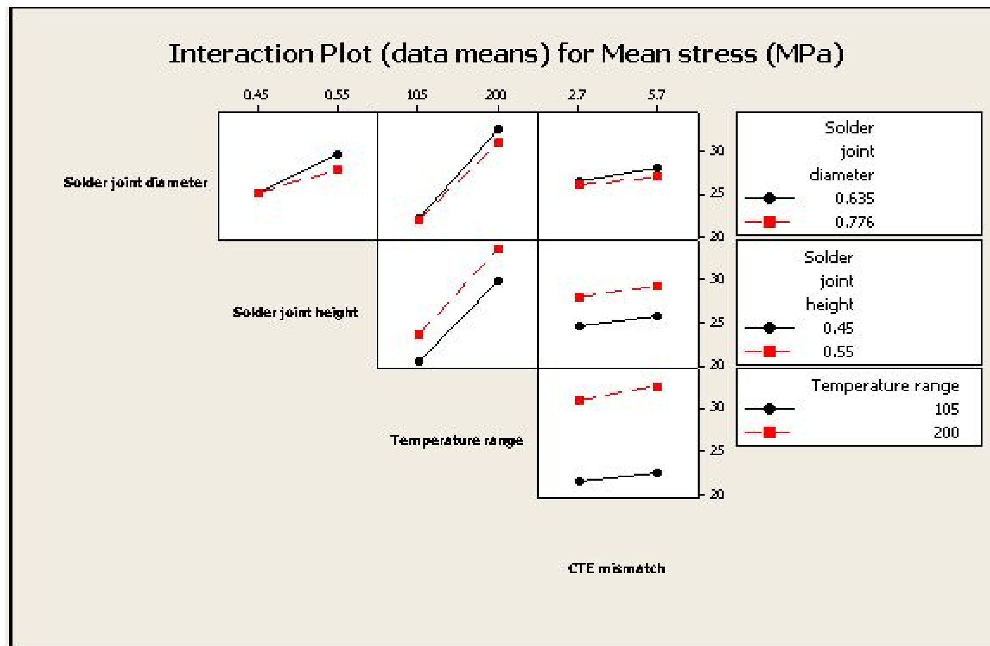

Figure C.3 Interaction effects

C.1.4 Quick PCB deformation calculation

After the damage due to thermal cycling and mean stress calculation, the damage due to vibration was then calculated. The whole calculation includes quick PCB deformation calculation, bending moment calculation, interconnect stress/strain analysis and damage assessment. In this section, PCB deformation calculation was described. This work was done by using calcePWA®. The procedure is as the following:

1) Create a PCB with the layers as the test vehicle
2) Choose the plastic ball grid array (PBGA) package from the library and locate the PBGAs on the board the same as the test vehicle layout
3) Specify the component and board dimensions and material properties at desired temperature level (e.g. T_{mean}, 50 °C in this study)
4) Apply the PSD profile and boundary condition as the vibration loading
5) Generate the FEA modeling using built-in quick FEA tool
6) Run the stress/strain function to obtain the board curvature distribution
7) Repeat step 3)–6) for different temperature levels (e.g. high T, 150 °C and low T, -50 °C)

In this study, board curvatures (Kyy) under PBGA U6 at three temperature levels (T_{max}, 150 °C; T_{mean}, 50 °C and T_{min}, -50 °C) are -1.97E-5 (1/mm), -1.48E-5 (1/mm), -1.40E-5 (1/mm), respectively.

Using the plate moment-curvature relations, the bending moments was then calculated at different temperature levels: -1.80E-3 (N-m/m), -6.47E-3 (N-m/m), -6.70E-3 (N-m/m). Equation C.4 gives the calculation formula:

$$M = \frac{1}{12} E h^3 / \left(1 - \nu^2\right) \kappa \qquad \text{(Eqn. C.4)}$$

where M is the external bending moment, E is board modulus, h is board thickness, ν is the poisson ratio, and κ is the board curvature.

C.1.5 Interconnect stress/strain analysis

As described in Chapter 4.2.2, the interconnect stress/strain analysis were performed based on an analytical model [Siddharth, 1995]. Eqn. 4.9–4.16 already give the calculation formula. Figure C.4 shows the out-of-plane displacements of component and board along the component length. Figure C.6 shows the maximum stress on the interconnects along the component length. The results show the maximum stress locates on the outmost solder joint.

With assumption of elastic deformation range under vibration loading, the maximum strain of solder joint can be calculated as

$$\varepsilon = \frac{\sigma}{E} \qquad \text{(Eqn. C.5)}$$

where ε is the maximum strain, σ is the maximum stress, and E is solder joint modulus.

The strain range was then calculated as two times maximum strain with an assumption of complete reverse strain. Therefore, the temperature dependent strain

ranges were obtained from the curvatures at three different temperature levels: 0.011 for T_{max}, 0.0025 for T_{mean}, and 0.0016 for T_{min}.

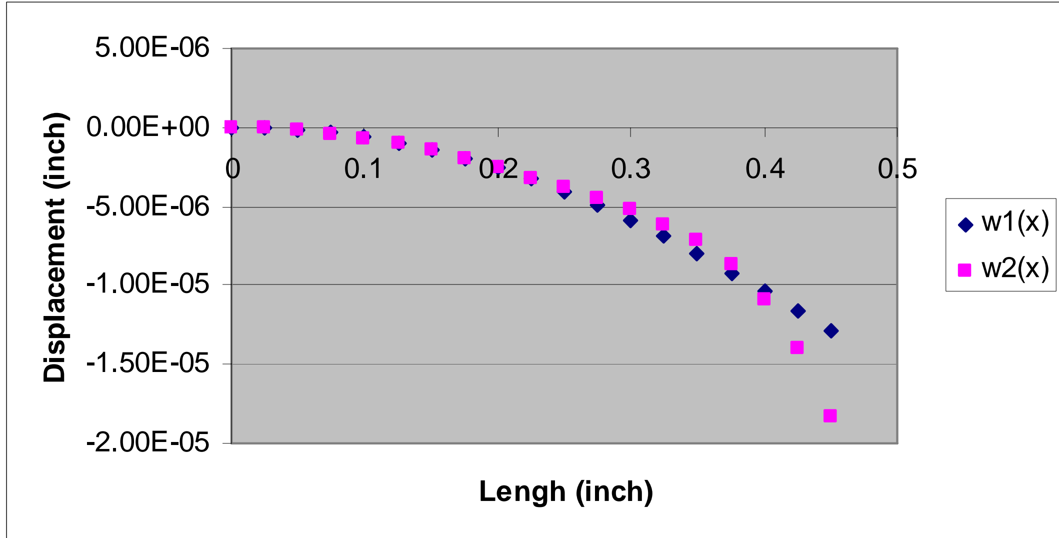

Figure C.4 Deflection of the component (w1) and the board (w2)

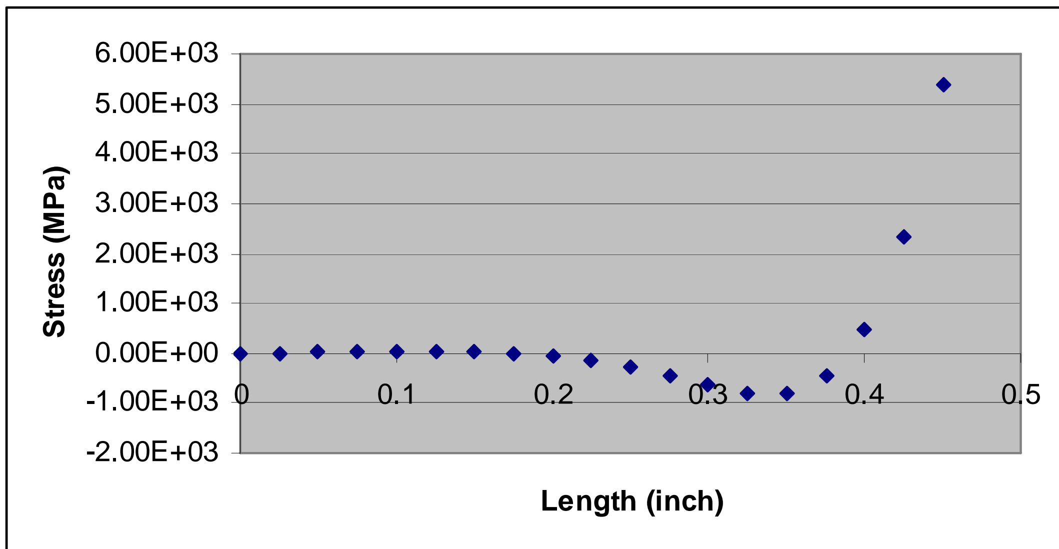

Figure C.5 Maximum stress developed in the solder joints of the PBGA package

C.1.6 Solder joint damage calculation due to vibration loading

When the strain ranges at three temperature levels were available, the solder joint damages were then calculated based on Equation 4.18. The detail calculation procedure was discussed in Appendix B.1.5. The difference is that no occurrence number in this calculation.

The Table C.2 gives the damage results for each temperature level. The accumulated damage due to vibration loading was the summary of the damage at each temperature level, 30.5E-8 (1/s).

Table C.2 Solder joint damage calculation due to vibration loading

	Damage (1/s)	Time fraction	Final damage (1/s)
High temperature (150 °C)	6.7E-7	15/78	12.9E-8
Mean temperature (50 °C)	9.26E-8	48/78	5.7E-8
Low temperature (-50 °C)	6.16E-7	15/78	11.9E-8

C.1.7 Damage superposition

Similar as described in B.1.6, the total damage under combined loading was equal to

$D_{total} = D_{th} + D_{vib} = 7.55E\text{-}8 + 30.5\ E\text{-}8 = 38.05\ E\text{-}8$ (1/s)

Then the predicted life was calculated as 1/38.05E-8/3600 = 730 hours.

The normalized life based on the life under pure vibration loading was calculated as

$N_{normalized} = N_f/N_{vib} = 730/2522 = 0.29$

The comparisons between test results, LDSA results, MIDSA and RLPA were shown in Figure 4.17.

C.2 Analysis on the difference between MIDSA and RLPA prediction

The simulation results show there is difference between MIDSA and RLPA predictions. Table C.3 compare the difference on each damage calculation. It is observed the damage due to thermal cycling in both MIDSA and RLPA is very close. The major life prediction difference is caused by the damage assessment under vibration loading. The 52% less damage was calculated using RLPA compared to MIDSA under vibration loading.

Table C.3 Solder joint damage calculation comparison

Damage (1/s)	Thermal cycling	Vibration loading		
		High Temperature	Room/T_{mean} Temperature	Low Temperature
MIDSA	8.12E-8	32.9E-8	20.1E-8	18.0E-8
RLPA	7.55E-8	12.9E-8	5.7E-8	11.9E-8
Relative difference	7%	61%	72%	34%

The damage calculation difference in two approaches can be due to two parts: the difference in global (PCB) deformation and the difference in the local stress analysis. In MIDSA, the PCB deformation was measured as board in-plane strain. In RLPA,

the PCB deformation was calculated as curvature. Based on the thin-plate small deformation theory, the curvature and strain relationship as

$$\kappa = \frac{\varepsilon}{t_{PCB} / 2} \qquad \text{(Eqn. C.6)}$$

Table C.5 shows the difference from MIDSA measurement and RLPA calculation. The average difference between MIDSA and RLPA on global deformation is 7 times.

Table C.4 PCB deformation calculation comparison

Curvature (1/mm)	Vibration loading		
	High Temperature	Room/T_{mean} Temperature	Low Temperature
MIDSA (Mean)	225E-6	136E-6	92
RLPA	20E-6	15E-6	12E-6
Times on difference	11	9	7

In MIDSA, the solder joint strain ranges were obtained from the response curves. In RLPA, the solder joint strain ranges were calculated using the curvature information and analytic stress calculation. By comparing the mean solder joint ranges in MIDSA and the calculation in RLPA, Table C.4 shows the difference between these two calculations. The average difference between MIDSA and RLPA on local stress analysis is 2.6 times.

Table C.5 Solder joint strain range calculation comparison

Strain range (με)	Vibration loading		
	High Temperature	Room/T_{mean} Temperature	Low Temperature
MIDSA (Mean)	1733	1495	612
RLPA	11000	2500	1600
Times on difference	0.15	0.60	0.38

Assuming the damage calculation difference is proportional to the deformation and stress analysis, the faction of difference between RLPA and MIDSA caused by local stress analysis is around 20% and 80% caused by global deformation calculation.

C.3 Discussion on the damage trend difference in Reference [Upadhyayula, 1999] and in this study using IDSA concept

In Reference [Upadhyayula, 1999], the leaded packages' durability under combined thermal cycling and vibration loading were studied. The test results showed the less damage and longer life of solder joint under combined loading conditions compared to under pure vibration loading at room temperature. However, in this study, PBGA solder joint durability tests showed the much more damage and shorter life of solder joint under combined loading conditions compared to either pure vibration loading or pure thermal cycling. Both studies used the incremental damage superposition approach concept and each simulation reflects the damage trends. To better

understand the incremental damage superposition approach, the qualitative and quantitative analyses were performed on the damage trend difference and described here.

C.3.1 Qualitative analysis on damage trend difference

Table C.6 gives the difference in test profiles and Table C.7 gives the difference in calculation in these two studies. Three major factors can cause the damage accumulation difference:

1) Mean stress at high temperature dwell. As explained previously, mean stress at high temperature dwell is compressive in nature, which can enhance the solder joint fatigue life. In Reference [Upadhyayula, 1999] study, the dwell time at high temperature is 33% longer than in this study. Also the magnitude of mean stress is 10 times than the one in this study. That means the less damage will accumulate during the high temperature dwell in the Reference [Upadhyayula, 1999] study compared to in this study.

2) Mean stress at low temperature. The mean stress during the low temperature dwell is tensile in nature, which can decrease the solder joint fatigue life. In this study, the magnitude of mean stress is 45% larger than the one in Reference [Upadhyayula, 1999]. That means the more damage will accumulate at the same period in this study.

3) Vibration response. While temperature increases, the vibration response increases, as Figure 2.3–2.5 show. Therefore the solder joint strain changes between high temperature and room temperature will affect the damage

accumulation. In this study, the strain range difference between high temperature and room temperature is around 1800 με. In Reference [Upadhyayula, 1999] study, major strain range differences are below 100 με. Therefore, the increase vibration response at high temperature does not contribute a lot damage compared to at room temperature. With consideration of mean stress effect at high temperature dwell, the less damage will be caused during the thermal cycling in Reference [Upadhyayula, 1999] study.

Table C.6 Test profile difference between Refence [Upadhyayula, 1999] and this study

	Ref. [4], PLCC84 (1 sample)	My work, PBGA272 (15 samples)
Time to failure under combined loading	38 hours	135 hours
Time to failure under vibration loading	21 hours	2252 hours
Time to failure under thermal cycling	None	2502 cycles
Thermal loading	-55/125 °C, 43 minutes/cycle 20 minutes dwell at high temperature and 5 minutes at low temperature 18 minutes ramp	-50/150 °C, 78 minutes/cycle 15 minutes dwell at extreme temperatures 24 minutes ramp
Vibration loading	Repetitive shock vibration Step loading: 20-60 Grms with a step size of 5 Grms and a dwell period of 5.6 hours at each level	Constant 0.1 G^2/Hz, 100~1000 Hz 0.1 G2/Hz, around 8 Grms

Table C.7 Simulation difference between Reference [Upadhyayula, 1999] and this study

	Ref. [4], PLCC84	My work, PBGA272
High T dwell time (minutes)	20	15
Low T dwell time (minutes)	5	15
Mean stress (High T)	-10 MPa	-1 MPa
Mean stress (Low T)	20 MPa	29 MPa
Strain range difference between High T and Room T	Below 100 με	Around 1800 με

C.3.2 Quantitative analysis on damage trend difference

In the above section, the qualitative explanation was given to describe the damage trend difference in two studies. Here more detail quantitative analysis was discussed. There are several equations used in damage superposition in IDSA and are listed here again to better discuss.

$$N_f = \frac{1}{D_{total}} \qquad \text{(Eqn. C.7)}$$

$$D_{total} = D_{th} + D_v \qquad \text{(Eqn. C.8)}$$

$$D_v = \sum_j \left(\sum_i \left(\frac{n_i}{N_i} \right)_{T_j} \right) t_j = \frac{1}{N_v} \qquad \text{(Eqn. C.9)}$$

$$D_{th} = \frac{1}{N_{th}} \qquad \text{(Eqn. C.10)}$$

$$\frac{\Delta\varepsilon(T)}{2} = \frac{(\sigma_f - \sigma_{o(T)})}{E}\left(2N_f\right)^b + \varepsilon_f\left(2N_f\right)^c \qquad \text{(Eqn. C.11)}$$

In both studies, the life under combined loading was normalized based on the life under pure vibration loading. Therefore, Equation C.12 gives the normalized calculation.

$$\frac{N_{v,pure}}{N_{combined}} = \frac{D_{total,combined}}{D_{v,pure}} = \left(\frac{D_{v,combined}}{D_{v,pure}}\right) + \left(\frac{D_{th,combined}}{D_{v,pure}}\right) \qquad \text{(Eqn. C.12)}$$

In the IDSA, the damage due to thermal cycling in combined loading is assumed not to be affected by vibration loading. Therefore the damage $D_{th,combined}$ will be equal to the damage D_{th} under pure thermal cycling. The Equation C.12 can be converted to

$$\frac{N_{v,pure}}{N_{combined}} = \frac{D_{total,combined}}{D_{v,pure}} = \left(\frac{D_{v,combined}}{D_{v,pure}}\right) + \left(\frac{D_{th,pure}}{D_{v,pure}}\right) \qquad \text{(Eqn. C.13)}$$

The following section, we will discuss several cases based on the Equation C.13.

Case 1: Equivalent damage due to thermal cycling and vibration loading

For this case, the last term of Eqn. C.12, $D_{th,pure}/D_{v,pure}$ will become 1. Since the term $D_{v,combined}/D_{v,pure}$ can not be negative, the $N_{v,pure}/N_{combined}$ has to be greater than 1. That means the damage under combined loading should be larger than the damage under pure vibration loading and the life should be shorter. In Reference [Upadhyayula, 1999] study, no information is available for life or damage under pure thermal cycling loading. Based on the test results, the product life under combined loading was longer than the product life under pure vibration loading, it can be concluded this study does not belong to this case.

Case 2: More damage due to thermal cycling than due to vibration loading

For this case, the last term of Eqn. C.13, $D_{th,pure}/D_{v,pure}$ will be greater than 1. Therefore, the same conclusion can be drawn that the life under combined loading has to be shorter than the pure vibration loading.

Case 3: Less damage due to thermal cycling than due to vibration loading

For this case, the last term of Eqn. C.13, $D_{th,pure}/D_{v,pure}$ will be less than 1. Therefore, the term $D_{v,combined}/D_{v,pure}$ will also control the damage under combined loading greater or less than the damage under pure vibration loading. In this study, the test results show the damage due to pure vibration loading is 11E-8 (1/s) and the damage due to pure thermal cycling is 8E-8 (1/s). Therefore, it belongs to this case. Furthermore, there are two subsets for this case:

Case 3.1 More damage due to vibration loading under combined loading than due to pure vibration loading

For this case, $D_{v,combined}/D_{v,pure}$ is greater than 1. The sum of $D_{v,combined}/D_{v,pure}$ and $D_{v,combined}/D_{v,pure}$ will be greater than 1. Therefore, the life under combined loading should be shorter than the life under pure vibration loading. In this study, the damage caused by vibration under combined loading condition was calculated as 71E-8 (1/s). It is much larger than the damage caused by pure vibration loading under room temperature 11E-8 (1/s). Therefore, the total damage ratio between combined loading and pure vibration loading is greater than 1. The reflection is the much shorter life under combined loading compared to the life under pure vibration loading at room temperature. The reasons caused more vibration damage under combined loading were discussed the above section and summarized here again:

1) Vibration response change. More deformation occurs at high temperature which means the short life from Eqn. C.11

2) Mean stress effect. With longer duration at low temperature and larger tensile mean stress, Eqn. C.9 and Eqn. C. 11 can contribute to more damage due to combined loading compared to pure vibration loading at room temperature.

Case 3.2 Less damage due to vibration loading under combined loading than due to pure vibration loading

For this case, $D_{v,combined}/D_{v,pure}$ is less than 1. If the sum of $D_{v,combined}/D_{v,pure}$ and $D_{v,combined}/D_{v,pure}$ is also less than 1, the life under combined loading should be greater than the life under pure vibration loading. Since there were no detail calculation information and intermediate results on $D_{v,combined}$ in Reference [Upadhyayula, 1999] study, it is assumed this case occurred in their study. Then it can explain why the life under combined loading was longer than the life under pure vibration loading under room temperature. The reasons caused less vibration damage under combined loading were discussed the above section and summarized here again:

1) Vibration response change. In the Reference study, it is observed major strain range increases were below 100 $\mu\varepsilon$ at high temperature level and the major strain range decreases were around 200 $\mu\varepsilon$ at low temperature level. Based on Equation C.11, more deformation occurring at high temperature will cause more damage and less deformation occurring at low temperature will cause less damage. The dominate part in their study was the less deformation and less damage.

2) Mean stress effect. As mentioned before, the mean stress at high temperature is compressive and will increase life. In the Reference study, the dwell time at high temperature is 4 times longer than the dwell time at low temperature. That means less damages were accumulated due to the longer high temperature dwell.

In a summary, the damage accumulation under combined loading has several scenarios:

1) If the damage caused by thermal cycling is equal or greater than the damage caused by vibration loading, the total damage under combined loading will be more and the life will be shorter than the vibration loading at room temperature
2) If vibration response at high temperature dramatically increases and the tensile mean stress effect is significant (e.g. longer low temperature dwell and larger tensile mean stress), the total damage under combined loading will be more and the life will be shorter than the vibration loading at room temperature
3) If vibration response at low temperature dramatically decreases and the compressive mean stress effect is significant (e.g. longer higher temperature dwell and larger compressive mean stress), the total damage under combined loading will be less and the life will be longer than the vibration loading at room temperature

C.3.3 One pseudo example for damage trend analysis

To better understand the damage trend affected by mean stress and vibration response, one pseudo example is given here. All strain range values and means tress values are assumed, not real values. The life and damage calculation were based on Equations C.7–C.11.

In this example, thermal cycling damage is assumed not the dominant one (Case 3). The life due to thermal cycling is assumed as 1000 hours, i.e., the damage is 2.8E-7 (1/s). The life due to vibration at the room temperature is calculated and listed in Table C.7. Table C.9 shows the vibration prediction at combined loading condition with mean stress effect and vibration response changes. The results show the vibration damage 4.24E-5 is less than damage under pure vibration loading, 5.03E-5. Since the damage due to thermal cycling is 2.8E-7, which is significant less than vibration damage, therefore the total damage under combined loading is less than the damage under pure vibration loading at room temperature (Case 3.2). By changing the mean stress value at high temperature and low temperature, Table C.10 shows new calculation for vibration damage under combined loading. Therefore, the new vibration damage is 5.95E-5, which is greater than the damage under pure vibration loading, 5.03E-5. The damage and life comparison for three conditions were listed in Table C.11. Therefore, the IDSA can be used to explain either damage trend in the tests.

Table C.8 Vibration damage at room temperature calculation

Solder joint strain range	Mean stress (MPa)	Fatigue strength coefficient (σf) (MPa)	Fatigue ductility coefficient (εf)	Fatigue strength exponent, b	Fatigue ductility exponent, c	Modulus, E (MPa)	Life (hrs)	Damage (1/s)
0.01	0	155	0.62	-0.12	-0.52	17687.2	5.5	5.03E-5

Table C.9 Vibration damage under combined loading calculation (condition 1)

	Solder joint strain range	Mean stress (MPa)	Fatigue strength coefficient (σf) (MPa)	Fatigue ductility coefficient (εf)	Fatigue strength exponent, b	Fatigue ductility exponent, c	Modulus, E (MPa)	Fraction of time, tj	Damage (1/s)
Mean T	0.01	0	155	0.62	-0.12	-0.52	17687.2	0.5	2.51E-5
High T	0.012	-50	155	0.62	-0.12	-0.52	17687.2	0.25	1.46E-5
Low T	0.005	50	155	0.62	-0.12	-0.52	17687.2	0.25	0.27E-5
Vibration damage (1/s)									4.24E-5

Table C.10 Vibration damage under combined loading calculation (condition 2)

	Solder joint strain range	Mean stress (MPa)	Fatigue strength coefficient (σf) (MPa)	Fatigue ductility coefficient (εf)	Fatigue strength exponent, b	Fatigue ductility exponent, c	Modulus, E (MPa)	Fraction of time, tj	Damage (1/s)
Mean T	0.01	0	155	0.62	-0.12	-0.52	17687.2	0.5	2.51E-5
High T	0.012	-1	155	0.62	-0.12	-0.52	17687.2	0.25	2.26E-5
Low T	0.005	150	155	0.62	-0.12	-0.52	17687.2	0.25	1.18E-5
Vibration damage (1/s)									5.95E-5

Table C.11 Comparison between combined loading life prediction and pure vibration loading condition

Loading	Damage (1/s)	Predicted life (hrs)	Normalized life
Pure vibration	5.0E-5	5.5	1
Combined loading (condition 1)	4.3E-5	6.5	1.2
Combined loading (condition 2)	6.0E-5	4.6	0.8

Bibliography

1. Adams, P. J., 1986 ‘‘Thermal fatigue of Solder Joints in Micro-Electronic Devices,’’ MS thesis, Dept. of Mechanical Engineering, MIT.

2. ASTM E 112-95, "Standard Test Methods for Determining Average Grain Size", *Annual Book of ASTM Standards,* Section 3, Volume 3.01, pp. 226-248, 1996.

3. Bannantine, J., Comer, J., and Handrock, J., *Fundamentals of Metal Fatigue Analysis*, Prentice Hall, New Jersey, 1990.

4. Barker, D. B., Gupta, V., and Cluff, K., “Solder Joint Crack Initiation and Crack Propagation in a TSOP using Strain Energy Partitioning”, Advances in Electronic Packaging, ASME, EEP-vol. 4-2, 1993

5. Barker, D. B., Vodzak, J., Dasgupta, A., and Pecht, M., “Combined Vibrational and Thermal Solder Joint Fatigue-A Generalized Strain Versus Life Approach”, Trans. of ASME, Journal of Electronic Packaging, Vol.112, pp.129-134, June 1990.

6. Barker, D. B., Vodzak, J., Dasgupta, A., and Pecht, M., “PWB Solder Joint Life Calculations Under Thermal and Vibrational Loading”, Journal of the IES, Vol. 35 (1), pp. 17-25, February 1992.

7. Basaran, C and Chandaroy, R., “Thermomechanical Analysis of Solder Joints Under Thermal and Vibrational Loading“, Transaction of ASME, Vol. 124, March 2002, pp. 60-66.

8. Basquin, O. H., "The Exponential Law of Endurance Tests", *ASTM Proceedings,* vol.10, 1910, pp. 625-630.

9. Boresi, A., Schmidt, R., and Sidebottom, O., *Advanced Mechanics of Materials,* John Wiley and Sons, 1993.

10. Busso, E. P., Kitano, M., and Kumazawa, T., 1992, ‘‘A Viscoplastic Constitutive Model for 60/40 Tin-Lead Solder used in IC package Joints,’’ ASME J. Eng. Mater. Technol., 114, pp. 331-337.

11. CALCE Circuit Card Assemblies Failure Mechanism Model Handbook, 2004

12. CALCE Consortium Technical Final Report, “Guidelines for Assembly and Reliability Assessment of BGAs”, 2002

13. Coffin, L. F., “A Study of the Effect of Cyclic Thermal Stress on a Ductile Metal”, *Transactions of ASME,* vol. 76, pp 931-950, 1954.

14. Darveaux, R. and Banerji, K., "Constitutive Relations for Tin-Based Solder Joints", IEEE Transactions on CHMT, Vol. 15, No. 6, pp. 1013-1024, Dec. 1992.

15. Darveaux, R., “Effect of Simulation Methodology on Solder Joint Crack Growth Correlations,” Proceedings of 50th Electronic Components & Technology Conference, pp. 1048-1058. May 2000.

16. Darveaux, R., Banerji, K., Mawer, A., Dody, G., “Reliability of Plastic Ball Grid Array Assembly”, *Ball Grid Array Technology*, J. Lau, Ed., McGraw Hill, Inc., New York, 1995

17. Dasgupta, A., et. al., “Material Failure Mechanisms and Damage Models”, - A tutorial series containing 14 articles in, IEEE Transactions on Reliability; Lead Article appeared: Vol 40, No.1, pp. 531. 1991.

18. Dasgupta, A., Oyan, C., Barker, D., Pecht, M., "Solder Creep-Fatigue Analysis by an Energy-Partitioning Approach", *ASME Trans. Electronic Packaging*, vol.144, pp.152-160, 1992.

19. Dowling, N. E., "Fatigue Failure Predictions for Complicated Stress-Strain Histories", *Journal of Materials*, JMLSA, Vol.7, No.1, 1972.

20. Dowling, N. E., *Mechanical Behavior of Materials,* Prentice Hall, New Jersey, 1993.

21. Downing, S. D., and Socie, D. F., "Simplified Rainflow Counting Algorithms*", Int. Journal of Fatigue*, Vol.4, No.1, 1982.

22. Engelmaier, W., "Chap. 17: Solder Attachment Reliability, Accelerated Testing, and Result Evaluation" in Solder Joint Reliability - Theory and Applications, edited by Lau, J. H., Van Nostrand Reinhold, New York, 1991, pp. 545-587.

23. IPC-SM-785, "Guidelines for Accelerated Reliability Testing of Surface Mount Solder Attachments," The Institute for Interconnecting and Packaging Electronic Circuits, Northbrook, IL, November 1992.

24. Lall, P., and Pecht, M., “An Integrated Physics-of-Failure Approach to Reliability Assessment Advances in Electronic Packaging”, ASME EEP-Vol.4-1, 1993.

25. Lau, J. et. al. HDPUG's Design for Lead-Free Solder Joint Reliability of High-Density Packages, Presented at IPC SMEMA Council APEX® 2003

26. Manson, S. S., "Fatigue: A Complex Subject-Some Simple Approximations", *Experimental Mechanics*, vol 5, pp 193-226, 1965.

27. McDowell, D. L., Miller, M. P. and Brooks, D. C., 1994 Fatigue Testing of Electronic Materials, ASTM STP 1153, pp. 42-59.

28. Miner, M. A., " Cumulative Damage in Fatigue", *Journal of Applied Physics,* A-159, September, 1945.

29. Morrow, J. D., "Cyclic Plastic Strain Energy and Fatigue of Metals"*, Internal Friction, Damping and Cyclic Plasticity,* ASTM-STP 378, Warrendale, PA., pp. 45-87, 1965.

30. Motorola part #: DSYCHN-272PBGA.

31. Palmgren, A., " Die Lebensdauer von Kugellagern," *VDI Zeitschrift,* No. 14, pp 339-441, 1924

32. Pecht, M., & Dasgupta, A., "Physics-of-failure: An Approach to Reliable Product Development", *Proceedings of Institute of Environmental Sciences*, Chicago, IL, pp.111-117, August 1995.

33. Pecht, M., Dasgupta, A., & Barker, D., "The Reliability Physics Approach to Failure Prediction Modeling," *Quality and Reliability Engineering International*, pp. 276-273, 1990.

34. Pecht, M., Dasgupta, A., Evans, J., and Evans, J., *Quality Conformance and Qualification of Microelectronic Packages and Interconnects*, John Wiley & Sons, New York, NY, 1994.

35. Qi, H., Lee, M., and Osterman, M., "Simulation Model Development for Solder Joint Reliability for High Performance FBGA Assemblies", In Twentieth Annual IEEE Semiconductor Thermal Measurement and Management Symposium, pp. 300-7, 2004

36. Rothman, T., "Physics-of-Failure Methodology for Accelerated Thermal Cycling of LCC Solder Joints", Masters Thesis, Department of Mechanical Engineering, University of Maryland College Park, 1995.

37. Rothman, T., Dasgupta, A. and Tsai, P. "Physics-of-Failure Methodology for Thermal Cycling of Solder Joints, T. *VIII International Congress on Experimental/Numerical Mechanics in Electronic Packaging*, Sponsored by Society of Experimental Mechanics, Nashville, TN, pp. 76-77, June 10-13, 1996

38. Siddharth, S., *Fatigue Life Estimation of Leads in Local Electronic Components Subject to Vibration,* Ph.D., Dissertation, University of Maryland, College Park, MD, 1995.

39. Skipor, et. al. "On the Constitutive Response of 63/37 Sn/Pb Eutectic Solder", J. of Engineering Materials and Technology, Vol. 118, p. 1, 1996

40. Solomon, H. D., *IEEE Trans. CHMT, vol.9, no. 4,* pp. 423-432, Dec. 1986.

41. Steinberg, D. S., *Vibration Analysis for Electronic Equipment*, John Wiley & Sons, New York, 2000.

42. Suhir E., "Could Compliant External Leads Reduce the Strength of a Surface-Mounted Device?", *38th Electronic Components Conference Proceedings*, 1988.

43. Timoshenko, S., and Goodier, J., Theory of Elasticity, McGraw-Hill, 1970.

44. Upadhyayula, K., "An Incremental Damage Superposition Approach for Surface Mount Electronic Interconnect Durability Under Combined Temperature and Vibration Environments", Ph.D. Dissertation, University of Maryland, College Park, 1999

45. Upadhyayula, K., and Dasgupta, A., "An Incremental Damage Superposition Approach for Reliability of Electronic Interconnects under Combined Accelerated Stresses", *9th Symposium on Mechanics of Surface Mount Assembly*, Dallas, Nov, 1997.

46. Vaynman, S., and Fine, M. E., Chapter 11, *Solder Joint Reliability: Theory and Application,* Ed. Lau, J., Van Nostrand Reinhold, 1991.

47. Vichare, N., Rodgers, P., Pecht, M., "Methods for Binning and Density Estimation of Load Parameters for Prognostics and Health Management", International Journal of Performability Engineering, Vol. 2, No. 2, April 2006

48. Wild, R. N., "Some Fatigue Properties of Solders and Solder Joints," IBM Tech. Rep. 73Z000421, January 1973.

49. Zhao, Y, Basaran, C, Cartwright, A, and Dishongh, T, "Inelastic behavior of microelectronics solder joints under concurrent vibration and thermal cycling." ITHERM 2000, Piscataway, NJ, 2000. pp. 174-80, vol. 2.